Some pages of this thesis may have been removed for copyright restrictions.

If you have discovered material in Aston Research Explorer which is unlawful e.g. breaches copyright, (either yours or that of a third party) or any other law, including but not limited to those relating to patent, trademark, confidentiality, data protection, obscenity, defamation, libel, then please read our Takedown policy and contact the service immediately (openaccess@aston.ac.uk)

Localising epileptiform activity and eloquent cortex using Magnetoencephalography

Michael Brathwaite Hope Hall

Doctor of Philosophy

Aston University

September 2017

©Michael Brathwaite Hope Hall, 2017 asserts his moral right to be identified as the author of this thesis

This copy of the thesis has been supplied on condition that anyone who consults it is understood to recognise that its copyright rests with its author and that no quotation from the thesis and no information derived from it may be published without appropriate permission or acknowledgement.

Aston University

Localising epileptiform activity and eloquent cortex using Magnetoencephalography

Michael Brathwaite Hope Hall

Doctor of Philosophy

2017

In patients with drug resistant epilepsy, the surgical resection of epileptogenic cortex allows the possibility for seizure freedom, provided that epileptogenic and eloquent brain tissue can be accurately identified prior to surgery. This is often achieved using various techniques including neuroimaging, electroencephalographic (EEG), neuropsychological and invasive measurements. Over the last 20 years, magnetoencephalography (MEG) has emerged as a non-invasive tool that can provide important clinical information to patients with suspected neocortical epilepsy being considered for surgery. The standard clinical MEG analyses to localise abnormalities are not always successful and therefore the development and evaluation of alternative methods are warranted. There is also a continuous need to develop MEG techniques to delineate eloquent cortex. Based on this rationale, this thesis is concerned with the presurgical evaluation of drug resistant epilepsy patients using MEG and consists of two themes: the first theme focuses on the refinement of techniques to functionally map the brain and the second focuses on evaluating alternative techniques to localise epileptiform activity. The first theme involved the development of an alternative beamformer pipeline to analyse Elekta Neuromag data and was subsequently applied to data acquired using a pre-existing and a novel language task. The findings of the second theme demonstrated how beamformer based measures can objectively localise epileptiform abnormalities. A novel measure, rank vector entropy, was introduced to facilitate the detection of multiple types of abnormal signals (e.g. spikes, slow waves, low amplitude transients). This thesis demonstrates the clinical capacity of MEG and its role in the presurgical evaluation of drug resistant epilepsy patients.

Keywords: Magnetoencephalography; Presurgical evaluation; Epilepsy; Interictal spikes; Beamforming

Acknowledgements

I would firstly like to thank my supervisor Professor Paul Furlong for his supervision and for providing me with great opportunities to facilitate my career. I hope we can continue to work together in the future and engage in more exciting science. I would also like to thank Dr Caroline Witton who has been a great role model and has provided me with valuable support throughout.

I am also indebted to all the people that have helped me along the way. This includes the Aston Brain Centre team, in particular Dr Siân Worthen and Mr Gerard Gooding-Williams for their friendship and advice over the years. I would also like to thank Professor Klaus Kessler for his guidance and for supporting me in recent career endeavours. A special thanks goes to Dr Matthew Brookes for his input in the Rank Vector Entropy project (Chapter 7), and to Dr Arjan Hillebrand and Dr Ida Nissen for our ongoing collaborative work (Chapter 5). I would also like to acknowledge the MRC-MEG UK partnership grant for funding me and providing me with the opportunity to work with some fantastic people.

I owe a debt of gratitude to my parents who have always been a source of love and support, from standing on the side of a rugby pitch in torrential rain to their unwavering support throughout my studies. I have learned much from them and hope to continue to make them proud.

I would finally like to thank my girlfriend Charlotte, for helping me through the tough times and being a constant source of support. You have many strengths that I draw inspiration from and without you this journey would have been exponentially more difficult.

Table of Contents

List of Abbreviations

AED	Antiepileptic Drug
ABC	Aston Brain Centre
ACMEGS	American Clinical Magnetoencephalography Society
ApEn	approximate entropy
ATL	anterior temporal lobe
BEM	boundary element model
BOLD	blood oxygen dependent level
CL	correlation limit
CT	computer tomography
D-EEG	dense array electroencephalography
ECD	equivalent current dipole
EEG	electroencephalography
ECG	electrocardiogram
EMG	electromyography
EOG	electroocoulogram
EPSP	excitatory postsynaptic potential
ESM	electrical simulation mapping
ERF	event related field
ESI	electrical source imaging
FLAIR	fluid-attenuated inversion recovery
FFT	fast-fourier-transform
fMRI	functional magnetic resonance imaging
$GABA_a$	γ-aminobutyric acid, type A receptors
GOF	goodness-of-fit
HPI	head position indicator
ICA	independent component analysis
IFG	inferior frontal gyrus
ILAE	International League Against Epilepsy
ITI	inter-stimulus interval
LCMV	linearly constrained minimum variance
LFP	local field potential

LORETA	low resolution electeromagnetic tomography
LTP	left temporal pole
iEEG	intracranial electroencephalography
MCP	multiple comparison problem
MEA	multiectrode array
MEG	magnetoencephalography
MRC	Medical Research Council
MRI	magnetic resonance imaging
MNE	minimum norm estimate
MNI	Montreal Neurological Institute
MSR	magnetically shielded rooms
MRS	magnetic resonance spectroscopy
MUSIC	multiple signal classification
OPMs	optically pumped magnetometers
PCA	principal component analysis
PET	positron emission tomography
PSP	postsynaptic potential
RMS	root-mean-square
RVE	rank vector entropy
SAM	synthetic aperture magnetometry
SFG	superior frontal gyrus
SMG	supramarginal gyrus
SNR	signal to noise ratio
SPECT	single-photon emission computed tomography
SQUIDS	superconducting quantum interference devices
SSS	signal space separation
STG	superior temporal gyrus
STS	superior temporal sulcus
SUDEP	sudden unexpected death
THOIP	a subsidiary of Sanrio based in the United Kingdom
TLE	temporal lobe epilepsy
tSSS	temporal signal space separation
VE	virtual electrode
VUmc	Vrije University Medical Center, Amsterdam

List of Figures

List of Tables

Chapter 1: Introduction

This PhD project was funded by the Medical Research Council (MRC) and is part of the MRC-MEG UK partnership grant (MR/K005464/1 & MR/K501086/1). This partnership grant is aimed to develop the clinical research capacity of magnetoencephalography (MEG) in the UK by facilitating collaborations between UK MEG centres, develop training programmes and to increase critical research mass in MEG. The partnership consists of 8 universities; Aston, Cambridge, Cardiff, Glasgow, Nottingham, Oxford, University College London, and York. Recently, two new UK MEG centres, Birmingham and Ulster, have joined the partnership and will engage in the goals set out by the lead site (Cardiff). These goals include developing standardised data acquisition and analysis pipelines, and the development of a normative database. Therefore, alongside the research detailed in this thesis, part of this PhD has involved collecting healthy control data for this normative database, whereby each site has committed to acquiring 80 datasets using common protocols. To further the clinical research capacity of MEG in the UK, this thesis has focussed on investigating the use of MEG in the evaluation of patients being considered for epilepsy surgery.

The aim of epilepsy surgery is to remove the epileptogenic zone, i.e. the region whose removal ensures seizure freedom (Engel, 1996, Rosenow & Luders, 2001; Luders et al., 2006). Typically, the epileptogenic zone is determined by the patient's clinical history, electroencephalographic (EEG), neuropsychological and neuroimaging assessments (Rosenow & Luders, 2001; Dorfer et al., 2015). MEG has been shown to provide non-redundant information to help generate hypotheses regarding the epileptogenic zone and information to guide the placement of intracranial electrodes (Mamelak, et al 2002; Fisher et al., 2005; Knowlton et al., 2006; Sutherling et al., 2008; Stefan et al., 2011; Agirre-Arrizubieta et al., 2014; Nissen et al., 2016). However, localising epileptiform activity with the standard MEG analyses is not always successful (Nissen et al., 2016). Therefore, the development and validation of alternative localising methods is warranted. There is also a continuous need to develop non-invasive techniques to accurately delineate eloquent cortex in patients being considered for surgery (Schevon et al., 2007). The accurate localisation of both epileptogenic and eloquent cortex is critical for enabling a successful surgical outcome.

This thesis therefore consists of two main themes: (1) Refining techniques to localise eloquent cortex responsible for language processing, and (2) evaluating alternative approaches for localising epileptiform activity. This introductory chapter aims to set the context of this thesis by describing epilepsy, drug resistance and the rationale for epilepsy surgery. Following this, a brief summary will be given on how non-invasive neuroimaging and MEG feeds into the presurgical evaluation process. Finally, the aims and structure of this thesis will be outlined.

1.1 Epilepsy

Epilepsy is a common neurological condition affecting approximately 50 million people worldwide (Brodie et al., 2000). In the United Kingdom, it is estimated that epilepsy affects almost 1% of the population (Ferro, 2011; Martinez et al., 2009; Wright et al., 2000; Morgan et al., 2002). Epilepsy is classically described as a diverse family of brain diseases characterised by unprovoked and recurrent seizures (Fisher et al., 2005; Fisher et al., 2014). The International League Against Epilepsy (ILAE) defines epileptic seizures as “a transient occurrence of signs and/or symptoms due to abnormal excessive or synchronous neuronal activity in the brain” (Fisher et al., 2005, p. 471). These two definitions reflect the diverse range of possible manifestations that are dependent on a multitude of factors. These factors often include the location of the seizure onset zone, neural pathways, brain development, and confounding disease processes (Fisher et al., 2005).

The generation of seizures are hypothesised to be a result of a complex interaction between two primary physiological factors; (1) neuronal deregulation, arising from mechanisms that affect membrane depolarisation and repolarisation, and (2) neural network abnormalities that involve the hypersynchronisation of neurons and propagation of discharges through the pathways (Engel, 1997). Anti-epileptic drugs (AEDs) aim to prevent epileptic seizures by targeting these two physiological factors.

Term	Definition
Epileptogenic zone	Region of cortex that can generate epileptic seizures. By definition, total removal or disconnection of the epileptogenic zone is necessary and sufficient for seizure-freedom.
Irritative zone	Region of cortex that generates interictal epileptiform discharges in the EEG or MEG.
Seizure onset zone	Region where the clinical seizures originate.
Epileptogenic lesion	Structural lesion that is causally related to the epilepsy
Ictal symptomatogenic zone	Region of cortex that generates the initial seizure symptoms.
Functional deficit zone	Region of cortex that in the interictal period is functionally abnormal, as indicated by neurological examination, neuropsychological testing and functional imaging or non-epileptiform EEG or MEG abnormalities.
Eloquent cortex	Region of cortex that is indispensable for defined cortical functions.

Table 1. ILAE definitions of epileptic brain areas (Luders et al., 1992). These terms are used throughout this thesis.

1.1.1 Antiepileptic drugs

The primary goal of AEDs is to prevent epileptic seizures by altering the bursting properties of neurons and reducing the abnormal synchronisation of local neuronal assemblies (Rogawshi & Löscher, 2004). Different AEDs target different molecules in the brain and can be classified into three main categories based on their action properties (Rogawshi & Löscher, 2004). These action properties include; (1) modulating voltage-gated ion channels to alter the firing of action potentials and the release of neurotransmitters, (2) potentiation of inhibitory systems mediated by $GABA_a$ (γ-aminobutyric acid, type A receptors), and (3) inhibiting synaptic excitation by blocking glutamate receptors. A comprehensive description of the current AEDs used in the UK can be found at https://www.epilepsysociety.org.uk/list-anti-epileptic-drugs.

1.1.2 Drug Resistant Epilepsy

AEDs are effective in preventing seizures in the majority of patients, however it is estimated that 20-30% of patients are resistant to these drugs and therefore do not achieve seizure freedom (Sander, 1993; Schmidt & Gram, 1995; Dichter & Brodie, 1996; WHO, 2009). The ILAE defines drug resistant epilepsy as a failure of two adequate trials of appropriately chosen and tolerated AEDs to achieve sustained seizure freedom (as a mono- or poly-therapy) (Kwan et al., 2010). Seizure freedom has been defined as a seizure-free period that is at least three times longer than the inter-seizure interval prior to starting a new intervention, or a period that lasts at least 12 months (Kwan et al., 2010). Drug resistant epilepsy patients are also frequently referred to as “pharmacoresistant”, “refractory”, or “intractable” patients. To stay consistent with the ILAE guidelines, these patients will be referred to as drug resistant epilepsy patients throughout this thesis.

The underlying cause for drug resistance is complex with several hypotheses attempting to explain the biological mechanisms involved, including the “target” and “transporter” hypotheses (Loscher et al., 2005). The transporter hypothesis refers to drugs failing to reach their targets due to an overexpression of efflux transporters that expel substrates out of the cell against the concentration gradient (Schmidt & Loscher et al., 2005). Alternatively, the target hypothesis postulates that intrinsic or acquired changes in AED targets (e.g. Na^{+} channels, Ca^{2+} channels, GABA system, Glutamate receptors) cause a loss of brain-target sensitivity resulting in resistance to AEDs (Loscher, 2005). These two putative biological theories provide a potential explanation for drug resistance, however there is still debate regarding the exact mechanisms underlying drug resistance (Schmidt & Loscher, 2005).

Importantly, patients with drug resistant epilepsy often have poor prognostic implications that may include physical injury, psychosocial dysfunction, reduced quality of life, and sudden unexpected death (SUDEP) (Leidy et al., 1999; Devisnky et al., 1995; Mohanraj et al. 2006; McCagh et al., 2009). In these patients, surgical intervention may offer a solution to eliminate or reduce the severity of seizures (Engel, 1996: 1993; Luders et al., 1992).

1.1.3 Epilepsy Surgery

The primary goal of epilepsy surgery is to completely remove the epileptogenic zone whilst avoiding permanent neurological deficits (Binnie & Polkey, 2000; Rosenow & Luders, 2001). This is achieved by accurately localising the epileptogenic zone and identifying nearby eloquent cortex (Knake et al., 2006). It has been reported that most epilepsy centres achieve a seizure free outcome in 70–90% of patients (Engel, 1993; Engel, 1996; McIntosh et al., 2001, Schmidt and Stavem, 2009; Engel et al., 2012). In a randomised control study, Wiebe et al., (2001) demonstrated that 64% of patients were free of disabling seizures at 12 months, relative to 8% who were assigned to further medical treatment. These figures demonstrate the utility of surgical intervention and how a favourable outcome can be achieved in a large proportion of patients.

Despite the benefits that can be gained from early surgical intervention, surgical treatment for epilepsy is often delayed or underutilised (Engel et al., 2003; 2012; 2013). The growing body of evidence supporting surgical intervention has aimed to increase efforts in providing earlier access to epilepsy surgery (Ryvlin, et al., 2014). This is reflected in a recent NHS England contract aimed at facilitating more surgeries per annum in conjunction with the Children's Epilepsy Surgery Service (NHS England, 2013). This increase in surgery demand means that identifying suitable candidates for surgery is of ever-growing importance.

Candidate selection for neurosurgery is often regarded as a two-step procedure involving the identification of drug resistant patients who experience disabling seizures and to secondly assess whether the risk to benefit ratio of surgery is acceptable (Ryvlin & Rheims, 2008). A key criterion for determining surgical suitability is whether the epileptogenic zone can be accurately localised during the pre-surgical evaluation phase. This is not always straightforward and multiple assessments are required to develop a precise hypothesis regarding its location. Therefore, the further refinement of pre-surgical evaluation techniques is continuously warranted to accurately localise the epileptogenic zone and to enable more patients to be selected for surgery.

1.2 Pre-surgical Evaluation

This section will outline the common pre-surgical assessments used and outline the added value of MEG in this process.

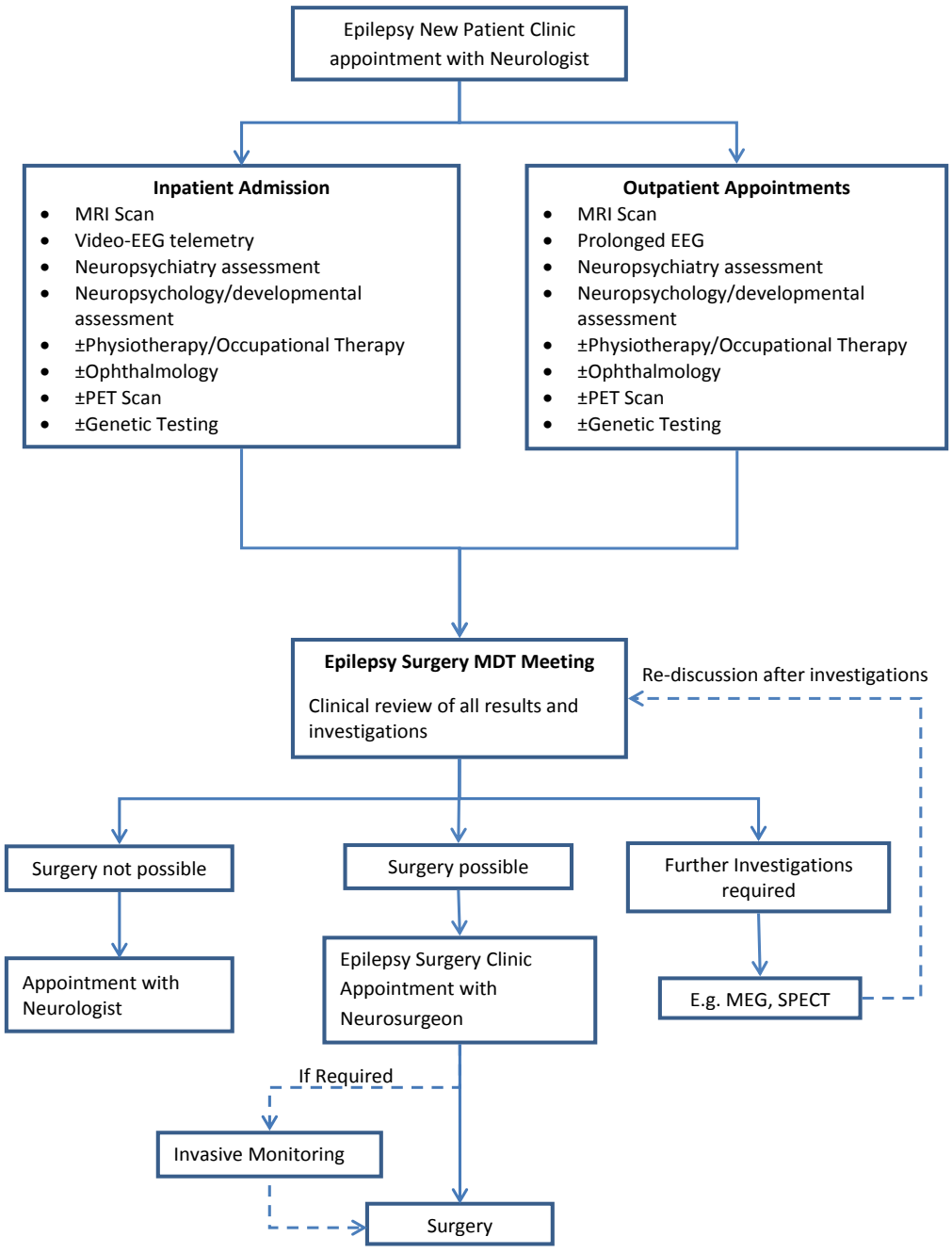

Figure 1.1 Children's Epilepsy Surgery Service patient pathway (NHS England, 2013).

1.2.1 Non-invasive Testing

There is currently no single measure or imaging modality that facilitates the identification of the epileptogenic zone in all patients, therefore a combination of methods is often required. These methods enable clinicians to not only determine the location of the epileptogenic zone, but to establish the distribution of epileptogenic tissue, i.e. whether epileptic discharges spread to epileptogenic cortex or tissue that would otherwise be considered normal (Rosenow and Luders, 2001). These evaluations often involve reviewing the patient's seizure history, neurophysiological, neuropsychological and neuroimaging assessments (Jayakar, 1999; Rosenow & Luders, 2001; Diehl et al., 2003; Dorfer et al., 2015). The following subsections will briefly describe each of these assessments and their contribution to the presurgical assessment of patients.

1.2.2 Seizure history and semiology

A comprehensive description of the patient's seizures is often acquired through conducting detailed interviews with the patient and their relatives (Ryvlin & Rheims, 2008). For example, if a patient reports unilateral somatosensory auras (e.g. "tingling" sensations), the contralateral primary sensory cortex is often revealed as the ictal symptomatogenic zone (Tufenkijan & Luders et al., 2012). In patients that report more distributed somatosensations, the seizure onset zone is likely to be located to the supplementary sensory motor area and/or the second somatosensory area (Pugnaghi et al., 2011). Seizure semiology is also assessed by reviewing video recordings of the seizure and linking the overt symptoms to areas in the brain (Tufenkijan & Luders et al., 2012). For example, if the recorded seizure indicates lateralised and prolonged febrile seizures, then the seizure onset zone is likely to be located in the temporal lobe contralateral to the affected side (Tellez-Zenteno et al., 2005; Tonini et al., 2004).

The use of seizure semiology to determine the epileptogenic zone is not always straight forward and conflicting symptoms can occur in a single seizure and inter-rater agreement can be variable (Tufenkijan & Luders et al., 2012). Therefore, the information gained from this assessment needs to be evaluated in the context of the other presurgical assessments described below.

1.2.3 Neuropsychological Assessments

Neuropsychological testing is an essential component of the candidate selection procedure (Rausch and Babb, 1993; Trenerry et al., 1993) and has shown to assist in lateralising the seizure onset zone (Williamson et al., 1993; Sayuthi et al., 2009). Furthermore, neuropsychological dysfunctions can be associated to specific seizure onset zones (Gotman et al., 1991; Wilson et al., 2015). For example, verbal memory impairments are often associated with left temporal lobe epilepsy (TLE) (Gotman et al., 1991). Alternatively, more wide spread neuropsychological deficits may be a marker of generalised epilepsy, suggesting a potentially poor outcome if a focal resection is pursued (Anhoury et al., 2000). With the advent of more sophisticated techniques (e.g. neuroimaging), neuropsychological testing is primarily used to provide further concordance to these measures and prognostic information regarding postsurgical neuropsychological deficits (Rosenow & Luders, 2001).

1.2.4 Neuroimaging assessments

The primary role of non-invasive imaging, such as magnetic resonance imaging (MRI) and x ray computed tomography (CT), is to help identify structural abnormalities that are likely to be responsible for the seizure disorder (Duncan et al., 1997; Carne et al., 2004; Knake et al., 2005). CT imaging permits the detection of large lesions, including tumours and infarcts, whereas MRI is able to also detect subtle malformations such as hippocampal sclerosis, focal cortical dysplasia, cavernomas and small tumours (Requena et al., 1991; Duncan, 1997; Bronen et al., 1997; De Camargo & Koroshetz, 2005). In the majority of cases MRI has replaced CT, however CT is still useful in the acute setting or when there are contraindications to MRI (e.g. pacemaker, cochlear implants, implanted iEEG electrodes) (Kuzniecky, 2005).

Despite the superior sensitivity of MRI in detecting both major and subtle abnormalities (Sperling et al., 1986; Cross et al., 1993), not all MRI assessments reveal abnormal findings (Duncan et al., 1997). Approximately, 30% of patients with drug resistant temporal lobe epilepsy have nonlesional MRI results (Cascino et al., 1991; Muhlofer et al., 2007). Berg et al., (2003) reported that 130 out 491 patients with MRI information showed no detectable abnormalities with a further 28 patients producing equivocal findings. More recent advances in MRI techniques, such as magnetic resonance spectroscopy (MRS) and ultra high field MRI, may enable the

detection of abnormalities in patients that were previously considered MRI negative (Mouthaan et al., 2016; De Ciantis et al., 2016; van der Kolk et al., 2013).

Other imaging techniques, including positron emission tomography (PET) and single-photon emission computed tomography (SPECT), have also been shown to complement MRI and may assist in determining the epileptogenicity of a lesion (Son et al., 1999; Hwang et al., 2001; Hong et al., 2002; Carne et al., 2004). PET imaging indicates the irritative zone by showing regional reductions in the uptake of glucose (hypometabolism) and significant increases during ictal activity (Henry, 1999). SPECT is particularly useful for localising seizure activity, as it is able to capture clinically overt seizures regardless of seizure-related movements (Knowlton et al., 2004; Ryvlin & Rheims, 2008). Typically, ictal SPECT shows a focal area of hyperperfusion relating to the ictal discharge (Kaiboriboon et al., 2005; Kilpatrick et al., 1997; Shin et al., 2002).

Figure 1.2. FLAIR MRI showing a focal cortical dysplasia of Taylor-s balloon cell type. The blue arrow depicts the hypoerintense subcortical aspect of the lesion. Taken from Urbach et al. (2002).

Being able to identify structural abnormalities is a key part of the presurgical evaluation of drug resistant epilepsy patients. However, not all lesions are epileptogenic and some radiographic lesions may be unrelated to seizure generation. For this reason, even when a radiographic lesion is identified, other methods are required to confirm whether this is the underlying cause of the patient's seizures and to establish the extent of the epileptogenic cortex (Rosenow & Luders, 2001).

1.2.5 Neurophysiological assessments

Another measure that is used to confirm whether a lesion is epileptogenic is EEG (Rosenow & Luders, 2001). EEG plays a key role in the diagnosis of epilepsy and can help to localise the epileptogenic zone (Engel, 1984; Noachtar & Rémi 2009) by providing a prolonged measure of interictal and ictal activity (Jobst et al., 2001; Pataraia et al., 2004). It can be argued that scalp EEG may be limited to being a confirmatory technique when localising the epileptogenic zone as its spatial sensitivity is limited by the spatial sampling used (16-21 electrodes). This confound is coupled with the field spread of currents as electrical signals pass through multiple layers of head tissue (Rosenow & Luders, 2001).

The use of dense array EEG (D-EEG) and electrical source imaging (ESI) has recently shown to be promising when attempting to counter the limitations of conventional EEG. The use of up to 256 electrodes in D-EEG increases spatial coverage whilst reducing inter-electrode distance to improve the spatial resolution of the data (Lantz et al., 2003; Holmes et al., 2008). Another advancement in ESI is the improved resolution of EEG forward models that take into account multiple types of head tissue and anisotropic conductivity profiles (Grech et al., 2008; Gramfort et al., 2010). The ability to construct more realistic head models is crucial to computing an accurate leadfield matrix to facilitate an accurate source estimate (Birot et al., 2014). There is still a limited amount of research clinically validating D-EEG and ESI, however recent studies suggest that D-EEG may provide useful information regarding the epileptogenic zone, particularly when the focus is deep (Holmes et al., 2008; Holmes et al., 2010; Yamazaki et al., 2012).

1.2.6 Invasive Monitoring

Appropriate candidates for invasive testing are patients with conflicting neuroimaging (MRI, SPECT, PET) and EEG findings (Sperling, 1997; Siegel, 2000). Invasive monitoring or iEEG involves the use of subdural strips, depth electrodes, and subdural grids (Dewar et al., 1996; Engel, 1996). Invasive monitoring is used in 25-40% of cases in large epilepsy centres (Faught et al., 2008) and is considered the gold standard for precisely localising the epileptogenic zone (Hader et al., 2004; Blount et al., 2008; Gompel et al., 2008). The percentage of patients that benefit from iEEG allowing them to be selected for surgery has shown to range from 75-90%

(Brekelmans et al., 1998; Schiller et al., 1998; Eisenschenk et al., 2001; Lee et al., 2003; Pondal-Sordo et al., 2007).

An important criterion to qualify for iEEG is that there is some form of hypothesis regarding the area to sample from (Siegel et al., 2000; Ryvlin and Rheims, 2008). This is crucial as electrode coverage can be limited to several cm^3 (Spencer et al., 1993; Seeck & Spinelli 2004). Given the costs involved and additional risks placed upon the patient, it is important to ensure that the implanted electrodes yield useful information to precisely determine the epileptogenic zone (Hamer et al., 2002; Stefan et al., 2011).

In cases where MRI and EEG findings are conflicting or inconclusive, MEG has shown to be useful in guiding the implantation of electrodes and determining whether the epilepsy if focal or if there are multiple seizure onset zones (Rodionov et al., 2013; Agirre-Arrizubieta et al., 2014; Nowell et al., 2015). Furthermore, it has been demonstrated that in some cases the use of MEG may reduce the need for invasive monitoring (Knake et al., 2006; Knowlton et al., 2006). The next section will provide an overview of the literature outlining the role of MEG as an additional presurgical evaluation tool.

1.3 Clinical MEG

MEG is a non-invasive technique that measures the weak magnetic fields produced by neurons providing a sub-millisecond measurement of neural activity (Hämäläinen et al., 1993) (See Chapter 2 for more detail). Several studies have shown that MEG has superior temporal resolution relative to fMRI (Dale et al., 2000; Zotev et al, 2008), as it provides a direct measurement of intracellular neuronal ionic current flow (Hämäläinen et al., 1993). This is in contrast to the blood oxygen dependent level (BOLD) signal measured by fMRI which can take several seconds to develop and decay (Bandettini et al., 1993). Furthermore, the spatial resolution of MEG is often regarded superior to EEG as magnetic fields are relatively undistorted as they pass through the cranium (Ebersole and Ebersole, 2010). This means that less complex forward models are required for source localisation in MEG (Muthukumaraswamy, 2014). Ultimately, MEG provides a good method for investigating the spatiotemporal dynamics of the brain and is therefore well suited to studying conditions such as epilepsy (Hämäläinen et al., 1993).

A key role of presurgical MEG is to help form hypotheses regarding the location of the epileptogenic zone in patients whereby MRI or EEG has produced inconclusive or conflicting findings (Paulini et al., 2007; Stefan et al., 2003; Wilenius et al, 2013). Secondly, in a similar fashion to EEG, MEG can be used as a confirmatory technique to establish whether a radiographic lesion is epileptogenic (Cohen-Gadol et al., 2004; Paulini et al., 2007). Importantly, the additional information acquired from MEG may increase the number of patients eligible for surgery and allow iEEG to be avoided where possible (Stefan et al., 2011).

The above points provide a good rationale for using MEG in clinical practice, however it has been reported that some clinicians still question the value of MEG and are sceptical of its use in clinic (Kharkar & Knowlton, 2015). The following section will provide an overview highlighting the additional value that clinical MEG can provide in an attempt to overcome this criticism.

1.3.1 MEG and Epilepsy

Numerous studies have shown that MEG can localise epileptiform discharges that coincide with ictal activity recorded by iEEG (Sutherling et al., 1988; Stefan et al., 1992; Knowlton et al., 1997; Mamelak et al., 2002; Lamusuo et al., 1999). Studies have also shown concordance between MEG localisations and subsequently resected areas leading to seizure free outcomes (Bast et al., 2004; Fujiwara et al., 2012; Genow et al., 2004; Wilenius et al., 2013). In a prospective blinded study, Sutherling et al., (2008) reported that MEG provided non-redundant information in 33% of patients (n=69), which led to 13% additional iEEG electrode coverage and changes that influenced the surgical decision in 20% of cases. This information provided by MEG was key, as the information leading to these outcomes were not available through other techniques (e.g video EEG, MRI, PET, and SPECT).

As previously mentioned, the optimal placement of intracranial electrodes is crucial with some studies reporting that 49% of ictal onsets occur in regions not covered by iEEG electrodes (Widdess-Walsh, 2007). MEG has shown to be useful in guiding the placement of intracranial electrodes to ensure successful coverage (Knowlton et al, 2006; Sutherling et al., 2008; Agirre-Arrizubieta et al., 2014). This is evident in cases whereby the initial iEEG electrode placement did not capture ictal activity, but secondary MEG guided iEEG placement resulted in the identification of the seizure

onset zone (Sutherling et al., 2008). A more recent study demonstrated how MEG can provide unique information to help guide intracranial electrode placement in patients whereby other pre-surgical assessments were unable to provide a clear hypothesis regarding the implantation site (Agirre-Arrizubieta, et al. 2014).

When considering the added value of MEG relative to EEG, findings have shown that the signal to noise ratio (SNR) is higher in the frontal lobe, facilitating greater spike detection (De Jongh et al., 2005; Ossenblok et al., 2007; Iwasaki et al., 2005; Kakisaka et al., 2012). Several studies have also demonstrated that MEG is more consistently concordant with iEEG findings (Mikuni et al, 1997; Oishi et al., 2002; Sutherling et al., 1988). This increased sensitivity in MEG compared to EEG may be explained by the amount of synchronised cortex reportedly required to produce an observable signal (3-4cm^2 versus 6-10cm^2, respectively) (Mikuni, et al., 1997, Tao et al., 2005). Furthermore, in patients who have previously undergone a craniotomy (inducing further skull inhomogeneities), MEG has been used successfully for spike localisation (Lee et al., 2010; Mohamed et al., 2007; Yoshinaga et al., 2008).

Figure 1.3. **Left:** A patient with a normal MRI and MEG dipole cluster in the right lateral temporal cortex **Right:** Neurofilament staining of resected tissue from the same patient indicating cortical dysplasia. The removal of this tissue was based on the MEG localisations that led to iEEG implantation confirming the location. The patient was seizure free post-surgery. Taken from Knowlton and Shih (2004).

MRI-guided MEG has also shown to be useful in revealing epileptogenic abnormalities by guiding the review of MRI images in cases that were initially declared as being nonlesional (Heers, 2012). For example, Knowlton and Shih (2004) demonstrate how MEG dipole analysis can localise small areas of cortical dysplasia (Figure 1.3). In conditions such as tuberous sclerosis complex, MEG can also be useful in establishing the epileptogenicity of cortical tubers and identifying the most epileptogenic tuber (Evans et al., 2012; Wu et al., 2006).

1.3.2 Interictal MEG

Based on the short time window to conduct MEG recordings (45-60 minutes) and movement related artefacts, ictal events are rarely captured in MEG (Iwasaki et al., 2005). It is argued that the neural assemblies responsible for generating interictal spikes are not necessarily identical to the neural assemblies responsible for generating seizures (Jensen and Yaari, 1988; Engel, 1997). Therefore, MEG largely relies on localising irritative zones to help form hypotheses regarding the location of the epileptogenic zone.

Interictal spikes are often expressed by high-amplitude (>50 mV) synchronous events that last <250ms followed by a slow wave lasting several hundreds of milliseconds[1] (de Curtis & Avanzini, 2001; Staley & Dudek, 2006; Walczac and Jayakar, 1997) (see figure 4). The neural mechanism thought to support these paroxysms is the synchronous depolarisation of cell membranes belonging to populations of hyperexcitable neurons (de Curtis & Avanzini, 2001).

[1] There is not a formal definition of what constitutes a spike in MEG (Nowak et al. 2009).

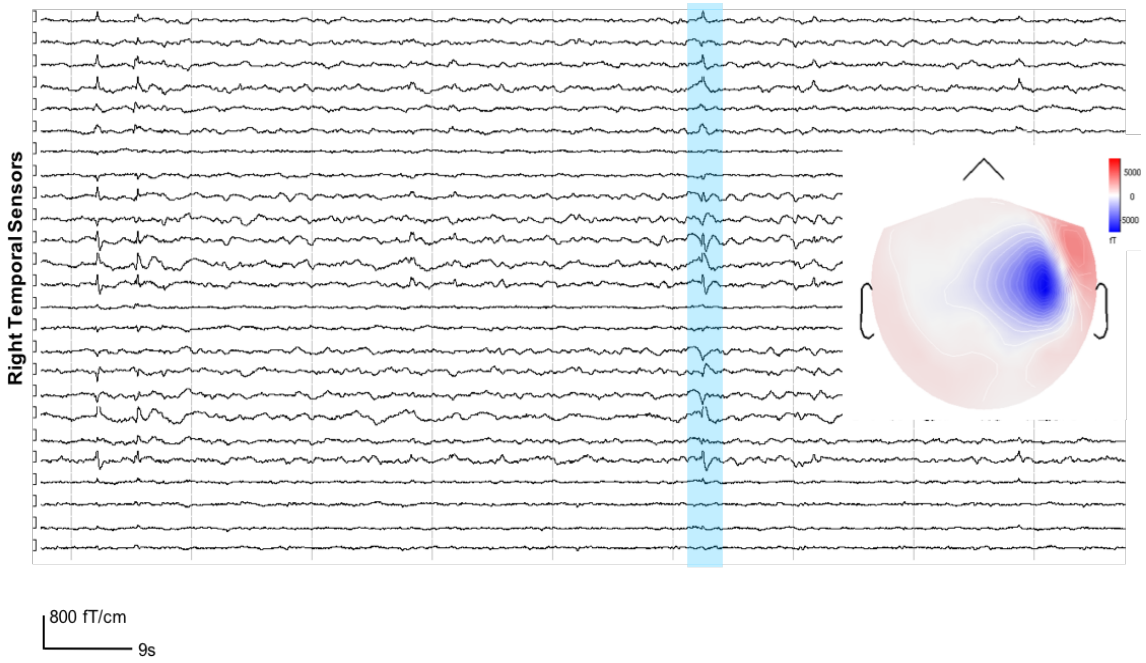

Figure 1.4. 9 seconds of MEG data (right temporal sensors) containing interictal spikes. The topographic map represents the time point correlating to the peak of the interictal spike contained within the shaded blue box.

Despite the added value of clinical MEG, the localisation of epileptiform activity with the current standard analyses (e.g. Equivalent Current Dipole fitting) are not always successful (Nissen et al., 2016). This may be due to an absence of clear interictal spikes during the recording period or due to insensitivities of the analysis methods. Therefore, there is a need to test alternative analysis approaches and develop novel techniques that may assist in localising epileptiform activity. This forms one of the objectives of this thesis with the aim of improving the sensitivity of clinical MEG (Chapters 5-7). The next section will outline the case for mapping eloquent cortex in epilepsy patients prior to surgergy and the challenges faced. This forms Chapters 3 & 4 of this thesis.

1.3.3 Functional Mapping in MEG

Patients being evaluated for surgery require eloquent cortex to be identified before the resection of epileptogenic tissue due to the risk of paralysis and possible disruptions to integral sensory areas (Rosenow & Luders, 2001). In clinical MEG, mapping of the primary somatosensory cortex is the most established method with

studies demonstrating its robust and accurate localisation (Gallen et al., 1993; Gallen et al., 1994; Roberts et al., 1995). The precise localisation of the motor cortex and somatosensory cortex is commonly required for frontal lobe epilepsy and fronto-parietal lesions (Witton et al., 2014). However, the most common type of drug resistant neocortical epilepsy is TLE (Zemskaya, 1998; Semah et al., 1998; Engel et al., 1998). Therefore, in this population, the localisation of language areas is critical. This is usually determined by establishing which hemisphere is dominant for language processing and has typically involved the use of invasive methods to achieve this.

1.3.4 Language Lateralisation

Historically, the method used to determine language lateralisation is the intracarotid administration of sodium amobarbital (WADA; Wada & Rasmussen, 1960). This technique works by assessing whether language deficits occur in the hemisphere sedated by the drug. A limiting factor of this procedure is that it can only identify the language dominant hemisphere and disregards bilateral language representation and the underlying neural substrates involved (Fisher et al., 2008). To gain more precise information about language functioning, electrocortical stimulation mapping (ESM) can be used to assess changes in language performance (Penfield & Rasmussen, 1950). Despite being the gold standard for language localisation, patient discomfort may reduce the efficiency of ESM and intra-operative mapping is limited to electrode coverage (Hamberger & Cole, 2011). Therefore, it is critical to develop non-invasive methods that samples the whole cortex to reduce the need for invasive methods where possible.

Non-invasive alternatives, including fMRI and MEG, have been used to identify language critical areas (Swanson et al. 2007; Salmelin et al., 2007). Typically, letter fluency and verb generation tasks have been used as measures of language lateralisation (Singh et al., 2002; Fisher et al., 2008). The overlapping nature of language processing lends itself well to MEG, allowing the temporal separation of multiple components with relatively accurate source localisation (Salmelin, 2007). Several studies have validated MEG localisations of language with WADA outcomes (Papanicolaou et al., 2004; Hirata et., 2004; Hirata et al., 2010) and ESM (Salmelin, 2007).

At the Aston Wellcome Trust Laboratory for MEG studies, language areas are often identified using a verb generation task. The original publication outlining this task

demonstrated beta desynchronisations in the dominant language hemisphere which was confirmed using WADA in a small group of patients (Fisher et al., 2008). This finding demonstrated a robust lateralised response and indicated a quantitative laterality measurement of the source data was not warranted**.** This study was conducted using CTF data from the previous MEG system at Aston and analysed using the CTF SAM software tools. More recently, the Aston MEG laboratory has acquired an Elekta Neuromag Triux system (see Chapter 2 for description), which has presented several issues in regards to source analysis, making these original results hard to replicate due to the Elekta beamformer software leading to erroneous localisations.

1.3.5 Functional Mapping using Elekta data

Until recently, the Aston MEG laboratory relied on the Elekta Beamformer software, which works well under some conditions (e.g single state for epilepsy protocols/resting state) but unpublished findings have shown that the dual-state beamformer (i.e. comparing the power estimate of two brain states) often leads to inaccurate deep localisations.

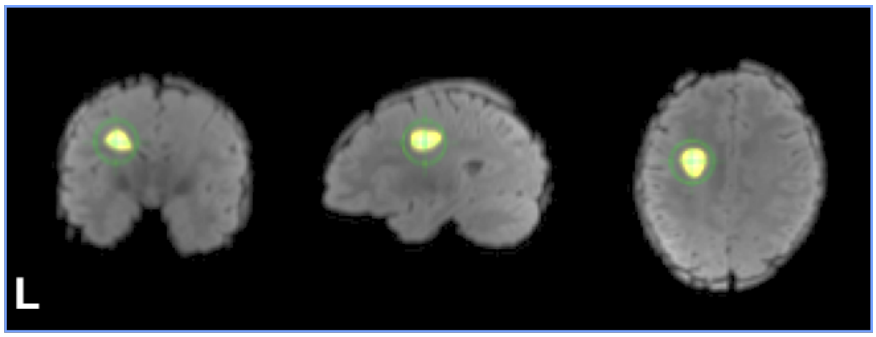

Figure 1.5. An example of a white matter localisation in response to stimulation of the median nerve. Source analysis was conducted using the Elekta Neuromag dual state beamformer.

The requirement of a source analysis pipeline that allows the investigation of ongoing oscillations is critical for cognitive paradigms such as the verb generation task. This has led to the exploration of alternative software packages, including Brainstorm (Tadel et al., 2011), MNE python (Gramfort et al., 2013) and SPM (Litvak et al., 2011), with little progress in regards of formalising a beamformer based pipeline. In this thesis, a Fieldtrip (Oostenveld et al., 2011) beamformer pipeline was outlined and tested (Chapter 3), and subsequently applied to language data in chapter 4.

1.4 Aims

To reiterate the aims stated at the beginning of this chapter, this thesis consists of two distinct, yet related themes: (1) Refining techniques to localise eloquent cortex responsible for language processing, and (2) developing and validating alternative approaches for localising epileptiform activity. Due to the imperative nature of localising both eloquent and epileptogenic tissue, this thesis aims to bring these two themes together to provide further insights into the use of MEG for the presurgical evaluation of epilepsy patients.

1.5 Chapter Outline

Chapter 2 will outline specific details about MEG and the methods that are referred to and used in this thesis. Chapters 3 & 4 will focus on the first theme of the thesis. Specifically, chapter 3 aims to develop an alternative source analysis pipeline for Elekta data that can be used to facilitate the localisation of eloquent cortex in epilepsy patients. This will also test some of the parameters specific to Elekta data (e.g. Maxfilter, sensor selection). Chapter 4 will then apply this pipeline to verb generation data and introduce a novel MEG language task with the aim of establishing the language dominant hemisphere. Conclusions will be drawn based on the analysis pipeline and paradigms used.

Chapters 5, 6 & 7 will then focus on the second theme of this thesis. Chapter 5 aims to evaluate the kurtosis beamformer, an alternative technique for localising interictal spikes. This evaluation is carried out on a cohort of patients that have undergone epilepsy surgery and have postsurgical outcome measures. In the interest of the MRC-MEG UK partnership goals, and to facilitate more multi-centre clinical studies, chapter 6 briefly outlines an open source pipeline to compute the kurtosis beamformer and provides an initial validation of this approach. Chapter 7 then involves applying a novel technique, rank vector entropy (RVE), to epilepsy resting state data to investigate its use in clinical MEG analysis.

Finally, Chapter 8 aims to bring the two themes together by reviewing the respective findings and discussing how they provide further insights into clinical MEG. Final discussion points will allude to recent advancements in MEG technology and how this may impact the future of clinical MEG.

Chapter 2: Magnetoencephalography (MEG) Physiological basis, hardware and analysis techniques.

2.1 Introduction

The purpose of this chapter is to introduce the methods used in this thesis and acts as a reference point throughout. This chapter begins with a brief description of MEG and the instrumentation used to acquire data in this thesis. It then continues to describe the methods used at the ABC for MEG-MRI coregistration and head localisation. Following this, the challenges faced in MEG are outlined and discussed in the context of the signal we can detect. Finally, different approaches to solving the inverse problem are outlined. This includes a brief description of common source localisation techniques featured in this thesis, with a more detailed description of methods that are implemented in the experimental chapters.

2.2 MEG Overview

MEG is a non-invasive technique that measures weak extracranial magnetic fields providing sub-millisecond measurements of neuronal activity (Hämäläinen et al., 1993). MEG has provided insights into the cortical dynamics of a broad range of functions including language (Salmelin 2007; Cornelissen et al., 2009), vision (Hall et a., 2005; Muthukumaraswamy & Singh, 2009), somatosensory (Worthen et al., 2011) and social processing (Wang et al., 2015). MEG has also been used in the clinical setting to localise epileptiform activity (Fujiware et al., 2012) and to guide the implantation of intracranial electrodes (Agirre-Arrizubieta et al., 2014).

A key advantage of MEG over its electrical counterpart, EEG, is that magnetic fields are less perturbed by biological tissue (e.g. skull, scalp, cerebrospinal fluid) (Barkley, 2004). This allows for less complex forward models to be used in the source localisation of MEG signals (Muthukumaraswamy, 2014). In this thesis whereby paediatric and adult patient data is used, this is important for a number of reasons. Firstly, epilepsy patients that have undergone a craniotomy or burr hole surgery present with additional skull inhomogeneities causing further distortions to the EEG signal (Flemming et al., 2005). Secondly, the computation of head models for children with central nervous system pathology (e.g. epilepsy) may also be complicated due

to variations in skull thickness and anisotropic tissue (Lew et al., 2013). MEG is not immune from the inaccurate modelling of head tissue, however studies have shown that this only weakly affects MEG inverse solutions (Hämäläinen and Sarvas, 1987;1989).

A practical advantage of MEG relative to EEG is that it allows patients to be assessed without the need for skin abrasion or the application of many electrodes. This facilitates patient compliance and can reduce the setup time required before a measurement can begin (Witton et al., 2014). It can also be argued that MEG is a friendlier environment compared to other techniques that require patient cooperation for extended periods of time. To further increase patient comfort, the ABC has recently installed a new hydraulic MEG chair to optimise the patient's head and body position. This enables further comfort and allows more effective sensor array coverage. This is particularly useful for paediatric patients that are referred to the ABC for presurgical evaluation.

2.3 MEG Signal and Instrumentation

Before discussing topics directly relevant to the methods used in this thesis, a brief overview of the MEG signal and hardware is given to establish what is being measured and how it is being measured.

2.3.1 The MEG Signal

The MEG signal is thought to originate from the apical dendrites of pyramidal neurons as a result of postsynaptic potentials (PSPs) (Hämäläinen et al., 1993). An excitatory PSP (EPSP) occurs when an action potential propagates along the axon reaching the synaptic terminal leading to an influx of calcium (Ca++) and causing the release of the excitatory neurotransmitter glutamate (Glu). The released Glu then diffuses through the synaptic cleft and attaches to receptors located on the postsynaptic cell. This causes an influx of sodium ions (Na+) into the postsynaptic membrane by increasing its permeability to this ion. Once a certain threshold is reached, the cell depolarises causing a primary current to travel down the dendrite. A key feature of pyramidal neurons is that they are relatively large with dendrites arranged parallel to one another and oriented perpendicular to the cortical surface (Ahonen et al., 1993). This facilitates current flow that is also perpendicular to the cortical surface producing magnetic fields that can be detected extracranially by the MEG sensors (Hämäläinen

et al., 1993). Generally, it is assumed that only primary currents are detectable in MEG but research has suggested that secondary volume currents in extracellular space may also contribute to the signal (Uitert et al., 2003).

Action potentials along the axon are unlikely to contribute to the observable MEG signal as they consist of two opposing dipoles producing a quadropular field. This field decreases with a distance ($1/r^3$) much faster than a dipolar field ($1/r^2$) (Hämäläinen et al., 1993). Another key difference between action potentials and PSPs is the temporal summation that occurs due to PSPs lasting for 10ms relative to an action potential lasting 1ms. This temporal summation is critical as neuronal currents generate very weak magnetic fields (10^{-13} Tesla) and it is estimated that 50,000-100,000 synchronous currents are required to generate a measurable MEG signal (Okada, 1983). Therefore, the decrease in field propagation coupled with the lack of temporal summation in action potentials makes measurable synchronised firing unlikely.

2.3.2 SQUIDS

The magnetic field generated by the human brain is extremely small, far smaller than the earth's magnetic signal and other physiological signals. Superconducting quantum interference devices (SQUIDs) allow the measurement of weak neuromagnetic fields (10^{-13} T) in the presence of strong environmental noise (Hämäläinen et al., 1993). SQUIDs are superconducting loops containing Josephson junctions that convert magnetic flux into voltage. Superconductivity is achieved by immersing the SQUIDs in liquid helium (4.2K). Modern MEG systems often use SQUIDs that are approximately 0.1mm in size and therefore require additional pick-up coils to increase their detection capability. Due to the magnetic field sensitivity of the SQUID, these pick-up coils also act as a flux-transforming device before flux is transferred to the SQUID.

2.3.4 Pickup coils

In modern MEG systems, such as the systems used in this thesis, there are tree types of pickups coils that are used to form the sensor array: (1) Magnetometers, (2) axial first-order gradiometers, and (3) planar first-order gradiometers (see Figure 2). Magnetometers consist of a single pickup coil and are sensitive to both deep and superficial sources but with the limitation of being more sensitive to noise. First-order gradiometers have a counter wound compensation coil that measures the gradient of the magnetic field to eliminate large homogenous signals (Vrba, 1997). Axial first-order gradiometers are arranged on top of one another in the vertical plane whereas planar gradiometers are arranged on the same horizontal plane.

Figure 2.1. A schematic of pickup coils used in modern MEG systems: (a) Magnetometer, (b) Axial first-order gradiometer, and (c) Planar first-order gradiometer. Taken from Lee & Kim (2014).

2.3.5 Elekta Neuromag System

The Elekta Neuromag (Elekta Neuromag, Oy) is the current system used at the Aston Wellcome Laboratory for MEG studies. This system has a sensor array consisting of 102 magnetometers and 204 planar gradiometers, and is housed in a magnetically shielded room (MSR). The Elekta system largely relies on the vendor provided Maxfilter software as a means of interference suppression. Maxfilter applies signal space separation (SSS) by resolving the measured data into components arising within and external to the sensor array (Taulu & Kajola, 2005). In order to reject interfering sources from within the helmet (e.g. dental artefacts), the temporal extension of SSS can be applied (tSSS). This involves applying a statistical method

to determine whether the compartmented signals are temporally correlated and if so, removed from the data (Taula and Simola, 2006). The use of tSSS and its implications are discussed further in Chapter 3.

2.3.6 CTF 275 System

MEG data used in this thesis was also collected on the previous Aston CTF MEG system (MISL, CTF). This system had a sensor array consisting of 275 axial gradiometers and was housed in an MSR. Third order noise cancellation was applied online to remove interfering magnetic signals from the data. This is achieved by calculating the field at each coil in the sensor and in a set of reference channels. The fields measured at the reference channels are then subtracted from the MEG sensors by multiplying them by a set of data-driven weights.

2.3.7 Head Movement

For the Elekta measurements, 5 head position indicator (HPI) coils were attached to the participant's head. Continuous HPI coil measurement was applied during acquisition in order to measure head movement across the duration of the scan. During HPI monitoring, continuous sinusoidal signals (290-320Hz) are emitted from the HPI coils whereby a minimum of 3 coils are required by the software to exceed the goodness-of-fit limit. Head movement is determined and can be compensated for by applying the motion correction algorithm in the Maxfilter software. Movement compensation is an extension of the signal separation method (SSS). In movement compensation, the harmonic amplitudes from the continuous HPI recordings are calculated and then the movement of the subject is modelled as movement of the sensor array. Signals are then calculated in a virtual array, which are locked to the participant's head. The output of motion correction must be inspected carefully to ensure the algorithm has produced a reasonable output. For example, in instances whereby the participant has rapidly moved their head, the algorithm is unable to compensate for the movement and can introduce a spurious artifact.

In this thesis, motion correction was applied to the healthy control data to determine the amount of head movement but only temporal SSS (tSSS) filtered data was used for data analysis in Chapter 3 & 4 (the rationale for this is outlined in the chapter). In these datasets participants with head movement exceeding 5mm were not further analysed. Clinical data used in Chapter 5 from the VU Medical Center (Amsterdam, Netherlands) were not motion corrected to stay in concordance with their clinical

preprocessing protocol. However, clinical data in Chapter 6 & 7 were motion corrected to stay in line with the ABC clinical protocols.

For the CTF data included in chapter 6 & 7, head localisation was performed in a similar manner by attaching three coils to the patient's head. Head localisation was monitored continuously throughout the recording and a warning message appeared if movement exceeded 5mm. Motion correction software is not available in the CTF platform therefore these measurements were not further analysed if movement exceeded 5mm.

2.3.8 Coregistration

At the ABC, MEG coregistration is performed using a T1-weighted structural MRI of the participant. In data acquired from both MEG systems, an outline of the scalp and the position of three fiducial landmarks (nasion, left- and right-preauricular) are digitised using a 3D digitiser (Fastrak, Polhemus, Colchester, VT, USA). The digital headshape and landmarks are then aligned with the MRI extracted head surface using an iterative least squares surface-matching algorithm (Adjamian et al. 2004). For this method to be effective, distinctive landmarks including the nose, eyebrows and inion must be captured during head digitisation. In each recording, approximately 300-400 points are acquired to form the digital head shape. It has been estimated that a 4mm error can be incurred during this coregistration procedure (Whelan et al., 2008).

2.4 Challenges in MEG

2.4.1 Radial Sources

One challenge often discussed in MEG analysis is the issue of radial sources (e.g. the apex of a cortical gyrus). MEG mainly measures tangential sources (e.g. sulcal walls) that are parallel to the scalp as the resulting magnetic field can be measured by the tangentially positioned MEG sensors. This insensitivity to radial sources also has implications for the detectability of deep sources, as dipoles closer to the centre of the head tend to be radially oriented.

Using a gradiometer array, Hillebrand and Barnes (2002) investigated signal detectability and demonstrated that sources within a 15° radial limit were considered

invisible. Based on neuroanatomical information, the authors determined that these invisible sources comprise of thin strips of cortex (2mm wide) present on the gyri crown and only account for 5% of neocortical areas. This suggests that although MEG is not sensitive to truly radial sources, this limitation is confined to a small percentage of the neocortex when using a single sphere forward model. However, more recent research has argued that these invisible sources are partially mediated by the use of a single-spheres forward model and that there are no truly radial sources (to all sensors) when using a multi-spheres forward model (Johnson et al., 2011). Therefore, the use of a multi-spheres forward model may assist in overcoming the challenge of localising radial sources (see section 2.5.1 for further information on forward modelling).

2.4.2 Deep Sources

Another important conclusion of the Hillebrand & Barnes (2002) study was that source depth, not orientation, was the main factor that detrimentally affected MEG sensitivity. This can be explained by Biot and Savart's law that states a dipolar magnetic field falls off to the square of the distance from the current source ($1/r^2$). This conclusion is concordant with Johnson et al. (2011) who reported that deeper sources were less accurately reconstructed when oriented radially. Therefore, careful consideration must be taken when attempting to localise deep structures and this may affect the sources of interest in this thesis (e.g. in cases of mesial temporal lobe epilepsy).

2.4.3 Spatial Resolution

Despite the spatial resolution of MEG typically being superior to that of EEG (Barkley et al., 2003), it is well known that fMRI offers a higher spatial resolution allowing the accurate mapping of anatomical areas (Belliveau et al., 1991; Kwong et al., 1992; Stam et al., 2007). This advantage however is confounded by the indirect nature and slow response latency of the heamodynamic response (Liu et al., 2006). Therefore, the rationale for using MEG is that it can measure rapid neurophysiological changes (Liu et al., 2006) providing a relatively good spatiotemporal assessment of the patient's ongoing neural activity. It has been reported that under favourable circumstances, MEG can localise sources with a 2-3mm accuracy (Hämäläinen et al., 1993). However, this is dependent on a number of factors including noise in the recording, source strength and the sensor configuration used (Hari et al., 1998).

2.5 Source localisation

With the aforementioned challenges in mind, a common goal faced in MEG is the estimation of neuronal sources that underlie the MEG signal. Source estimation is not straightforward and has resulted in different MEG laboratories adopting different methods. This section will discuss the forward and inverse problem before describing commonly used source inversion methods that are referred to throughout this thesis.

2.5.1 The Forward Problem

The forward problem is a mathematically well-posed problem and states that given a known source in the brain we can compute the electromagnetic distribution observed outside the head. This is based on the Biot-Savart Law that dictates the magnetic field generated by an electrical current (Mosher et al., 1997; Mosher et al., 1999). To solve the forward problem, two approximations are required; the current dipole and volume conductor approximation. A neuronal source is typically modelled as a current dipole (Okada, 1982) and can be considered as a layer of current dipoles generated by a large group of dendritic currents.

In MEG it is sufficient to use a single sphere as a volume conductor model unlike EEG whereby the conductivity of different head tissue needs to be modelled more precisely (e.g. using three-shell models based on the cranial volume, skull and scalp: Hämäläinen and Saravas, 1989). Sphere models can be dissected into three main categories: single sphere, locally optimal sphere and local sphere models (Huang et al., 1999).

In clinical MEG the ACMEGS guidelines advocate the use of a single sphere model (Bagic et al., 2011). However, there may be limitations when using a single sphere if the source is unknown or distributed. This may be a result of a sub-optimal sphere fit due to error incurred based on the geometry of the head. For example, Stenroos et al. (2014) suggested that with a single sphere model, areas close to the central sulcus are likely to be represented well by the model but anterior frontal and posterior occipital regions maybe missed. Therefore, it can be argued that a multi-spheres forward model can overcome these limitations to provide a model that takes into account all sources in the head. As previously mentioned in section 2.4.1, a multiple-spheres model may also provide better sensitivity to detect radially oriented sources (Johnson et al., 2011).

Realistic head modelling may also be used to overcome limitations associated with a single sphere approach. Realistic head models include the boundary element model (BEM) (Fuchs, et al. 2002) and corrected-sphere model (Nolte, 2003). The corrected sphere model introduced by Nolte (2003) operates by fitting a single sphere to the cranial volume. This sphere is then corrected by the harmonic function based on the geometry of the volume that is derived from the single-shell model.

In this thesis a number of forward models are used based on the analysis software and clinical protocols used and are stated in the relevant method sections.

2.5.2 Leadfields

Once an appropriate head model has been computed, a source space grid containing all leadfields for each grid point can be calculated. Leadfields refer to the forward model at each grid point and consist of three numbers specifying how the current in that voxel (x, y and z orientations) produce a magnetic field measured at sensor *i*. There is a set of leadfields for each location in the grid and for each sensor. The leadfield for grid point *k* and sensor *i*, can be represented as L_{ik}:

$$\left[l_{ikx}\ l_{iky}\ l_{ikz}\right] \tag{2.1}$$

Leadfields for the whole head are represented as a matrix *L*, in order to specify the scaling and additions for all sensors around the head.

2.5.3 The Inverse Problem

The inverse problem refers to estimating the underlying current distribution from the MEG data. Unlike the forward problem, the inverse problem is mathematically ill-posed as there are an infinite number of source solutions that can explain the measured signal (Larson et al., 2014). An inverse solution is derived from the signals measured on the scalp, the sensor configuration, the head and source model used.

The magnetic field observed around the head is the sum of the fields produced by all sources within the brain (with the addition of noise). To illustrate the inverse problem, consider this equation:

$$B = LQ \tag{2.2}$$

Where *B* is a matrix containing the magnetic field measured by *M* sensors across *N* time samples, *L* is the leadfield matrix and *Q* is the underlying neuronal source. A simple working example of this would be to consider a four channel MEG system with 2 underlying dipoles generating an observed magnetic field *B* at time point N:

$$\begin{bmatrix} b_{1n} \\ b_{2n} \\ b_{3n} \\ b_{4n} \end{bmatrix} = \begin{bmatrix} l_{11} & l_{12} & l_{13} \\ l_{21} & l_{22} & l_{23} \\ \vdots & \vdots & \vdots \\ l_{41} & l_{42} & l_{43} \end{bmatrix} \begin{bmatrix} q_{1} \\ q_{2} \end{bmatrix} \tag{2.3}$$

We know *B* from our sensor data and can calculate *L* from theory, however we need to estimate *Q*. It is the estimation of *Q* that is referred to as the inverse problem.

Most inverse solutions can be seen as a weighted sum of sensor measurements and are mathematically very similar (Hillebrand et al., 2005). Hillebrand et al. (2005) suggests that the difference between linear inverse solutions are the assumptions that the methods impose on the shape of the source covariance matrix. Figure 2.2 demonstrates how each of these solutions are different cases of covariance component estimation formulated on different assumptions and optimisation rules (Nagarajan & Sekihara, 2014).

Figure 2.2. Schematics of the source covariance matrices for 4 different inversion algorithms: Weighted minimum norm, LORETA, Dynamic SPM and SAM. Taken from Hillebrand et al. (2005).

2.5.4 Source inversion methods

Many of the traditional source inversion techniques are suitable for studying the evoked response which refers to the short lasting (~100ms) neuronal responses that are both time- and phase-locked to the stimulus (see Figure 8). In order to extract the evoked response, data is often averaged to increase its signal to noise ratio (SNR) (Schimmel, 1967). Non-phase locked activity or induced activity, is lost in this averaging process but has been shown to be integral in cognition (Singh et al., 2002; Wang et al., 2016). In order to localise induced activity, beamformer-based source solutions have been developed to study increases and decreases in power across time points of interest (Hillebrand et al., 2005).

Figure 2.3. The difference between evoked and induced responses (adapted from Adjamian, 2014). The traces in the left column represents the evoked response and shows phase locking indicated by the grey vertical line. Traces in the right column represent induced activity consisting of ongoing oscillations that are not phase locked to the stimulus. When averaged (bottom row), only the phase-locked activity remains.

A brief overview of the inverse solutions that are referred to and used throughout this thesis will now be given.

2.5.4.1 Equivalent Current Dipole Fitting

Equivalent Current Dipole (ECD) fitting is widely used in localising evoked responses (Okada et al., 1984; Meunier et al., 2003) and is advocated by the ACMEGS for modeling interictal spikes (Bagic et al., 2011). The ECD algorithm estimates the direction, strength and orientation of the dipole in order to minimise the residual variance between measured and predicted field patterns using a least squares approach (Scherg, 1985).

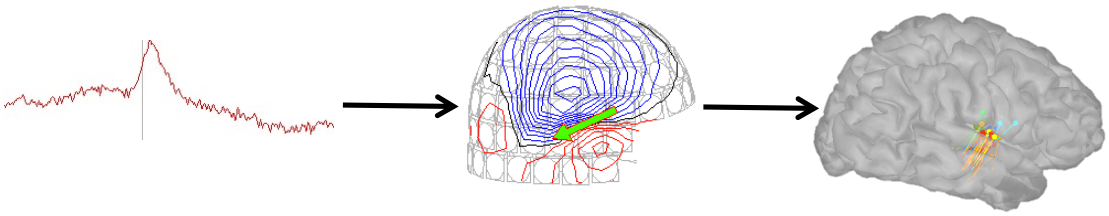

Figure 2.4. An interictal spike from a single sensor is marked (left) and modelled using the Xfit dipole algorithm (middle). These dipoles can then be represented onto the subject's anatomical MRI (right).

In Chapter 5, moving dipoles were implemented to model inerictal spikes iteratively in time using the Elekta Neuromag Xfit software (Elekta Neuromag Oy, Helsinki, Finland). This included fitting a dipole at each time sample from the ascending limb of the spike to the peak of the spike. The quality of the dipole fit was evaluated using a goodness-of-fit (GOF) measure:

$$g = 100 * \left(1 - \frac{(\mathbf{b}-\hat{\mathbf{b}})^{\mathrm{T}}(\mathbf{b}-\hat{\mathbf{b}})}{\mathbf{b}^{\mathbf{T}}\mathbf{b}}\right) \qquad (2.4)$$

Where $\mathbf{b}$ and $\hat{\mathbf{b}}$ are vectors that consist of the measured and modelled magnetic fields, respectively.

Despite performing well when the source is expected to be focal, the assumption that a small number of ECDs can explain the measured topography presents problems when multiple distributed sources are active. To account for multiple sources, multiple

dipole models can be implemented. This requires multiple dipole starting locations and a priori knowledge regarding the location and extent of the sources.

2.5.4.2 Multiple Signal Classification (MUSIC)

The MUSIC algorithm (Schmidt, 1986) can be used to localise multiple asynchronous dipolar sources. This inversion method assumes that the signal and noise components within the data are orthogonal and can therefore be partitioned into separate subspaces. The MUSIC algorithm uses a single dipole to scan through a three-dimensional source grid and projects the forward model for each position against a signal subspace generated from the data. Dipole locations are estimated based on the source space locations that yield the best projections onto the computed signal subspace. The user is then required to manually determine the source by searching for multiple local peaks in the head volume (Mosher & Leahy, 1998). This manual search is subjective and time consuming however further modifications (e.g. recursive-MUSIC) allows for the automatic extraction of sources (Mosher & Leady, 1999). The sensitivity of classifying signal and noise components into different signal subspaces is crucial to the performance of this method and (like most techniques) careful consideration to data quality must be given.

2.5.4.3 Minimum Norm Estimation (MNE)

MNE is a non-adaptive spatial filtering approach and is used in the localisation of evoked responses and their wide-spread activation across time (Hämäläinen & Ilmoniemi, 1994). The MNE procedure localises the underlying current distribution by applying a distributed source model in which 3-dimensional current dipoles are fixed to each location. The inverse solution is determined by varying the amplitude parameter of the dipoles to recover a source distribution where the predicted data is consistent to the measured data whilst searching for a solution that yields minimal overall energy.

2.5.4.4 Low Resolution Electromagnetic Tomography (LORETA)

A limitation of MNE is that it is prone to a superficial bias and has been criticised for mislocalising deep sources onto the cortical surface (Pascual-Marqui, 2002). LORETA takes the current density estimate provided by MNE and standardises it by the variance of each estimated dipole source (Pascual-Marqui, 1994). This standardisation acts as a depth weighting mechanism to counteract the superficial

bias of the minimum norm solution. LORETA has been subjected to various modifications including sLORETA which uses a different standardisation method to counteract the superficial cortical bias (Pascual-Marqui, 2002).

2.5.4.5 Beamformers

Beamformers have been used frequently at the ABC for a number of years and are used throughout this thesis. The rationale for using a beamformer is that it can localise induced changes in cortical oscillatory power (Pfurtscheller and Lopes da Silva, 1999) and provide virtual electrode time series that can be subjected to further analysis (Hillebrand and Barnes, 2005). These features are important for the analysis of oscillations in relation to cognitive tasks and also when interrogating the source time series with metrics to localise epileptiform activity (Chapters 5, 6 & 7).

A key advantage of the beamformer is that multiple sources can be reconstructed independently without requiring *a priori* knowledge regarding the number and location of active sources (Vrba & Robinson, 2001; Hillebrand et al., 2005). Further, the spatial filtering properties of the beamformer have shown to attenuate sources of magnetic noise (e.g. EMG, ECG, EOG) (Brookes et al., 2005; Litvak et al., 2011), increasing the signal to noise ratio (SNR) of the signal (Adjamian et al., 2009). It has been demonstrated that physiological interfering signals can be localised to their sources using a beamformer (Furlong et al., 2004; Muthukumaraswamy, 2013).

Figure 2.5. Beamformer results for the active phase of a tongue thrust. The EMG resulting from the tongue itself produced significant activation in the 25- to 40-Hz bands. This activity is localised external to brain tissue to the tongue region positioned under the glass brain. Taken from Furlong et al. (2004).

The fundamental difference between beamformers and other source inversion methods is that they do not attempt to explain the whole of the measured magnetic field, instead they reconstruct the contribution of each brain position to the measured field. The main assumption in beamforming is that sources are not temporally correlated.

In order to estimate the location and strength of neuronal activity at each location and orientation in source space, $\mathbf{Q}_{kd}$, beamformer weights, $\mathbf{W}_{kd}^{\mathbf{T}}$, must be applied to the measured signal over time, **B**(t):

$$\mathbf{Q}_{kd} = \mathbf{C}_{\mathrm{j}}\, \mathbf{L}^{\mathbf{T}} \mathbf{C}_{\mathbf{b}}^{-\mathbf{1}}\, \mathbf{B} = \mathbf{W}_{kd}^{\mathbf{T}}\, \mathbf{B} \qquad (2.5)$$

Where $\mathbf{C}_{\mathrm{j}}$ is the source covariance matrix, **L** is the lead field vector and $\mathbf{C}_{\mathrm{b}}$ is the data covariance matrix. The data covariance matrix, $\mathbf{C}_{\mathrm{b}}$, contains information from all the sensors in the system configuration. The diagonal entries of the matrix contain information regarding the spatial distribution of signal and noise power within sensor space. The off-diagonal entries represent the spatial correlations between the sensors. The source covariance matrix, $\mathbf{C}_{\mathrm{j}}$ is not known and must be estimated from the lead field vectors and the data covariance matrix allowing us to calculate weights for each individual location:

$$\mathbf{C}_{\mathbf{j}} = (\mathbf{L}_{kd}^{T}\, \mathbf{C}_{\mathbf{b}}^{-1}\, \mathbf{L}_{\boldsymbol{\theta}})^{-\mathbf{1}} \qquad (2.6)$$

Synthetic aperture magnetometry (SAM) is a scalar beamformer that optimises for power by iteratively searching for the dipole orientation that gives the optimal SNR. This is achieved by computing the pseudo-Z deviate at each source point (Robinson & Vrba, 1999). This pseudo-Z statistic is computed based on the source power *P,* and the noise power, *n*:

$$Z = \sqrt{\frac{P}{n}} \qquad (2.7)$$

2.5.4.6 Vector Beamformers

Vector beamformers operate in a similar way to scalar beamformers however there is no fixed orientation based on power optimisation (Van Veen et al., 1997). Therefore, the forward model and weights are 3-dimensional for each source position, Q:

$$q = \begin{pmatrix} q_x \\ q_y \\ q_z \end{pmatrix} \quad (2.8)$$

Throughout this thesis scalar beamformers are used based on its extensive use previously in the ABC. However, optimising the spatial filter orientation for power may not always be the optimal method and the use of a vector beamformer may have advantages in accurately characterising signals that have a predominantly radial representation (Johnson et al., 2011; Prendergast et al., 2013).

2.6 Statistical Analysis

2.6.1 Single Subject Statistics

Functional mapping of healthy control and patient data included in this thesis (Chapter 3 and 4) were subjected to statistics implemented in the Fieldtrip software (Oostenveld et al. 2011). Non-parametric testing for a number of inverse solutions has been implemented in the literature including minimum variance beamformers (Singh et al., 2003), MNE (Pantazis et al., 2005) and within the Fieldtrip software (Maris & Oostenveld, 2007). In this thesis, cluster-based nonparametric randomisation testing as described by Maris & Oostenveld (2007) was applied using the Fieldtrip software (Oostenveld et al., 2011). This non-parametric framework allows great flexibility with freedom to choose any test statistic (i.e. *t-, F-,* etc.) and does not hold the same assumptions as parametric methods (e.g. normally distributed data).

Briefly, this method involves randomising the single trial source space data (i.e. baseline and active) across two partitions and computing a dependent-samples *t* value between them. Samples that exceed <0.05 are then clustered based on spatial adjacency (i.e. grid points). The cluster-level statistics are then calculated by taking the sum of the *t* values within a cluster. The cluster with the maximum statistic is used as the test statistic. The data is randomised 1000 times across the two partitions and the test statistic is calculated each time. The resulting test statistics form a reference distribution. The proportion of random partitions that resulted in a larger test statistic than the observed statistic is the Monte Carlo significance probability (i.e. *p*-value).

2.7 Virtual Electrodes Analysis

Virtual electrode (VE) analysis was conducted by multiplying the MEG signal with the spatial filter for a given region of interest to reconstruct the electrical density series at that location across time (Singh et al., 2002; Barnes & Hillebrand, 2003).

2.8 VE Time-Frequency analysis

In the experimental chapters of this thesis, time-frequency analysis was carried out using the Fieldtrip software platform (Oostenveld et al., 2011). Time-frequency analysis was implemented using a multitaper time-frequency decomposition based on multiplication in the frequency domain. Wavelets are created with 1 wavelet per frequency and the length parameter is defined based on the frequency of interest. The wavelet is tapered (discrete prolate spheroidal sequences) and the fast-fourier-transform (FFT) is computed on the raw data and the wavelet. These two are then multiplied with each other across each frequency. The inverse Fourier transform is then calculated on this output. To ensure a reliable estimate of the frequency power within a time window, at least 3 cycles of the frequency of interest was used.

2.9 Conclusion

The purpose of this chapter was to introduce the reader to the methods that are frequently referred to in this thesis and to provide fundamental background knowledge to the signal that is being recorded using MEG.

Chapter 3: Functional Brain Mapping

3.1 Introduction

The Aston MEG laboratory has typically used Elekta software to perform source analysis for the localisation of eloquent cortex. This software is particularly good for visualising sensor data, performing averages and modelling dipoles in the Xfit program. There is a good level of confidence in the spikiness (Foley et al., 2012; Hall et al., 2017, in review) and event-related beamformer, however in unpublished data from the ABC, mislocalisations have frequently been reported when using the Elekta dual state beamformer. This has included the mislocalisation of various somatosensory stimulations (median nerve, single digit), physiological artefacts (similar method to Furlong et al., 2004), and expressive language areas (similar method to Fisher et al., 2008). The dual-state beamformer allows the comparison between two brain states and is therefore important for functional brain mapping in patients.

This chapter aims to describe and test an alternative source analysis pipeline using the Fieldtrip toolbox (Oostenveld et al., 2011). Secondly, the effects of tSSS filtering and MEG sensor selection (gradiometers, magnetometers, or combined) on the beamformer analysis will be explored. The conclusions drawn in this chapter will inform the subsequent analysis in Chapter 4 with the aim of establishing a pipeline that can be used for the lateralisation of language in epilepsy patients. This section will first discuss issues relating to the analysis of Elekta data (tSSS and combining sensors), and will state the specific aims of the study followed by a brief explanation of the MEG paradigm used.

3.1.1 Temporal Signal Source Separation

Signal Source Separation (SSS) (Taula and Jajola, 2005) divides the measured MEG signal into two partitions: signals coming from sources outside of the sensor array and signals generated from within the sensor array. Residual signal may remain after SSS, which cannot be exclusively modelled into either partition. This leads to temporally correlated signals between the two SSS-reconstructed partitions. Temporal SSS (tSSS) aims to solve this by removing correlated waveforms that appear in both parts of the SSS-reconstructed data by means of orthogonal projection (Taula and Simola, 2006). A correlation limit (CL) to quantify the degree of synchrony

between the magnetic signals is used to determine which signals should be removed. Typically, clinical laboratories have adopted a 0.9 CL (Wang et al., 2013; Hillebrand et al., 2013; Nevalainen et al., 2012). The CL of 0.9 is also implemented throughout this thesis.

The rationale for using tSSS is based on the noise reduction properties that it provides (see Figure 3.1) and literature suggesting that it is a necessary pre-processing step for the beamformer analysis of Elekta data (Hillebrand et al., 2013). Hillebrand et al. (2013) demonstrated that tSSS filtering is crucial when attempting to accurately localise somatosensory evoked fields (SEFs) and hand movements. The results demonstrated that raw Elekta data (no tSSS) can lead to errors larger than 1cm, or even complete mislocalisation. The authors state that the noise reduction properties of tSSS outweigh the caveat posed by tSSS in that it reduces the degrees-of-freedom within the data.

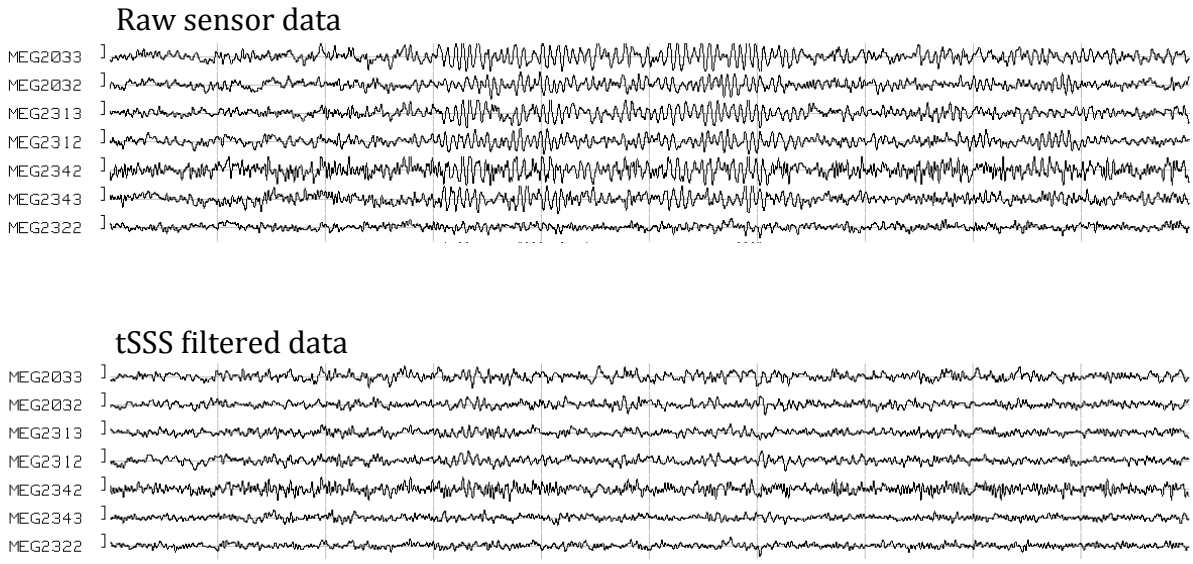

Figure 3.1. Raw (top) and tSSS filtered (bottom) data of the same participant across the same 10 second time window.

After applying tSSS using Maxfilter software (Elekta Neuromag, Oy), MEG data is typically left with an approximate rank of 68 (i.e. 68 non-zero eigenvalues). In general terms, rank deficiency refers to a lack of data to accurately estimate the desired model. This may arise in MEG from using too few trials, narrow frequency bands or small time windows (Woolrich et al., 2011). In the context of tSSS, rank deficiency

may occur due to the removal of components within the data, particularly in datasets contaminated by large artefacts. This may lead to a lack of sufficient data to accurately estimate the beamformer covariance matrix leading to poor source reconstructions (Woolrich et al., 2011).

To integrate the use of rank reduced data, Elekta have developed an SSS-beamformer that combines both tSSS and beamforming (Vrba et al., 2010). The SSS-beamformer operates on the time-dependent expansion coefficients of spherical harmonics estimated by tSSS. Vrba et al (2010) stated that the SSS-beamformer allows for computationally more efficient processing and provides equal and in some cases, better spatial resolution relative to conventional beamformers (that operate on the full data covariance matrix). Vrba and colleagues demonstrated in simulated data that the SSS-beamformer can increase the spatial resolution for deeper sources relative to a conventional beamformer. The extent and conditions to which the SSS-beamformer provides better spatial resolution still requires further testing and does not necessarily compensate for rank reduced data. The use of SSS-beamforming would benefit from further testing in open source platforms, however the ability to do so is challenging as the source code is closed[2]. Therefore, this chapter is limited to investigating the source estimates of tSSS filtered data when using a conventional beamformer in Fieldtrip.

In the Fieldtrip documentation, the only reference to compensating for Maxfilter (SSS/tSSS) is by using principal components analysis (PCA) to remove small components that are likely to be poorly conditioned to 'stabilise' the covariance matrix. The documentation suggests using PCA to retain the top 50 components of the data (http://www.fieldtriptoolbox.org/workshop/meg-uk-2015/fieldtrip-beamformer-demo). This approach therefore removes a large number of components from the data causing further rank reduction. In this chapter, the use of 'tSSS-PCA' will be investigated but will use a less aggressive approach by retaining 99% of the variance in the covariance matrix, allowing more degrees of freedom to be retained.

[2] Elekta have recently announced that they will open the source code and share with the open source community. Initial SSS-Beamformer implementations in SPM are currently being developed.

3.1.2 Combining Magnetometers and Gradiometers

The Elekta Neuromag Triux system contains 102 magnetometers and 204 planar gradiometers. A question faced when analysing Elekta data is whether to combine magnetometers and gradiometers or to select only one sensor type for further analysis. The fundamental difference between the two sensor types is that magnetometers measure the magnetic field component perpendicular to the surface of a single pick-up coil, whereas gradiometers measure the magnetic gradient between two counter-wound coils (Mohseni et al., 2012). Magnetometers therefore measure the total magnetic flux in Tesla and gradiometers measure the difference in flux using Tesla per meter (Henson et al., 2009). The difference in scaling and signal to noise ratio (SNR) between these two types of sensors must be considered when combining them for a beamformer analysis. This is supposedly solved in the Elekta software, however limited testing has been carried out in external software platforms.

A recent study using Fieldtrip to analyse Elekta data selected gradiometers for source analysis but did not explain why only gradiometers were selected and whether Maxfilter was used to pre-process the data (Cousijn et al., 2014). The online literature supporting the Fieldtrip toolbox suggests that the software is able to solve the scaling of the forward solution and that source analysis using combined sensors is supported[3]. However, no empirical research has yet aimed to measure the differences in source localisations when using combined sensors versus gradiometers or magnetometers alone.

3.1.3 Aims

Based on the issues raised, the aims of this chapter are to; (1) establish a beamformer pipeline for Elekta data using Fieldtrip, (2) determine the feasibility of using tSSS filtered data in this pipeline (using raw, tSSS, and tSSS-PCA data), and (3) investigate the effects of source localisation using different sensor types (gradiometers, magnetometers and combined sensors). The differences between the various conditions will be summarised and quantified using relevant statistics. These

[3] This was verified by personal communication with Robert Oostenveld (Fieldtrip developer).

differences include the MNI coordinates of the peak source and corresponding source values.

3.1.4 MEG stimulus

In order to select an appropriate paradigm to address the research questions of this chapter, it is necessary to choose a stimulus that elicits a well characterised response. Based on this criterion, a stationary square-wave grating, presented in the lower-left quadrant of the visual field was used[4]. Based on knowledge of the visual system and related MEG studies, it can be hypothesised that the stimulus should yield a peak gamma response in the contralateral occipital cortex (Adjamian et al., 2004; Hall et al., 2005; Muthukumaraswamy & Singh et al., 2008; Muthukumaraswamy & Singh et al., 2013). Presenting the stimulus in only one quadrant relative to all four (i.e. foveal stimulation) is also useful for testing the effects of tSSS in lower SNR conditions, as lower induced gamma responses are reported when using non-foveal stimulation (Swettenham et al., 2009). Furthermore, the psychophysical properties of a stationary, square-wave grating should yield lower amplitude gamma oscillations relative to other types of visual stimuli, such as a moving, annular-grating (Muthukumaraswamy & Singh et al., 2013).

3.1.5 Hypothesis

It is hypothesised that all methods will produce a peak localisation in the right occipital lobe as the visual grating is presented in the lower left quadrant of the visual field. Due to the lack of published data that has used tSSS data for source localisation in Fieldtrip, it is uncertain how tSSS data will perform. As suggested in previous tSSS studies (Hillebrand et al., 2013) it can be argued that the benefits of tSSS (less interfering components) outweigh the caveat of reducing the rank of the data. Furthermore, the use of PCA post tSSS may enable poorly estimated components to be removed and thus improve the source estimate.

[4] This paradigm is the visuomotor task used in the MRC-MEG Partnership normative database.

3.2 Methods

3.2.1 Participants

Data was collected from 18 adult participants (10 female, mean age = 20). All participants had normal vision with no reported history of neurological or psychiatric conditions.

3.2.2 MEG task

A vertical, stationary, maximum contrast, three cycles per degree, square-wave grating subtending a 4° angle in both horizontal and vertical planes was presented in the lower left quadrant of the visual field for 100 trials. The grating was presented for 1.5-2 s (jittered) with an inter-stimulus interval (ITI) of 4 or 8s (50 trials for each ITI). Participants were instructed to maintain fixation on a red dot presented in the centre of the screen and asked to perform a right index finger abduction at the offset of the visual grating. In this study only the visual grating component was analysed. The visual stimulus was programmed in the Psychophysics toolbox for MATLAB (Brainard & Pelli, 1997) and gamma corrected for the presentation monitor used. The stimuli were projected using a Panasonic 3-Chip DLP^{TM} projector, with a screen solution of 1400 x 1050 and 60Hz refresh rate.

Figure 3.2. Visuomotor task. Participants were instructed to fixate on a centrally presented red dot and perform a finger abduction on the grating offset. Only the visual grating component of this task was analysed.

3.2.3 MEG data collection

MEG data was recorded in a magnetically shielded room (VacuumSchmelze GmbH, Hanua, Germany) using a 306-channel Elekta Neuromag Triux (102 magnetometers and 204 planar gradiometers), at a sampling rate of 1000 Hz. Participants were recorded in the 68° upright seated position. In the tSSS and tSSS-PCA conditions, noise reduction was achieved with the Maxfilter software (Elekta Neuromag Oy, version 2.2.10). The temporal extension of signal space (tSSS) was applied using a sliding window of 10 seconds and a subspace correlation limit of 0.9. Bad channels were identified using Xscan (Elekta Neuromag, Oy) and excluded in all analysis conditions. A bipolar EEG channel was used to record electrocardiogram (ECG) and electrooculogram (EOG). Prior to data acquisition 5 head localisation coils were attached to the participants' head and 3 fiducial points were digitised using a polhemus fast-trak digitizer ((Fastrak, Polhemus, Colchester, VT, USA). Additional head points were collected to allow a surface based alignment with the participant's T1-weighted MRI using the method described in Chapter 2. Continuous head position indication was used and a head movement threshold of 6mm was implemented (none of the datasets in this chapter exceeded this threshold).

3.2.4 MEG analysis

MEG data was analysed using the MATLAB toolbox Fieldtrip (Oostenveld et al., 2011). Data was down-sampled offline to 300Hz and epochs were extracted from -2s prestimulus to the grating onset to 2s post-stimulus. Trials containing eye blinks during visual grating presentation and large electromyography (EMG) artefacts were removed via visual inspection. A single shell head model was used (Nolte et al., 2003) and source analysis was computed in MNI standard space using a 5mm source space grid. An LCMV beamformer was computed on bandpass-filtered data (35-75Hz) using a covariance time window from -1.5s to 1.5s post stimulus. Source power was projected through using common beamformer weights computed across the whole covariance window and applied separately for the baseline (-1.2 to 0 s) and active period (0.3 to 1.5 s). Single subject source statistics were computed on the individual's source reconstructed active and baseline trials using non-parametric permutation testing as described in Chapter 2. Cluster-based correction was used to correct for

the multiple comparison problem (alpha level = <.01) (Maris & Oostenveld et al., 2007).

Virtual electrodes were recomputed on the original sampled data (1kHz) at the maximum peak voxel identified by the beamformer analysis (-2s to 2s). Time-frequency analysis was computed between 10-100Hz with a FFT using 3 Slepian multitapers (+/- 8 Hz spectral smoothing) applied to the baseline time window (-2s to 0s) and active time window (0s to 2s). Time-frequency statistics were computed between the two conditions using cluster-based permutation testing (<0.01).

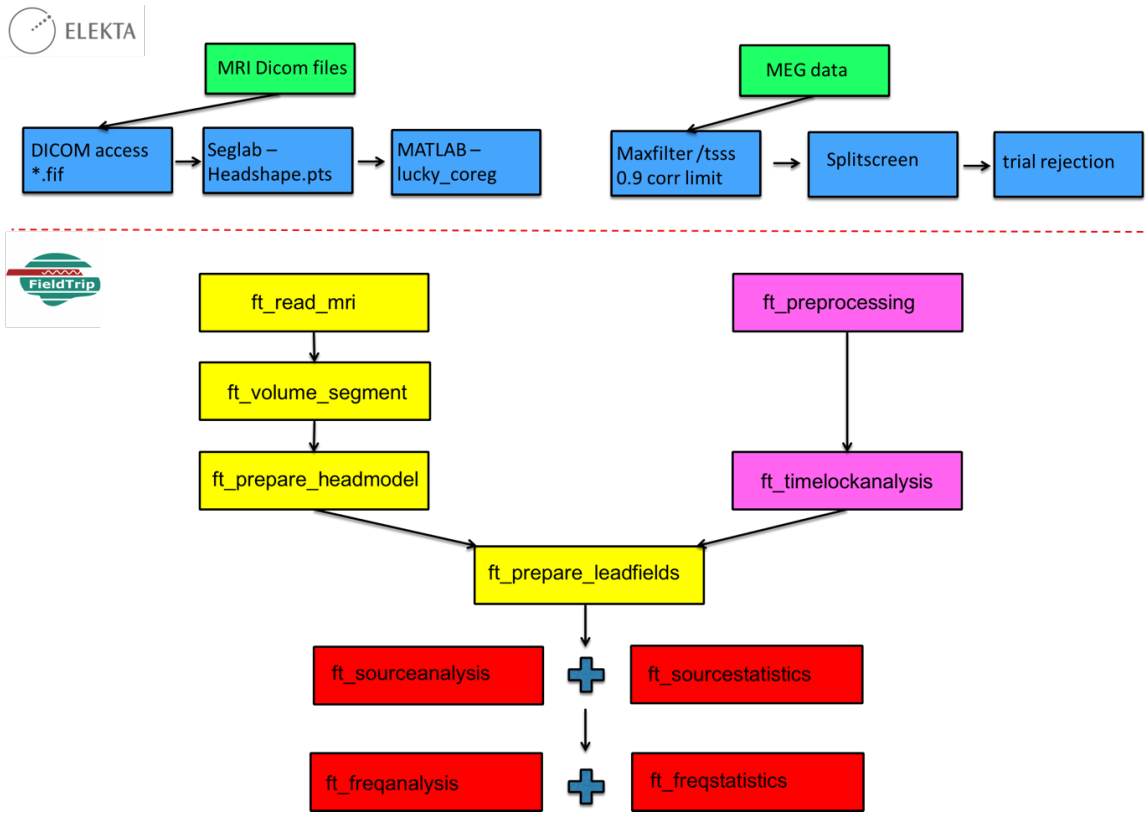

Figure 3.3. The general analysis pipeline and fieldtrip functions used for source analysis in this chapter. The pipeline is split up into 2 sections; the first section involves data pre-processing and MRI coregistration in the Elekta software, the second section is completed in the Fieldtrip toolbox.

3.2.5 Source localisation comparison

The 9 different analysis conditions included; (1) raw gradiometers, (2) raw magnetometers, (3) raw combined sensors, (4) tSSS gradiometers, (5) tSSS magnetometers, (6) tSSS combined sensors, (7) tSSS-PCA gradiometers, (8) tSSS-PCA magnetometers, (9) tSSS-PCA combined sensors. The raw conditions (1,2,3) were not subjected to tSSS, the tSSS conditions (4,5,6) were subjected to tSSS filtering, and the tSSS-PCA conditions (7,8,9) were subjected to tSSS followed by PCA in Fieldtrip to retain 99% of the variability of the data. The PCA process resulted in an average of 4 components being removed for each participant (i.e. leaving an average of 64 components).

3.3 Results

A peak gamma localisation was found in the right occipital cortex in all participants across all conditions, except for one subject in the raw gradiometer (subject 8), raw magnetometer (subject 8), tSSS-PCA gradiometer (subject 6), tSSS-magnetometer (subject 6), and tSSS-PCA combined (subject 6) condition. Figures 3.4–3.6 show plots of the LCMV beamformer gamma band activity (35 – 75Hz, $p<0.01$ cluster corrected) on the right hemisphere for 5 randomly selected participants alongside time frequency representations of the peak virtual electrode ($p<0.01$ cluster corrected) for each analysis condition (see Appendix 1 for beamformer and time-frequency plots for all participants).

Figure 3.4 depicts the raw data results, whereby the source plots indicate larger t-values in the occipital region for the magnetometers and gradiometers conditions relative to the combined sensors condition. The time frequency spectra show a typical response in the magnetometers and gradiometers, consisting of an initial broadband amplitude increase in the gamma frequency band (>40Hz). This is then followed by a sustained increase in gamma power across the time window. The raw combined sensors do not resemble this typical response and show much lower source values in the occipital lobe with diminished gamma power in the time frequency plots. Figure 3.5 shows the source plots and time frequency spectra for the tSSS filtered data. The source values and time frequency spectra are more uniform for the tSSS filtered data, showing a typical gamma band response, but also an initial transient onset response

followed by an alpha/beta power decrease. This initial power increase in alpha/beta is considered a characteristic of the visual evoked response (Muthukumaraswamy et al., 2010). Finally, figure 3.6 represents the tSSS-PCA data, showing a similar pattern of responses to the tSSS filtered data.

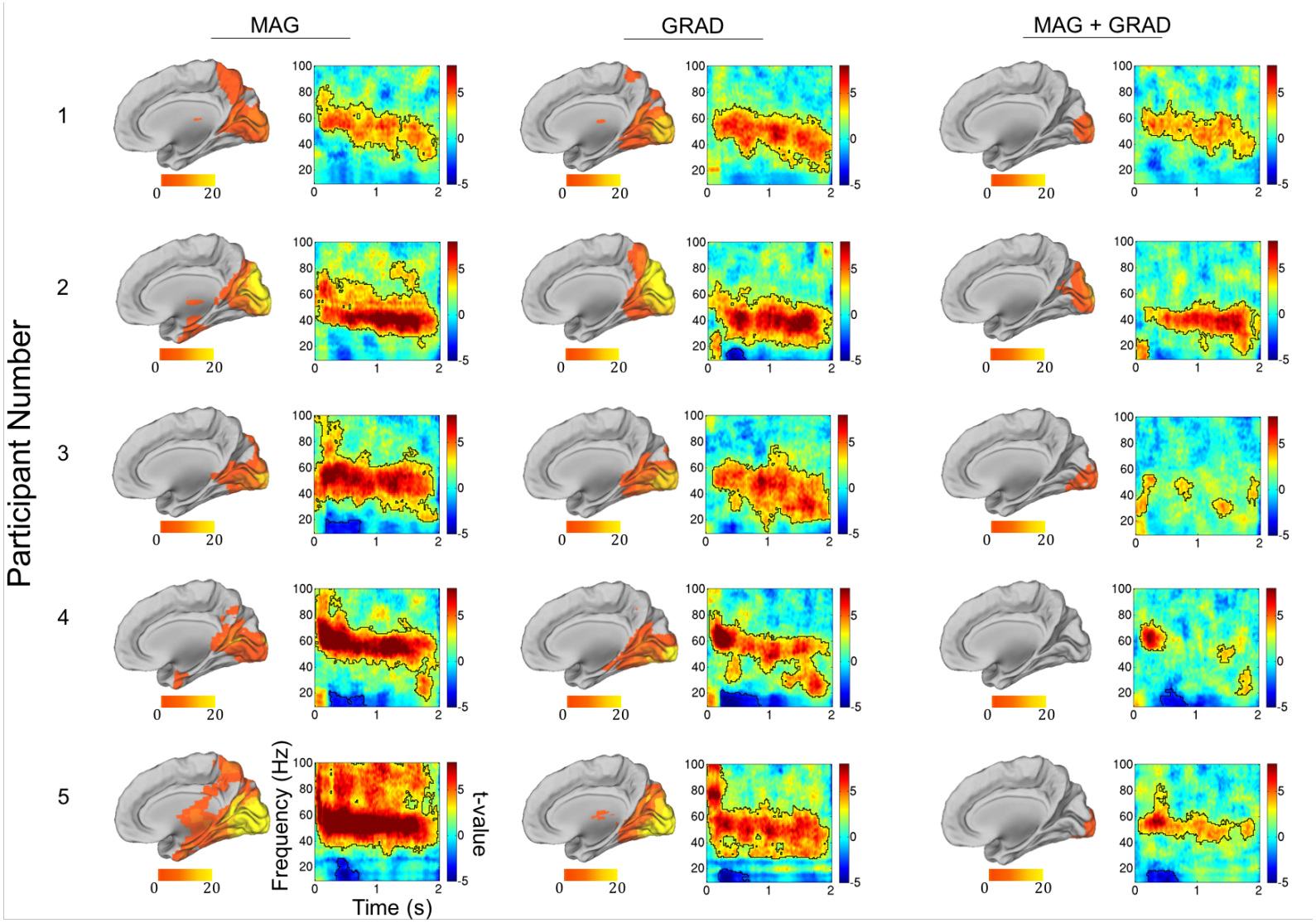

Figure 3.4. LCMV 35-75Hz beamformer results and corresponding peak virtual electrode time-frequency plots for the raw data (10-100Hz). Significant voxels (<0.01) are plotted on the right hemisphere. Significant time-frequency bins (<0.01) are identified by the black outline.

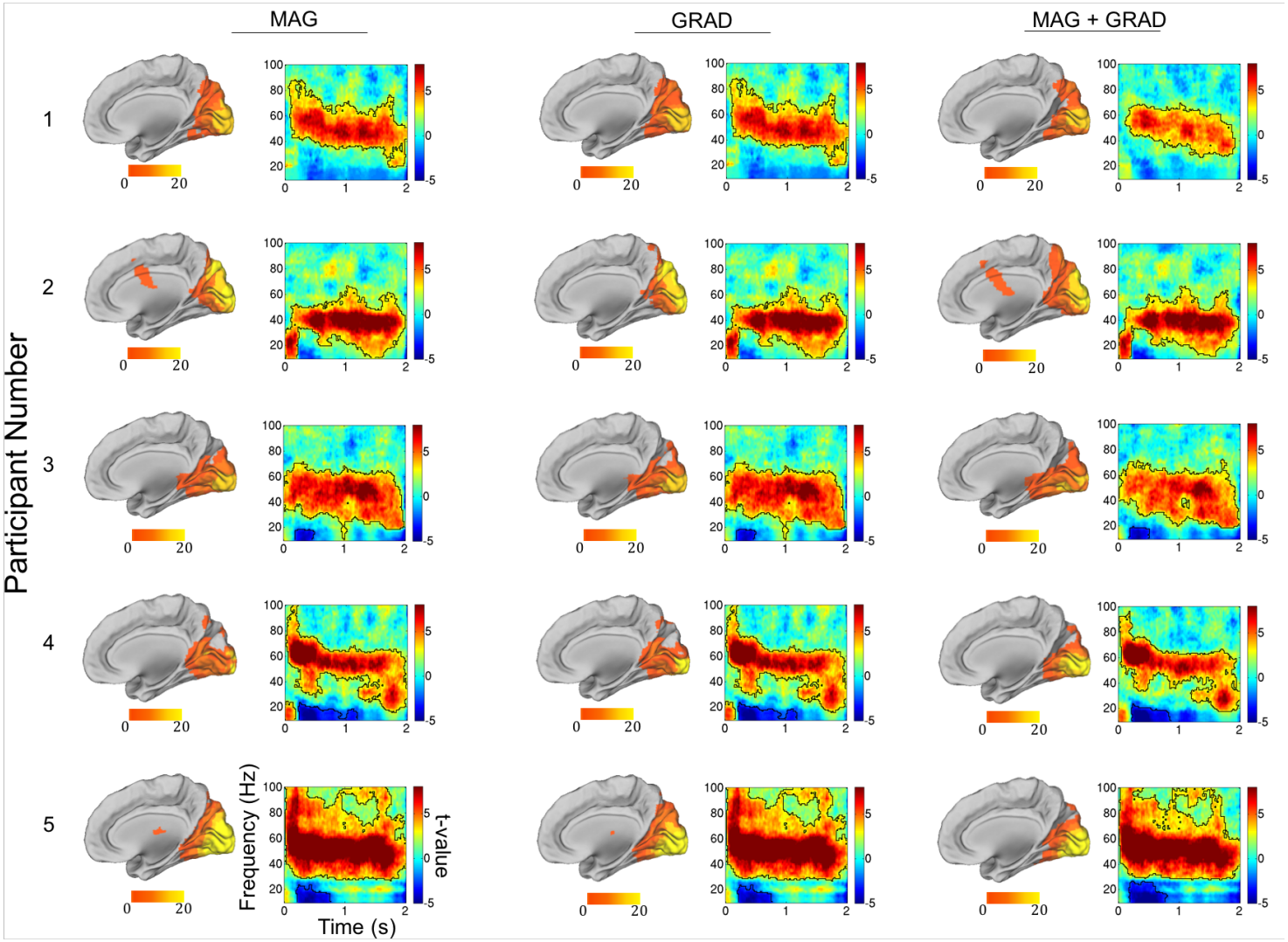

Figure 3.5. LCMV 35-75Hz beamformer results and corresponding peak virtual electrode time-frequency plots for the tSSS filtered data (10-100Hz). Significant voxels (<0.01) are plotted on the right hemisphere. Significant time-frequency bins (<0.01) are identified by the black outline.

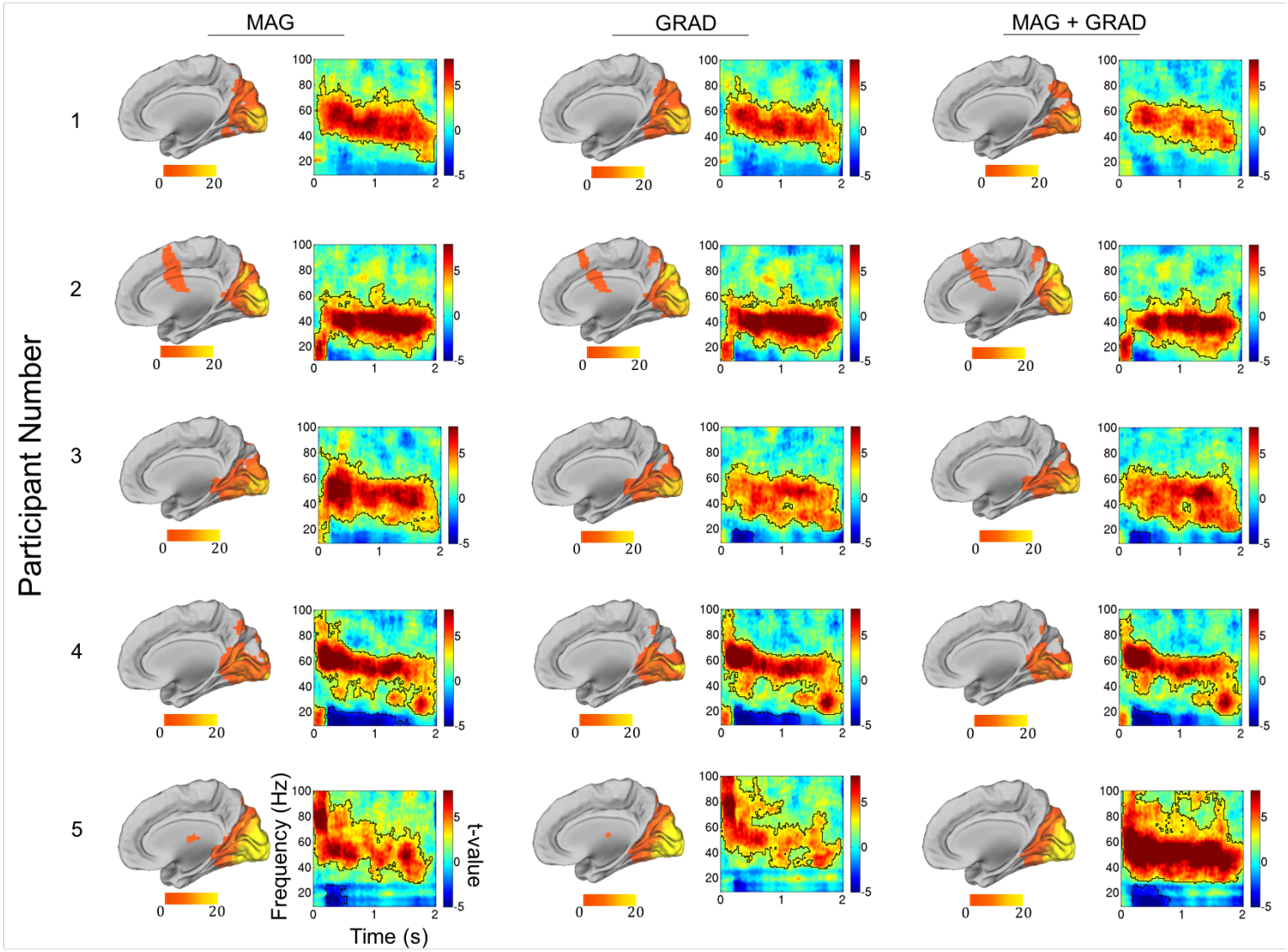

Figure 3.6. LCMV 35-75Hz beamformer results and corresponding peak virtual electrode time-frequency plots for the tSSS-PCA data (10-100Hz). Significant voxels (<0.01) are plotted on the right hemisphere. Significant time-frequency bins (<0.01) are identified by the black outline.

3.3.1 Source values

These findings indicate that the largest source values (*t*-statistic) at the peak voxel were observed in the tSSS-PCA gradiometers and the tSSS-PCA combined condition (Table 3.1). To investigate the differences between the analysis conditions, the resulting peak source values for each condition were compared using a one-way repeated measures ANOVA. Mauchly's test shows that the assumption of sphericity had been violated, χ^2 (14) = 61.28, p<.001, therefore degrees of freedom were corrected using Greenhouse-Geisser estimates of sphericity (ε = .36). The one-way repeated measures ANOVA showed that there was a significant effect of the method used and the peak source value gained, F(2.86, 48.62) = 12.22, p <.01 (η_p^2= .42). Bonferroni-corrected pairwise comparisons revealed that the raw magnetometer (M = 16.28, SD = 1.56), raw gradiometer (M = 16.99, SD = 1.47), tSSS magnetometer (M = 16.84, SD = 1.54), tSSS gradiometer (M = 16.72, SD = 1.54) , tSSS-PCA magnetometer (M = 16.25, SD = 1.50), tSSS-PCA gradiometer (M = 17.05, SD = 1.55) and tSSS-PCA combined (M = 17.06, SD = 1.58) conditions yielded significantly higher peak source values (p<0.05) relative to the raw combined sensor condition (M = 12.24, SD = 1.30). In summary, the condition yielding the significantly lowest source values were the raw combined sensors condition.

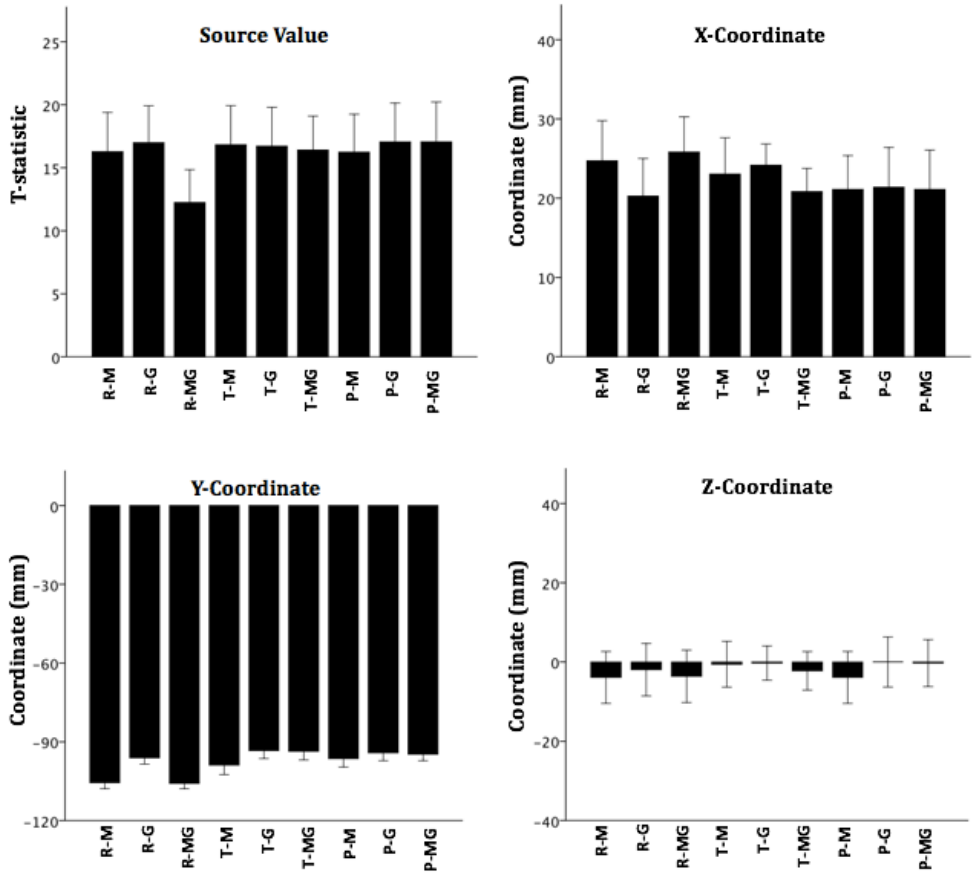

Figure 3.1. Mean peak source values and mean X, Y and Z MNI coordinates for the different analysis conditions**: R-M:** Raw magnetometers**, R-G:** Raw gradiometers, **R-MG:** Raw magnetometers and gradiometers (combined), **T-M:** tSSS magnetometers, **T-G:** tSSS gradiometers, **T-MG:** tSSS magnetometers and gradiometers (combined), **P-M:** tSSS-PCA magnetometers, **P-G:** tSSS-PCA gradiometers**, P-MG:** tSSS-PCA magnetometers and gradiometers (combined).

3.3.2 Spatial location

Due to non-normal distributed data, non-parametric statistics were used to study the differences between the peak source locations in the X, Y and Z directions (MNI coordinates). A Freidman test found no significant differences in the X and Z direction but did indicate a significant difference between the conditions in the Y direction (anterior-posterior), $\chi 2(8, N=18) = 79.26$, $p < .01$. Post hoc-tests (Wilcoxon signed-rank test, bonferroni corrected) found that there was a significant difference between the raw gradiometer (Mdn = -95), tSSS-magnetometer (Mdn = -100), tSSS-gradiometer (Mdn = -95), tSSS-combined (Mdn = -95), tSSS-PCA magnetometer

(Mdn = -98), tSSS-PCA gradiometer (Mdn = -95), and tSSS-PCA combined (Mdn = -95) conditions relative to the raw magnetometer condition (Mdn = -105, $p < 0.05$) and raw combined condition (Mdn = -105, $p<0.05$). In summary, there were no differences between the peak value locations in the X and Z directions, however the raw magnetometer and the raw combined conditions differed on the Y axis compared to the other methods.

3.3.4 Grand-averaged Time Frequency Plots

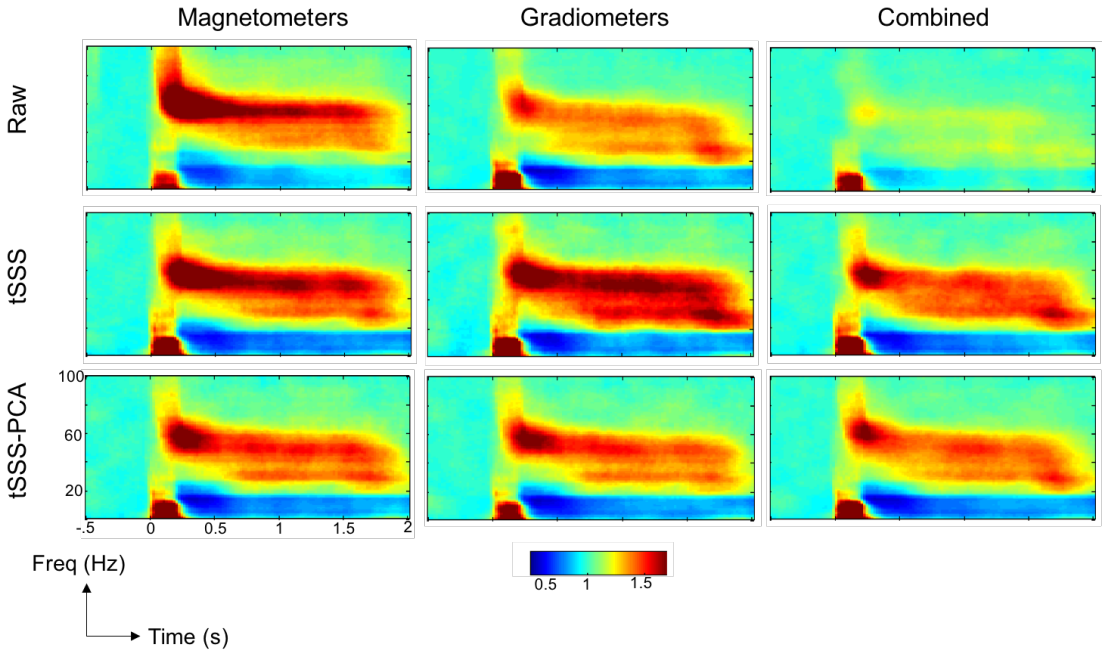

Figure 3.7. Grand-average time frequency plots based on the peak virtual electrode time series from 18 participants (10-100Hz). Time frequency plots are normalised using a relative baseline [-2 2] and changes are expressed as a ratio.

The grand averaged time frequency plots (Figure 3.7) provide a useful overview of the results, showing how the raw combined sensor condition produced a diminished gamma response relative to the other conditions. Notably, the raw magnetometer plot shows the strongest initial broadband gamma response and the tSSS gradiometers show the strongest sustained gamma power increase. In all time frequency plots, the initial evoked response is observed in the alpha/beta band and characteristically followed by a reduction in power.

3.3.5 Event Related Fields (ERFs)

Figure 3.8 shows that the smallest ERFs are found in the tSSS-PCA conditions, with the largest responses observed in the tSSS gradiometer condition. The amplitudes of the c2 (~100ms) and c3 (~150ms) components of the visual grating onset (Harding et al., 1996), were compared to investigate if there was a significant difference between the conditions. A Freidman's test revealed that there were no significant differences between conditions for the peak amplitudes of the c3 component, however a statistical difference was found for the c2 component, $X^2(8) = 17.60$, $p<.05$. Post-hoc Wilcoxon tests show that this difference was observed between the tSSS gradiometer condition and the tSSS-PCA gradiometer condition ($Z = -3.38$, $p<0.05$, bonferroni corrected) indicating a larger c3 response for the tSSS gradiometer condition.

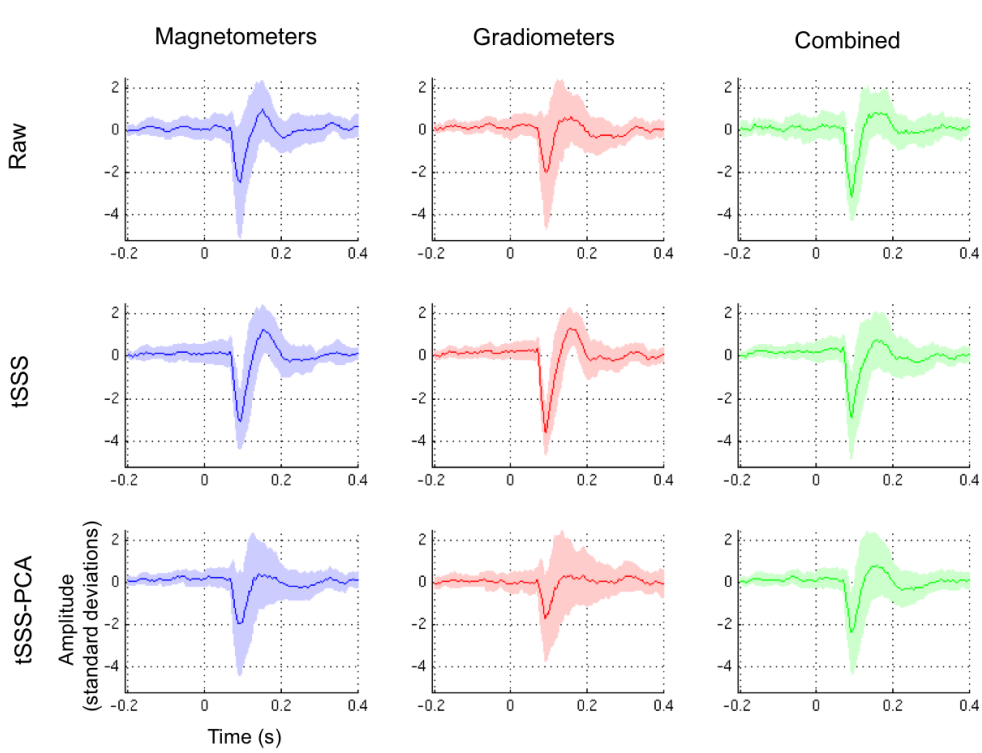

Figure 3.8. Grand-averaged ERF plots based on the peak virtual electrode time series from 18 participants (shaded area represent the standard error).

3.4 Discussion

The purpose of this chapter was to establish a source analysis pipeline in Fieldtrip to accurately identify functional cortex in order to overcome issues relating to the Elekta dual-state beamformer. This chapter investigated the peak source localisations and their values when using different sensor selections (magnetometers, gradiometers, combined), and preprocessing methods (raw/no-tSSS, tSSS, tSSS-PCA). Based on previous work (Muthukumaraswamy et al., 2013), it was hypothesised that a peak source within the gamma range (>35Hz) would be found in the right occipital lobe in response to a stationary, square-wave grating presented in the lower left quadrant of the visual field.

Overall, each analysis condition produced similar localisations (Table 1), with a right visual cortex peak found in all participants, except for one participant in the raw gradiometer, raw magnetometer, tSSS-PCA gradiometer, tSSS-magnetometer, and tSSS-PCA combined condition. The statistical analysis comparing the peak source locations revealed that the raw magnetometer and raw combined conditions differed significantly in the Y (anterior - posterior) direction relative to the other analysis conditions. A second comparison was made based on the peak source value. This revealed that the raw combined analysis condition resulted in the lowest peak values and was significantly lower than all other analysis conditions except for the tSSS combined condition.

Figure 3.4 indicated that the Fieldtrip LCMV beamformer, or perhaps beamformers in general, provide less useful source reconstructions when combined sensors have been used without applying tSSS. This is also evident in the Figure 3.4 time-frequency plots that show diminished gamma responses relative to the raw magnetometer and raw gradiometer conditions. This could be a result of the covariance matrix containing cross terms from both sensor types. The Fieldtrip toolbox corrects the scale difference between magnetometer and gradiometer signals and their corresponding leadfield values, however these sensors are still likely to contain differing noise profiles. The tSSS procedure may act to reduce the difference between the noise profile of both sensor types allowing the covariance between these sensors to be computed more effectively.

The visual ERFs (Figure 3.8) computed at the peak source indicated that the tSSS conditions produced the largest responses with the smallest standard error. In contrast, the tSSS-PCA analysis showed less pronounced ERFs, with diminished amplitudes and larger standard errors. However, the only statistical difference found was for the c2 component between the tSSS gradiometers and tSSS-PCA gradiometers. Despite the tSSS-PCA conditions having similar spatial localisations and source values to the majority of the other conditions, the application of PCA after tSSS seemed to produce poorer ERFs than using tSSS alone. This could be a result of the PCA procedure removing components critical for forming the ERF. This may be explained by the transient nature (<300ms) of the ERF resulting in its components being 'smaller' relative to other components contained within the whole 4 second epoch (e.g. the long sustained gamma increase, alpha/beta decrease). The ERF may have therefore benefited from the PCA method being applied to shorter epochs of data (e.g. -400ms to 400ms).

The perceived rationale for using PCA post tSSS is to 'stabilise' the data matrix by removing the smallest components (and likely poorly estimated components) to prevent unpredictable behaviour when the inverse of the covariance matrix is calculated. This approach is stated on the Fieldtrip user documentation and suggests retaining the first 50 components, however this explicit rank reduction seems to be overzealous. Therefore, in the application of the PCA method in this chapter, a data driven approach was taken to retain the number of components that described 99% of the variance in the data matrix. The use of PCA may prove to be more useful when concatenating multiple datasets that have been separately maxfiltered (e.g. in the case of the fiff 2GB file limit causing the file to split) where the low-rank subspace may vary for each dataset. After concatenation, it is more likely that the 'higher' components will represent noise and therefore the removal of these components may improve the subsequent source estimate.

As previously mentioned, this chapter aimed to establish whether the Fieldtrip LCMV beamformer is fit for purpose and to establish a source analysis pipeline when using Elekta data. Despite this chapter not necessarily producing optimal solutions to the challenges specific to Elekta data, observations can be drawn regarding the use of methods that are currently available in the Fieldtrip toolbox. These observations are stated below:

1) Analysing raw combined sensors produces lower source values and localisations that deviate from the other analysis conditions (except the raw magnetometer condition).
2) The time frequency representations of the raw combined sensors also show a much more diminished gamma power increase and alpha/beta decrease relative to the other analysis conditions. This raises scepticism about the use of raw combined sensors when using the Fieldtrip LCMV beamformer.
3) The tSSS conditions were the only analysis conditions in which all peak sources were contained in the right occipital lobe as hypothesised.
4) In the grand averaged time-frequency plots, the raw magnetometers were able to reveal the early broadband gamma increase more clearly relative to the other analysis conditions.
5) Applying PCA after tSSS produced smaller ERF components with higher inter-subject variance relative to the other conditions. This raises doubt on whether the tSSS-PCA method is useful in clinical MEG when the study of ERF responses forms an important part of the clinical protocol.
6) Beamforming suppresses magnetic artefacts and produces relatively good source reconstructions despite the raw data containing more noise relative to the tSSS filtered data.

It is feasible to suggest that based on these observations, tSSS filtering offers useful noise reduction in order to gain more accurate spatial localisations. The additional use of PCA after tSSS is still undetermined in this context and may remove useful components from the data. This leads to the conclusion that using tSSS alone is the optimal method out of the analysis methods investigated in this chapter. In regards to sensor selection, the tSSS-gradiometers show the largest ERF response and the grand-averaged time frequency spectra indicates that this analysis condition shows larger gamma power increases than the tSSS-magnetometer and tSSS-combined conditions. Therefore, given the current methods available and the comparisons included in this chapter, it is recommended that data should be tSSS filtered and gradiometers should be selected for source analysis. This selection avoids the issues faced when attempting to combine different sensor types, whilst still making use of a large number of sensors (204 planar gradiometers).

Currently, there is no unanimous agreement within the Elekta user community on how to optimally compensate for Maxfilter and combine different sensor types. In attempt to address these issues, a beamformer workshop was recently organised by Aston involving various Elekta users and open source software developers (e.g. SPM, Fieldtrip, MNE). The Aston beamformer workshop is an active project and aims to address issues concerning the source analysis of Maxfiltered data and the combination of different sensor types. The overarching goal of this project is to provide optimal solutions to these problems with the view of developing a more standardised source analysis approach within the Elekta user community. These solutions will first be implemented in the Fieldtrip toolbox, however code will be distributed and implemented in other platforms including SPM and MNE.

One initial suggestion from the Aston beamformer workshop was to zero out the cross terms of the covariance matrix, i.e. zero the elements that contained a product of a magnetometer and gradiometer channel. This essentially would solve issues relating to the calculation of covariance between sensors of different scales and different noise profiles, however this approach does not take full advantage of the combined information from the sensors. Other sensor fusion methods that have previously been suggested involve normalising the leadfields and the sensor data based on their power prior to source reconstruction (Henson et al., 2009).

A potential method to ensure the stable estimation of the covariance matrix post-tSSS is to apply a regularisation parameter, μ, to amplify the on-diagonal elements of the covariance matrix. A limitation of this approach is that by increasing μ, the spatial specificity of the beamformer decreases as the weights become less specific due to the increase in spatial averaging (Woolrich et al,. 2011). Furthermore, the amount of regularisation to be used is relatively subjective, with the most common method using the lowest eigenvalue of the covariance matrix (Robinson and Vrba, 1999). More recently, a Bayesian PCA approach for adaptive covariance matrix regularisation was proposed by Woolrich et al., (2011) to estimate the dimensionality of the data and objectively choose the amount of regularisation required. There has been limited evaluations of this method and therefore should be included in future research.

A limitation of this study was that the stimulus used is known to have a variable peak localisation within the contralateral visual cortex (Swettenham et al., 2009), therefore making it difficult to determine the true source location. This could have been overcome by using a stimulus with a more known localisation, for example a motor task or somatosensory stimulation. The reason for choosing this non-foveal, stationary grating was to investigate tSSS and beamforming in a more moderate SNR condition (relative to the high SNR often encountered in tactile stimulations). The additional use of phantom data could have also been used to further test the accuracy of the beamformer and forms part of ongoing work.

When attempting to construct an analysis pipeline, there are countless pre-processing methods that can be applied to the data. In this chapter, tSSS was the primary noise reduction method alongside the visual inspection and removal of excessively noisy trials. Interestingly, the beamformer performed well in the raw condition. This supports previous research that demonstrates the noise filtering properties of the beamformer even in the presence of large environmental and physiological noise (Adjamian et al., 2004; Cheyne et al., 2007).

3.4.1 Conclusion

In conclusion, the rationale for this chapter was to develop an alternative source analysis pipeline to the Elekta dual-state beamformer. It was demonstrated that the Fieldtrip LCMV beamformer is fit for purpose for localising functional brain areas when using tSSS filtered data. More systematic testing is ongoing and the integration of solutions from the Aston Beamformer workshop will form future investigations. The analysis pipeline outlined here will inform the analysis in the next chapter in order to localise language areas using a verb generation and a novel passive language task.

Chapter 4: Lateralising Expressive Language using MEG

4.1 Introduction

Drug resistant epilepsy patients put forward for surgery require eloquent cortex to be identified before the resection of tissue to reduce the risk of surgically induced neurological deficits. TLE is the most common type of drug resistant epilepsy, therefore identifying language critical areas prior to surgery is imperative in these patients. This is usually determined by establishing which hemisphere is dominant for language processing and is often achieved by using invasive techniques such as WADA or ESM. These invasive techniques can be uncomfortable and pose additional risks to the patient, therefore there is a need to develop non-invasive measures to investigate language representation.

The use of fMRI has frequently been used to lateralise language in patient cohorts (Binder et al., 2008; Szaflarski et al., 2006; Anderson et al., 2006), however the use of MRI in the paediatric assessment of language may be faced with cooperation issues due to the unfriendly scanner environment. Alternatively, MEG may be used to potentially overcome these issues. In the ABC, an expressive language task has been used to determine the language dominant hemisphere by instructing patients to covertly generate verbs (Fisher et al., 2008). However, this type of paradigm may pose challenges to young patients that do not understand the task or in patients with developmental delays. In these patients, the use of a passive language task may allow language lateralisation to be investigated. This is of particular importance to the clinical work done at the ABC, as paediatric patients with TLE are frequently referred for MEG evaluation.

This chapter aims to replicate previous verb generation findings using Elekta Neuromag data and the analysis pipeline developed in the previous chapter. Further, a novel MEG language task will be piloted to seek a passive alternative that may be more practical in children and non-compliant patients.

4.1.1 Lateralising Language

The left hemisphere dominance of language is a well-documented finding dating back to the 19th century (Broca, 1861; Wernicke, 1911). Research has consistently shown support for this unilateral dominance in healthy individuals with only a small proportion of dextrals (approximately 4%) expressing bilateral or right hemisphere language dominance (Knecht et al., 2000a; Springer, Binder et al., 1999). The incidence of atypical language lateralisation increases to 20-27% in healthy left-handed individuals (Knecht et al., 2000b; Springer et al., 1999; Pujol et al., 1999).

Atypical language representation has also shown to increase approximately by one-third in drug resistant epilepsy patients (Rasmussen & Milner, 1977; Gaillard et al., 2007). This increase is thought to represent cortical reorganisation as a result of chronic epileptogenic activity whereby language-processing regions have moved or additional areas have been recruited (Thivard et al., 2005). Inter-hemispheric shifts in language processing are often thought to occur (Staudt et al., 2001, 2002; Gaillard et al., 2002; Gaillard & Sachs, 2003; Gaillard et al., 2004; Gaillard et al., 2007) resulting in right sided dominance or bilateral language representation (Hertz-Pannier et al., 2002; Pataraia et al. 2005). Therefore, measures of handedness are not appropriate or accurate enough in determining language dominance in healthy participants or in epilepsy patients.

More direct measures used to investigate language representation has often involved the administration of intracarotid sodium amobarbital, referred to as ISAP or WADA (Wada & Rasmussen, 1960). This technique works by sedating one hemisphere of the brain and assessing whether language deficits occur in order to determine its role in language. A limiting factor of this procedure is that it can only identify the language dominant hemisphere and disregards bilateral language representation and the underlying neural substrates of language (Fisher et al., 2008). Another issue is that WADA testing carries a certain level of risk due to its invasive nature and can only be used on a selective group of patients (Hajek et al., 1998; Abou-Khalil, 2007). Furthermore, WADA is an uncomfortable procedure and not patient friendly, particularly in paediatric patients.

To gain more precise information about language functioning, electrical current stimulation (ESM) can be employed to assess changes in language performance (Penfield & Rasmussen, 1950). This involves delivering electrical currents to the cortical surface whilst the patient performs various language tasks to measure disruptions in performance. Despite being the gold standard for language delineation, this procedure places additional health risks to the patient (Abou-Khalil, 2007; Hamberger & Cole, 2011) and may cause significant distress. It has been reported that WADA and ESM success rates are lower in paediatric populations (Hamer et al., 2000; Schevon et al., 2007) and therefore friendlier, non-invasive alternatives are warranted.

4.1.2 Non-invasive Language Measures

fMRI and MEG have been used as non-invasive alternatives to identify language critical areas. Despite the spatial accuracy of fMRI, the scanning environment maybe intimidating for children (Byars et al., 2002) and therefore affecting task compliance (Schweitzer, 2010). In uncooperative paediatric patients undergoing MRI, the use of general anaesthesia or sedation can be used to ensure a successful recording (Johnson et al., 2002; Malviya et al., 2000). This strategy is limited when completing functional tasks in MRI and therefore more practical non-invasive modalities need to be sought. In this context, MEG may provide a more patient and child friendly environment (Colon et al., 2010; D'Arcy et al., 2013).

4.1.2.1 MEG Language Paradigms

MEG measurements of language functions have been validated to some degree against WADA testing (Papanicolaou & Simos, 2004; Hirata et al., 2004; Hirata et al., 2010) and ESM (Salmelin, 2007). Previously, expressive language tasks, such as covert letter fluency (Singh et al., 2002) and verb generation (Fisher et al., 2008), have been used to determine the language dominant hemisphere. Using a covert letter fluency task, Singh et al., (2002) demonstrated strongly left biased beta dysynchronisations (15-25 Hz) and spatially correlated fMRI BOLD increases at the group level. An extension of this work using a verb generation task also reported similar lateralised beta dysnchrosinations within single subjects (Fisher et al., 2008).

This study demonstrated how spectral power distributions in single subjects could provide a qualitative assessment of language dominance.

It must be highlighted that data used by Fisher et al. (2008) were collected and analysed at Aston University using a CTF 275 MEG system and the accompanying software. Crucially, these findings have not since been replicated at the ABC since the installation of the Elekta Neuromag system due to the aforementioned issues with the beamformer software. In this chapter, the pipeline established in the previous chapter will be applied to verb generation data with goal of replicating Fisher and colleagues. This forms the first aim of this chapter.

Figure 4.1. Verb generation SAM beamformer in the 0 to 3 second time window and in the 15-25Hz frequency band (Taken from Fisher et al. 2008). Colour bars show pseudo-*t* values.

4.1.2.2 Passive Language Tasks

The second aim of this chapter is concerned with the introduction of a passive language task to assist in determining the language dominant hemisphere. Despite previous studies showing the potential clinical utility of expressive language tasks, a limitation with these paradigms are that participants may not be able to perform the task effectively due to young age or developmental delays. Therefore, the use of a passive language task may permit the lateralisation of language in order to circumvent the practical issues associated with complex active paradigms. In this chapter, a

passive listening task, referred to as rotated speech, is used in an attempt to provide a lateralisation of language by contrasting intelligible and unintelligible speech signals.

Spectrally rotating speech signals was introduced by Blesser (1972) as a method to destroy the intelligibility of speech signals whilst retaining its structural acoustic complexity. Rotated speech involves spectral inversion of the original speech stimuli and sounds like 'alien' speech. The advantage of this method is that it allows the internal structure to be maintained therefore providing a good contrast condition to intelligible speech when attempting to reveal speech perception processes. Previous research using filtered and spectrally rotated speech in PET demonstrated clear left hemispheric dominance, indicating that intelligible speech processing is associated with a left anterior temporal pathway (Scott et al., 2000). This left hemispheric dominance is also consistent with the neuropsychological literature into language organisation (Caplan, 1987).

Figure 4.2 (A) Intelligible speech, (B) Spectrally Rotated Speech. Taken from Scott et al. (2000).

The potential utility of a passive listening task is that it can be adapted to children to include more engaging content, such as that from a popular children's book. To date, the use of spectrally rotated speech has not been used in MEG and not as a clinical tool to passively probe language dominance. The advantage of this task being carried out in MEG relative to fMRI is that the scanner environment is friendlier and auditory signals can be delivered without scanner noise interference. Another potential advantage of MEG is that signals originating from anterior temporal lobe regions may be better measured as signal loss in these regions are often incurred in fMRI due to macroscopic field gradients (Devlin et al., 2000; Ojemann et al., 1997).

4.1.3 Aims

The first aim of this chapter is to replicate the findings from Fisher et al. (2008) in a sample of healthy control participants. To expand on Fisher et al's findings, robust source space statistics will be used (using cluster based permutation testing), as opposed to using unthresholded pseudo *t*-values. This first aim is important in establishing a method for analysing verb generation data at the ABC and to facilitate a larger study using patient MEG and iEEG data.

The second aim is to pilot the rotated speech paradigm on the same healthy control participants to investigate whether the task can provide useful information about language representation. Additionally, a dataset from a child and patient will be included to test the feasibility of this paradigm. As previous speech perception studies have shown BOLD increases in the left anterior temporal pathway (e.g. Narain et al., 2003), it is hypothesised that the MEG data will show increases in gamma band power in similar areas.

This hypothesis is based on local field potential (LFP)-BOLD coupling studies, that have showed positive correlations in the gamma band and negative correlations in the beta band (Conner et al., 2011; Mukamel et al., 2005). MEG studies investigating this relationship in the visual cortex have also demonstrated significant gamma band (40-60Hz) and BOLD responses arising from the same cortical regions (Muthukumaraswamy & Singh, 2009). However, the relationship between the BOLD and MEG signal is complex (Hall et al., 2014) as BOLD increases cannot be fully explained by increases in gamma-band power (Muthukumaraswamy & Singh, 2009). Therefore, the rotated speech paradigm will be investigated using the same beta-frequency band as the verb generation task (15-25 Hz) alongside two gamma-frequency bands (30-50 Hz) and (40-60 Hz).

4.2 Methods

4.2.1 Participants

Four right handed adults and two left handed adults (four females, age-range 18-61 years) with no reported neurological or psychiatric conditions took part in the verb generation experiment. Participants were recruited from an ad-hoc population of university staff and graduate students. The same participants also took part in the rotated speech experiment. In order to pilot the rotated speech paradigm further, data was also acquired from a healthy child (female, 12 years old) and a drug resistant epilepsy patient (male, age 46) with suspected TLE.

4.2.2 MEG Data Acquisition

MEG data was recorded in a magnetically shielded room (VacuumSchmelze GmbH, Hanua, Germany) using a 306-channel Elekta Neuromag Triux (102 magnetometers and 204 planar gradiometers), at a sampling rate of 1000 Hz. Participants were recorded in the 68° upright seated position. Noise reduction was achieved with the Maxfilter software (Elekta Neuromag Oy, version 2.2.10) using a sliding window of 10 seconds and a subspace correlation limit of 0.9. Bad channels were identified using Xscan (Elekta Neuromag, Oy) and were not included in the Maxfilter calculations and subsequent beamformer analysis. Prior to data acquisition 5 head localisation coils were attached to the participants' head and 3 fiducial points were digitised using a polhemus fast-trak digitizer (Fastrak, Polhemus, Colchester, VT, USA). Additional head points were collected to allow a surface based alignment with the participant's T1-weighted MRI using the method described in Chapter 2. Continuous head position indication was used and a head movement threshold of 6mm was implemented (none of the datasets in this chapter exceeded this threshold).

4.2.3 Verb Generation

The trial began with a passive phase where participants were instructed to focus on a central fixation cross for 3 seconds. After 3 seconds of fixation a noun was presented on the screen for a further 3 seconds (e.g. BALL). At this point participants were asked to covertly generate a single verb associated with the noun on the screen

(e.g. THROW). After 3 seconds of covert verb generation, a picture of Mr. Chatterbox© (THOIP) appeared on the screen for 3 seconds and participants were instructed to vocalise the verb that they had silently generated (see Figure 4.2). This final vocalisation stage was used to assess whether the participant was correctly engaging in the task. In this experiment, 60 trials were presented using the Presentation software (Neurobehavioral Systems, San Francisco, CA).

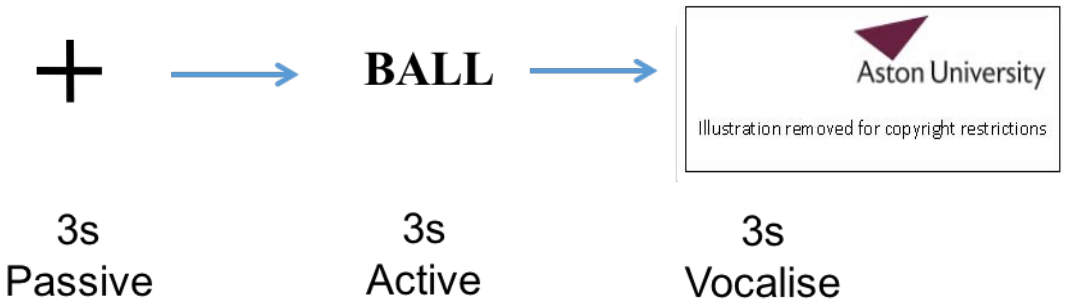

Figure 4.3. A schematic of the verb generation task.

4.2.4 Passive Listening Task

Participants were instructed to focus on a fixation cross in the centre of the screen whilst the speech stimuli were delivered binaurally through echoless plastic tubing and foam ear-tips at a comfortable hearing level. The speech stimuli consisted of filtered intelligible speech (active) and spectrally rotated speech (baseline). Six, five seconds trials of filtered speech were presented consecutively, followed by six, five second trials of spectrally rotated speech. This was repeated 5 times, resulting in 36 trials for each condition. The speech stimuli used in both conditions were taken from a shipping forecast, voiced by a male speaker. For the filtered speech condition (intelligible speech), stimuli were low pass filtered (3.8 kHz). To create the rotated speech stimuli the filtered speech was spectrally inverted using a digital version of the technique described by Blesser (1972). This involved first equalising the speech signal with a filter, giving the rotated signal approximately the same long-term spectrum as the original signal. This signal was then amplitude-modulated with a sinusoid at 4 kHz followed by low-pass filter at 3.8 kHz. The spectrally rotated speech signal has very similar temporal and spectral complexity to the original speech signals but is not intelligible without extensive training (Blesser, 1972).

4.2.5 MEG analysis

MEG data was analysed using the MATLAB toolbox FieldTrip (Oostenveld et al., 2011). The MEG data was down-sampled offline in both experiments to 300Hz and a single shell head model was used (Nolte et al., 2003). Source analysis was computed in MNI standard space using a 5mm source space grid.

4.2.5.1 Verb generation

Epochs were extracted from 2.5s prior to the noun onset to 2.5s post-stimulus. Therefore, only the covert verb generation phase of the experiment was analysed. A slightly shorter time window was used in this study relative to Fisher et al. to avoid potential desynchronisations in beta due to motor anticipation for the vocalisation phase of the trial. An LCMV beamformer was computed on bandpass-filtered data (15-25Hz). Source power was projected through using a common beamformer filter computed across the whole covariance window (-2.5s to 2.5s) and applied separately for the baseline (-2.5 to 0s) and active period (0s to 2.5s). Single subject source statistics were computed on the individual's source reconstructed active and baseline trials using monte-carlo testing. A cluster-based permutation correction method was used to correct for the multiple comparison problem (alpha level <0.01) (Maris & Oostenveld et al., 2007). Virtual electrodes were recomputed on the original sampled data (1kHz) at the left inferior frontal gyrus (pars opercularis, MNI: -48, 13, 17) and the contralateral site (MNI: 49, 12, 17) for a simple comparison. Time-frequency analysis was computed between 1-100Hz with a fast fourier transform (FFT) using 3 Slepian multitapers (+/- 8 Hz spectral smoothing) applied to the baseline time window (-2.5 s to 0s) and active time window (0s to 2.5s). Time-frequency statistics were computed between the two conditions using cluster-based permutation testing (<0.01).

4.2.5.2 Passive Listening Task

An LCMV beamformer was computed in three frequency bands, 15-25 Hz, 30-50Hz, and 40–60 Hz. Source power was projected through using a common beamformer filter computed across the whole covariance window and applied separately to the two experimental conditions (spectrally rotated and filtered speech). Single subject

source statistics were initially computed by contrasting the spectrally rotated speech (baseline) to the filtered speech (active) using cluster-based statistics (alpha level = <0.01) (Maris & Oostenveld et al., 2007). In a number of participants, no significant clusters were found at the alpha level of <0.01, therefore power differences were expressed as percentage change (the implications of non-significance at this alpha level are raised in the discussion).

In the child and patient example, virtual electrodes were reconstructed at the peak source identified by the beamformer using the original sampling rate of 1kHz. Time-frequency analysis was computed between 40-80Hz with a fast fourier transform (FFT) using 3 Slepian multitapers (+/- 8 Hz spectral smoothing) and applied to the spectrally rotated (baseline) and filtered speech (active) conditions separately. Time-frequency statistics were then computed between the two conditions using cluster-based permutation testing (alpha level = <0.01).

4.3 Results

4.3.1 Verb Generation

The verb generation task elicited decreases in spectral power in the 15-25 Hz frequency band in regions of the left frontal or temporal lobe in all of the right handed participants (participants 1 – 4). In the two left handed participants (participant 5 & 6), bilateral decreases in spectral power were observed (Figure 4.4). However, across all participants, the sites that showed the greatest spectral decreases are variable in location and additional areas including the superior frontal gyrus (SFG), middle frontal gyrus (MFG), and angular gyrus also showed power decreases. The results are shown in Figure 4.4, whereby the top 50% of significant t-values are plotted. In all participants, there were significant bilateral decreases in spectral power within the frequency band of interest, however in right handers this decrease was greater in the left hemisphere and masked out when applying the 50% image threshold.

The time frequency representations in Figure 4.4 shows the oscillatory power at the inferior frontal gyrus (IFG) (pars opercularis) site in both hemispheres. The significant changes in task-related power in the right handed participants are prominent within

the frequency band of interest, except participant 2 where the decreases in spectral power were observed primarily in the anterior temporal lobe. In participants 1,3, and 4, this significant decrease in power commences approximately at 250–500 ms after the noun appears on the screen, indicating early involvement of the left IFG. There are no significant power increases observed in the 15-25 Hz frequency band in the right handed participants.

In the left handed participants (5 & 6), there is much earlier bilateral IFG involvement, however these changes in spectral power only last for 1–1.5 seconds. The time frequency plots for these participants also show (non-significant) increases across a broad frequency spectrum. In participant 6, an earlier increase in power peaking in the alpha frequency is observed in the left IFG followed by a power decrease at 500ms. In participant 6's right IFG time frequency plot an early increase in gamma (50-70 Hz) is observed alongside the early decreases in the beta frequency band.

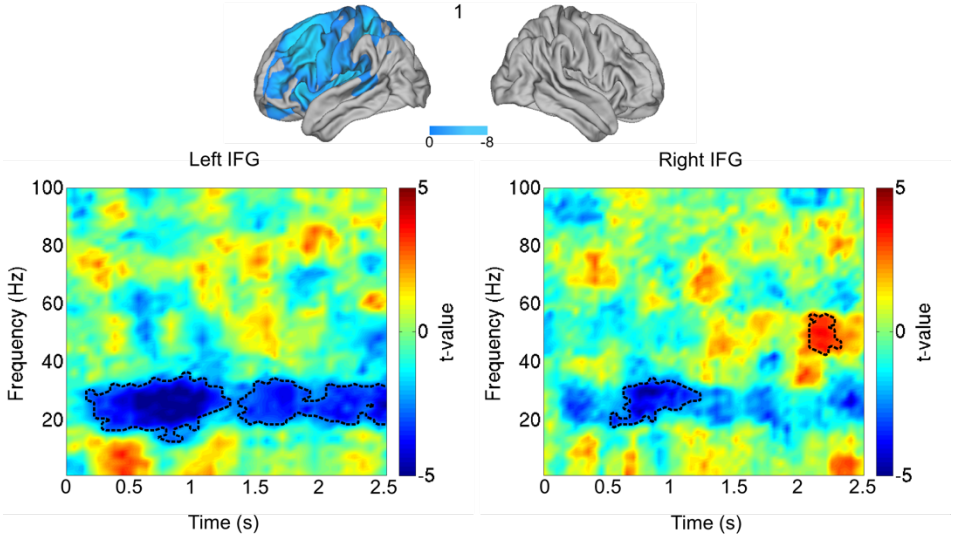
1
0
-8
Left IFG
Right IFG
Frequency (Hz)
Time (s)
t-value
5
0
-5

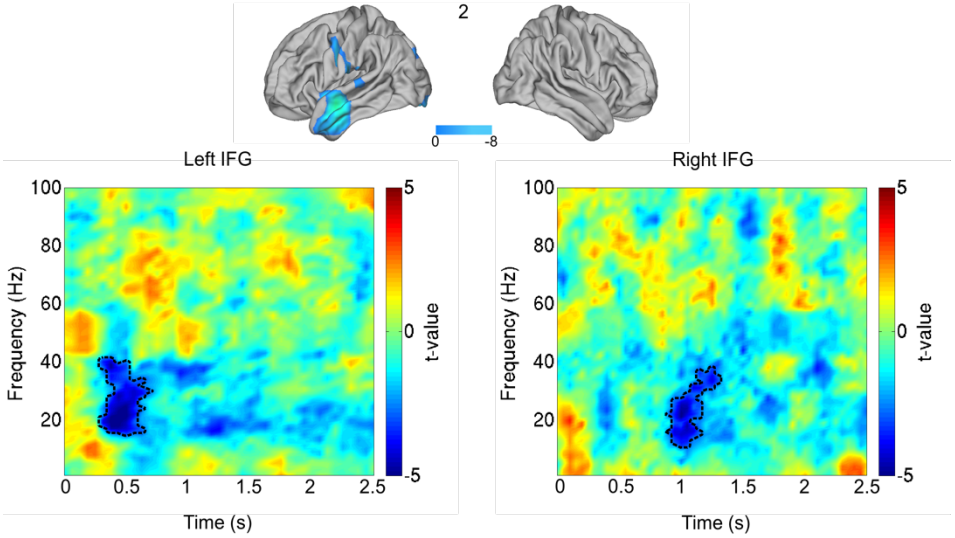
2
0
-8
Left IFG
Right IFG
Frequency (Hz)
Time (s)
t-value
5
0
-5

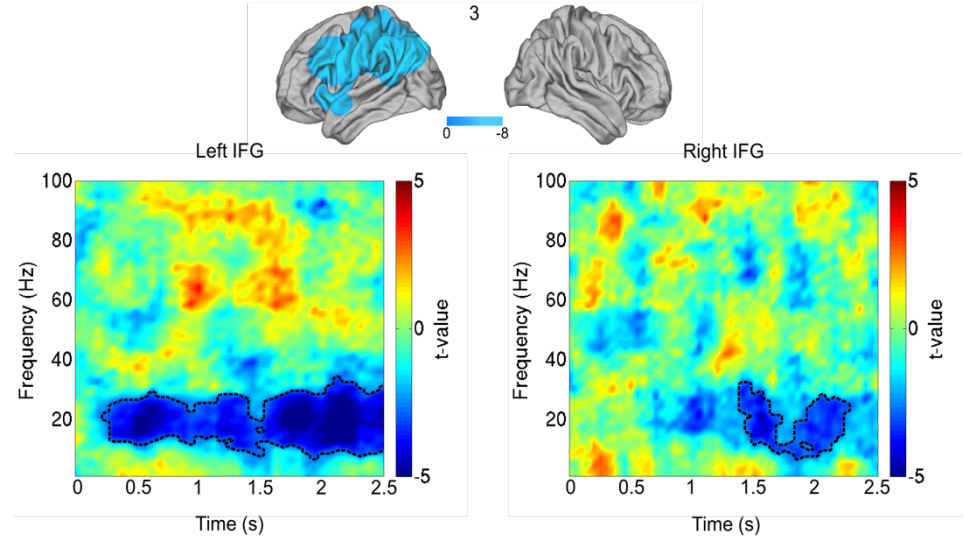
3
0
-8
Left IFG
Right IFG
Frequency (Hz)
Time (s)
t-value
5
0
-5

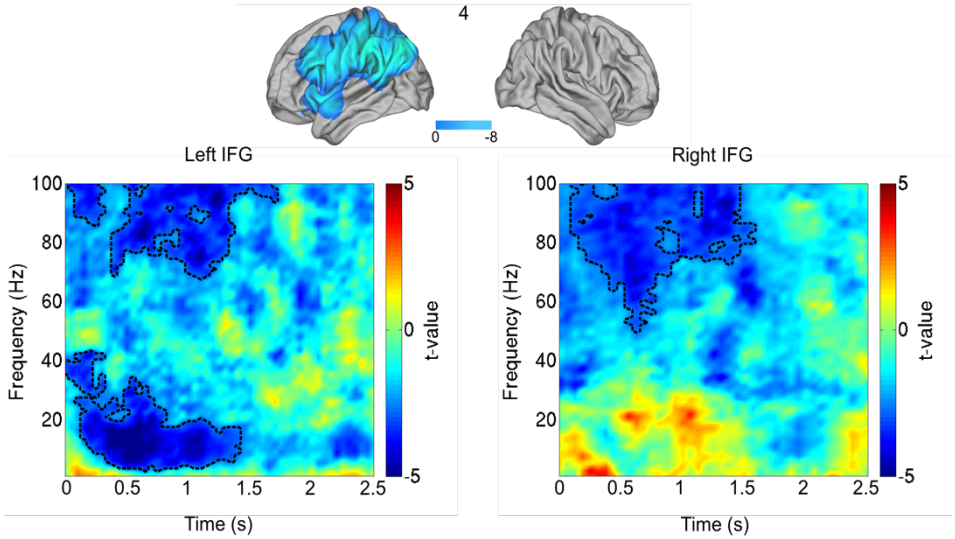
4
0
-8
Left IFG
Right IFG
Frequency (Hz)
Time (s)
t-value
5
0
-5

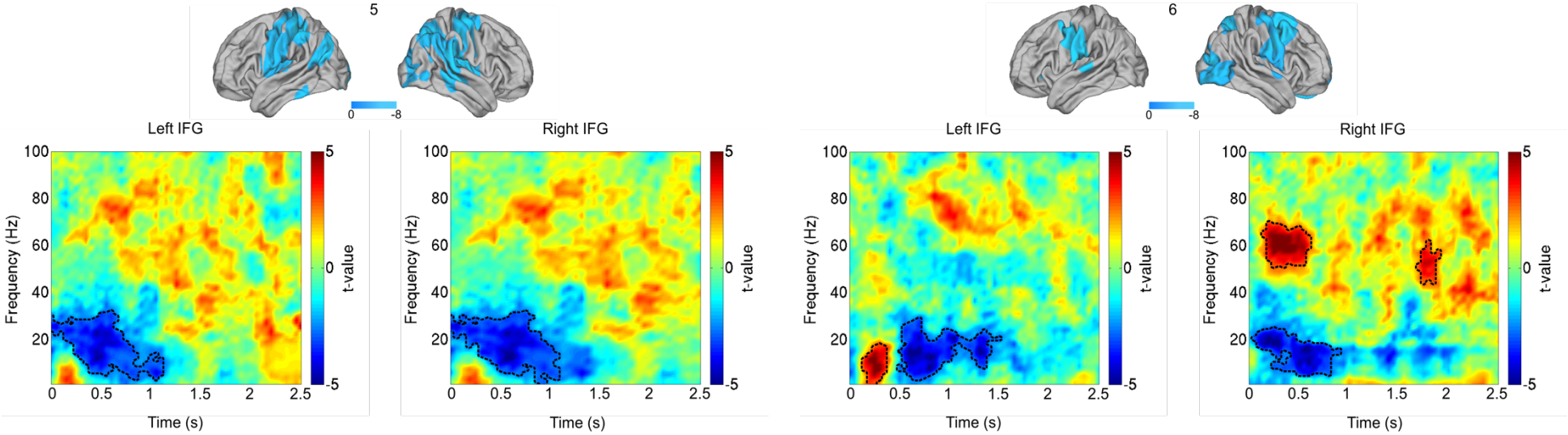

Figure 4.4. Verb generation results. Significant t-values (p<0.01, cluster corrected) are plotted on the brain (thresholded to show top 50% significant values). Time frequency plots of the left and right inferior frontal gyrus are plotted below beamformer results (<0.01, cluster corrected).

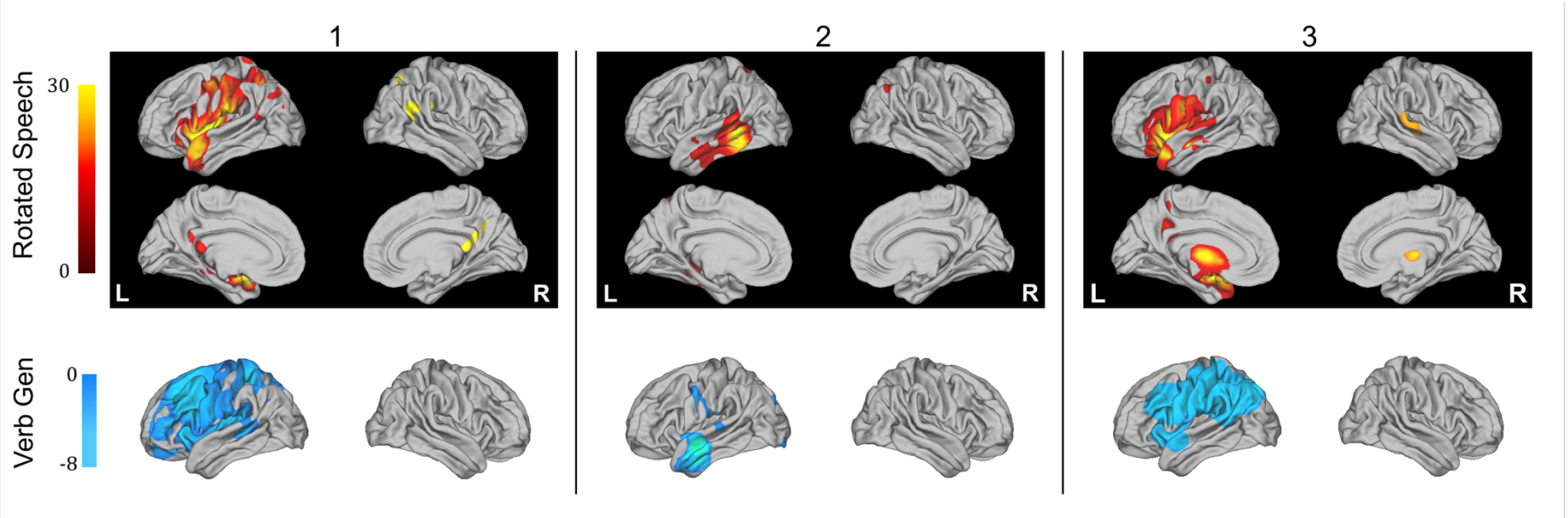

Figure 4.5. Passive listening results (40-60Hz) for participants 1-3 expressed in percentage change. Verb generation results for the same participants are plotted underneath (significant t-value, <0.01 cluster corrected).

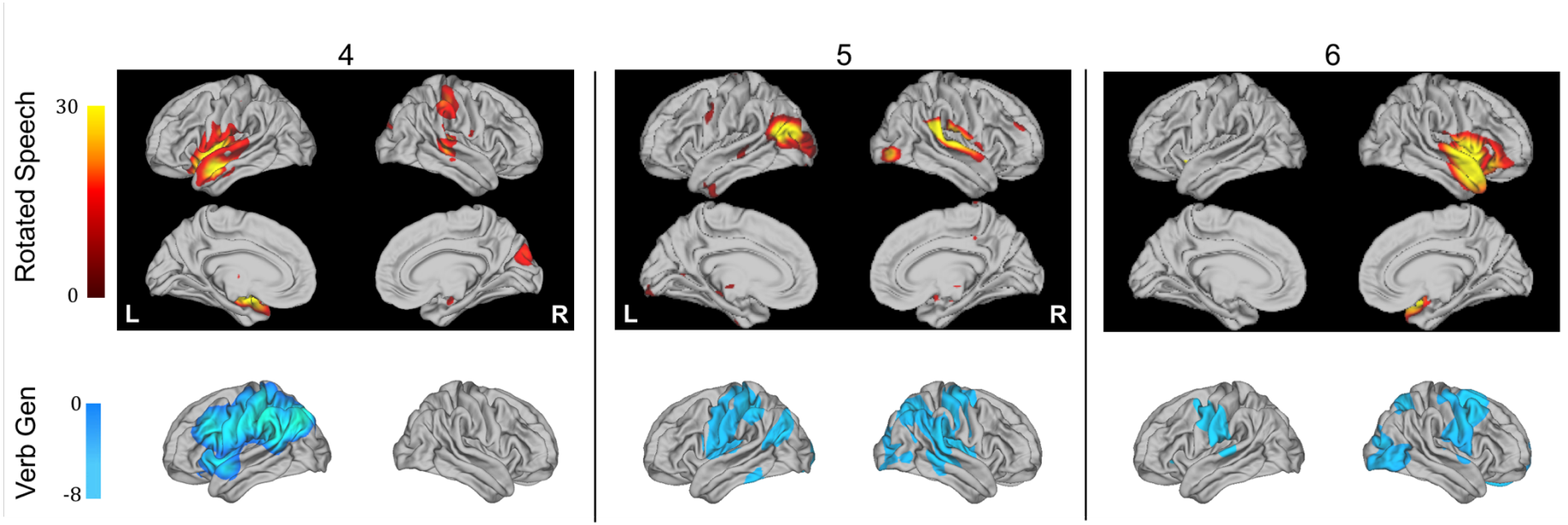

Figure 4.6. Passive listening results (40-60Hz) for participants 4-6 expressed in percentage change. Verb generation results for the same participants are plotted underneath (significant t-value, <0.01 cluster corrected). N.B. Participants 5 & 6 are left handed.

4.3.2 Rotated Speech

The rotated speech task elicited the greatest percentage changes in the 40-60 Hz frequency band, with little changes observed in the remaining two frequency bands of interest (15-25 Hz & 30-50 Hz) and therefore are not plotted. In the 40-60 Hz frequency band, predominately left temporal lobe increases were found in the right handed participants (1-4). In participants 1, 3 and 4, peak power increases were found in the left temporal pole (LTP) and left IFG. Participant 2 displayed greater power increases in the left posterior temporal lobe extending to anterior temporal regions. In comparison to the verb generation results for these participants (Figure 4.5 & 4.6), the rotated speech results identify the same hemisphere (left) for language dominance. Patient 4, showed a bilateral response to the intelligible speech with right sided power increases in the STG and supramarginal gyrus (SMG), however the greatest increases in power were observed in left LTP and IFG areas.

In the left handed participants (5 & 6), the increases in spectral power in the 40-60 Hz band did not show the same left hemisphere bias. Participant 5, shows bilateral increases in power in the left angular gyrus and parietal activations in the left hemisphere and superior temporal gyrus (STG) increases in the right hemisphere. Participant 6 resembles a similar activation profile to participants 1, 3, and 4, however these increases in power are lateralised to the right hemisphere. In participant 5, despite the results not spatially overlapping, bilateral language activations are observed in concordance with the bilateral power decreases observed in the verb generation results. The verb generation results for participant 6 also show bilateral language representation, however the rotated speech results do not show this bilateral response and is lateralised to the right ATL and IFG.

Finally, Figure 4.7 shows the child and patient data, indicating left lateralised increases in power. In the child dataset the peak activation is located on the left STG bordering with the left primary somatosensory cortex and an activation in the left anterior temporal lobe. The corresponding time frequency plot for the peak activation also indicates an increase in power in the 40-60Hz frequency band, with some time frequency bands reaching significance. In the patient dataset, the intelligible speech sounds are localised to the anterior portion of the left temporal lobe. This activation is consistent with the previous right handed results. The corresponding time frequency plots show increases in the gamma frequency band (40-60 Hz) for the child dataset and small increases in power in the patient dataset (40-80 Hz).

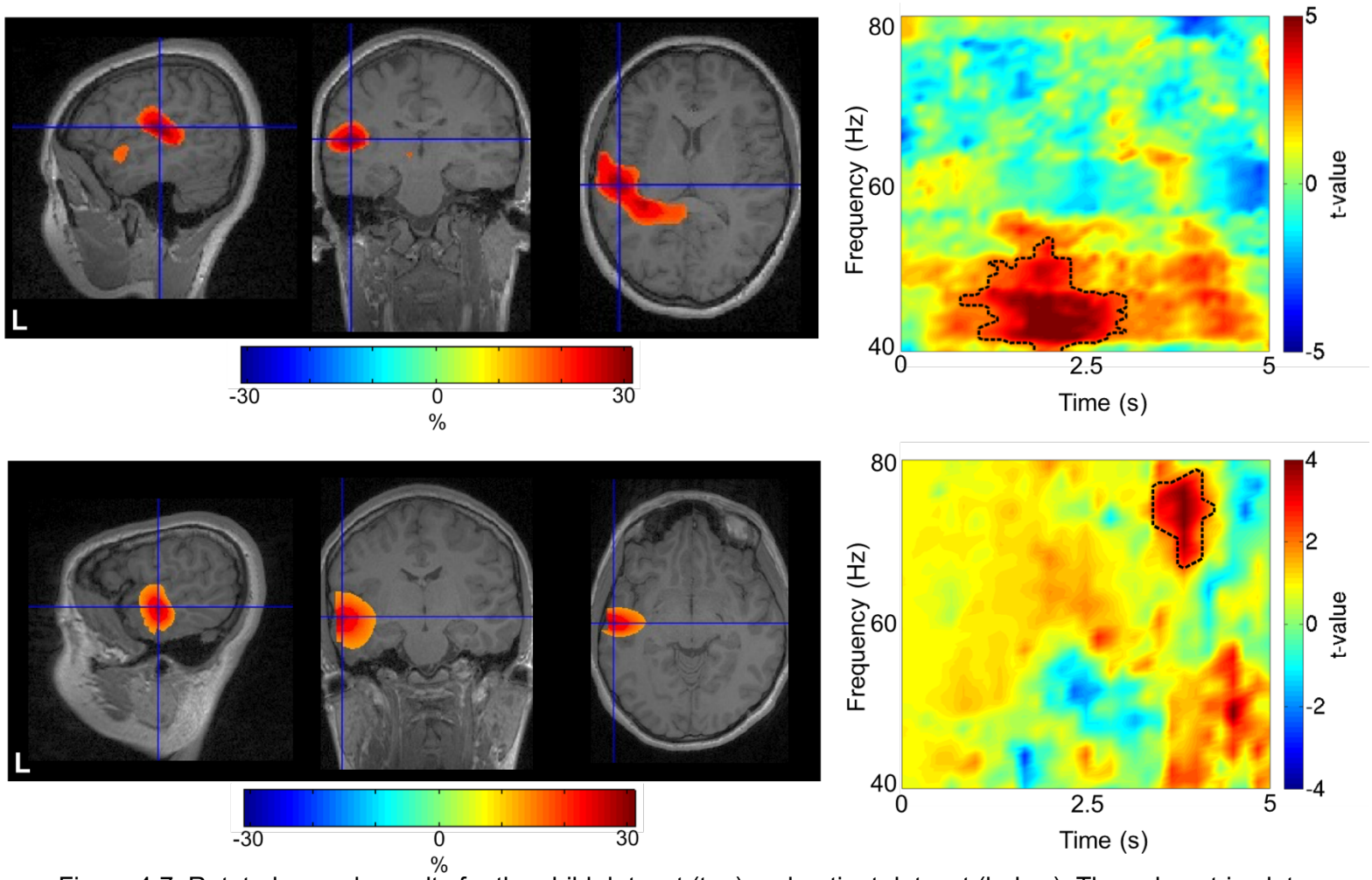

Figure 4.7. Rotated speech results for the child dataset (top) and patient dataset (below). The volumetric plots show percentage change and associated time frequency plots are displayed on the right.

4.4 Discussion

4.4.1 Key findings

The characterisation of language dominance prior to surgery is important in order to avoid removing eloquent cortex responsible for language processing. In this chapter, the aim was to replicate the findings from Fisher et al. (2008) using the analysis pipeline established in the previous chapter and to test a new passive language task. The rationale for using a passive task is of particular importance when assessing language in non-compliant patients, such as younger children and patients with developmental delays or language impairments.

The findings of this chapter demonstrate a replication of the beta band power decreases that were observed in the Fisher et al. (2008) study. This is important as previous unpublished verb generation findings using Elekta data has provided uninterpretable results that do not replicate the original CTF results. Secondly, this is the first study demonstrating the use of rotated speech to assess language dominance in MEG. The significance of this finding is that the use of a passive paradigm may permit the assessment of language in non-complaint patients, due to age or developmental delays. The discussion will first focus on the verb generation findings and then the rotated speech results.

4.4.2 Verb generation

At the ABC, verb generation has previously been used to identify the language dominant hemisphere as part of additional presurgical information that can be included in the clinical MEG report. This verb generation study is based on the work by Fisher et al. (2008) that showed spectral power changes in the 15-25 Hz frequency band in response to covert generation of a verb. Fisher and colleagues investigated a sample of right handed adults and found decreases in power in the left hemisphere indicating a left sided dominance for language. It was also found that increases in spectral power in the 15-25 Hz frequency band were found in the right hemisphere of participants, showing a clear spectral pattern. As mentioned in the introduction, there has been difficulty replicating these findings in the ABC using the Elekta Neuromag system and the associated Elekta beamformer software.

The verb generation results in this study showed similarities to Fisher and colleagues, replicating the main finding of spectral decreases in power (15-25 Hz) in the left hemisphere in right handed individuals. In the two left handed participants, the verb generation source plots indicated bilateral decreases in spectral power, which may be explained by research showing a higher prevalence of atypical language lateralisation in non-dextrals (Knecht et al., 2000; Springer et al., 1999; Pujol et al., 1999). Interestingly, unlike the Fisher et al. study, increases in power were not observed in the non-dominant hemisphere in the right handers. A key difference in the analysis in this chapter is that robust source space statistics were used (permutation testing, cluster based correction <0.01). In comparison, Fisher et al. presented unthresholded pseudo *t*-values. The use of more stringent statistical thresholding may explain why power increases were not observed in this study. In other studies, using similar covert language generation tasks, beta-band power increases have not been reported (Singh et al., 2002; Elk et al., 2010) and therefore this may raise scepticism over this finding.

In the verb generation task, the nouns presented often lead to the generation of action verbs (e.g. run). This may explain why sensorimotor beta power decreases were observed as the role of beta oscillations are classically related to motor processes (Weiss & Mueller, 2012). An explanation for beta desynchronisations in other regions could be related to the memory retrieval components of the task when engaging in the semantic processing of the noun. Beta desynchronisations have been demonstrated in both memory encoding and retrieval, and information load has shown to correlate with beta power decreases (Hanslmayr et al., 2012). Beta oscillations may also play a role in attention and expectancy violation (Engel and Fries, 2010; Jenkinson and Brown, 2011). Although a cognitive violation task was not used in this study (e.g. oddball), the presentation of a noun after a baseline period may have disrupted the ongoing cognitive state.

In summary, the verb generation results replicated Fisher et al's primary finding of beta spectral power decreases as a potential signature of language dominance. The ability to reproduce this key finding using Elekta data permits a larger study to be completed and to provide further clinical evaluations of the verb generation task. A

study of this nature is currently being carried out at the ABC comparing patient MEG data to data recorded using iEEG.

4.4.3 Passive Listening Task

The passive listening task revealed power increases (40-60 Hz) in the left IFG and ATL regions in the right handed control participants, and in the child and patient datasets. These results indicate that the left IFG and ATL are important for processing intelligible speech signals. Speech perception research carried out by Scott et al. (2000) using various speech stimuli demonstrated the role of the left anterior superior temporal sulcus (STS) in processing intelligible signals. The passive listening findings documented in this chapter also indicate the role of anterior portions of the temporal pole including the STS supporting the findings by Scott and colleagues. PET and fMRI studies have also demonstrated the role of the left anterior temporal cortex in response to single words, sentences processing and narratives (Binder et al., 1998; Wise et al., 2001; Humphries et al., 2005; Crinion et al., 2006).

The precise role of the left ATL is still debated but evidence from patients with semantic dementia affecting the ATL have exhibited deficits in semantic knowledge whilst retaining knowledge in other cognitive domains (Warrington, 1975; Patterson et al., 2007; Jefferries, 2013). Neuropsychological cases have also shown speech perception impairments as a result of left hemisphere lesions in the STS and anterior STG, whereby Heschl's gyrus and the planum temporale were spared (Barrett, 1910; Henschen, 1918). Anterior temporal regions have also shown stronger activation when processing speech at the sentence level relative to single words (e.g. Stowe *et al.*, 1998; Vandenberghe *et al.,* 2002). One potential explanation for this is that the ATL is responsible for binding together different components of a sentence into one message (Vandenberghe *et al.* (2002)). This hypothesis is concordant with studies that suggest that the left ATL acts an integrative hub in semantic memory (Holland & Ralph, 2010) and therefore is an important substrate in understanding sentences.

Interestingly, the results did not show peak activations in Wernicke's area except for in the right sided homologue in participant 5. This finding supports the notion that posterior STS regions maybe more responsive to speech acoustic signals (Mazoyer

et al., 1993; Binder et al., 1994; Fiez et al., 1995; Price et al., 1996; Warburton et al., 1996), as opposed to speech meaning (Belin et al., 2004). Therefore, it can be hypothesised based on the findings from this chapter and previous studies that posterior STS regions may be more responsive to the acoustic signals associated with speech, but more anterior STS regions are involved in the comprehension of these signals. Due to the spectrally rotated speech signal containing the same acoustic components as the intelligible speech, there was not a marked power change between the two conditions in posterior STS regions. Therefore, the use of spectrally rotated speech and the contrast used only revealed the semantic processing components of intelligible speech.

Notably, minimal changes in power were observed in the beta (15-25 Hz) and low-gamma (30-50 Hz) frequency bands. Previous research has suggested that beta frequencies act as a mechanism for binding the multiple components (e.g. physical, phonological, and semantic) that are contained in speech into a single coherent unit (Scott et al., 2009). These changes in beta may not have been observed in the current study due to the rotated speech matching the physical properties of the intelligible speech. The phonological content between the speech and rotated speech signals differ, however it has been reported that after extensive training spectrally rotated signals can be understood (Blesser, 1972). In previous sentence processing tasks, increases in beta coherence have been correlated with the activation of semantic working memory (Haarmann et al., 2002). However, it could be the case that increases in beta coherence only occur during more semantically challenging tasks. For instance, Haarman et al., (2002) used a gap-filling task to probe semantic working memory.

The 40-60 Hz passive listening findings showed concordance with the verb generation results in terms of determining the language dominant hemisphere. These results also show concordance to previous findings that implicate the role of anterior temporal regions in the processing of intelligible signals. However, the findings in this chapter should still be considered preliminary based on the sample size used and the lack of robust source space statistics. Given the alpha level used in the permutation testing and cluster based correction (<0.01), significant increases in gamma were not observed in the majority of participants and therefore results were expressed as percentage change. A less stringent alpha level could have been used (e.g. <0.05),

however this could have been considered as p-hacking. Due to the contrast used in the passive listening paradigm, the findings reveal only the semantic processing component of the intelligible stimuli as the acoustic features of the signal are controlled for. Based on this, more trials may be required to increase the power of the study to reveal this subtle effect. Currently, the passive listening paradigm lasts 6 minutes and therefore additional trials could be added without jeopardising participant compliance.

4.4.4 Conclusion

The findings in this chapter supports previous findings indicating that MEG can be used as a non-invasive method to investigate language and provide useful information in the presurgical evaluation of TLE patients. As previously mentioned, the findings presented here are only preliminary and a larger study is warranted using a larger sample size of patients whereby iEEG, ESM, or WADA data is available to confirm the MEG findings. The verb generation findings replicate the key beta desynchronisations observed in the Fisher et al. study indicating that the analysis pipeline developed in the previous chapter is fit for purpose in this context. Importantly, this chapter has also demonstrated the potential clinical utility of a passive listening paradigm that may be particularly useful in patients that are non-compliant or are unable to engage in active language tasks.

Chapter 5: Kurtosis Beamforming in Clinical MEG

5.1 Introduction

This chapter aims to focus on the second theme of this thesis and is concerned with the localisation of epileptiform activity. This chapter evaluates the use of kurtosis beamforming as an alternative method for localising interictal spikes in drug resistant epilepsy patients. Reports of the use of kurtosis beamforming for presurgical evaluation are limited, with few studies measuring its concordance with surgically resected areas and post surgical outcomes. The clinical data used in this study was provided by the VU University Medical Center (VUmc), Amsterdam, and co-analysed with Dr Ida Nissen.

5.1.1 Localising Epileptiform Discharges

As described in Chapter 1, MEG has been shown to provide unique information to help guide the placement of iEEG electrodes and inform surgical intervention in patients with inconclusive presurgical findings (Mamelak, et al 2002; Fisher et al., 2005; Knowlton et al., 2006; Sutherling et al., 2008; Stefan et al., 2011; Agirre-Arrizubieta et al., 2014; Nissen et al., 2016). Despite these findings, localising epileptiform activity with the standard clinical MEG analyses are not always successful (Nissen et al., 2016). One of the challenges faced in our patient population is that interical spikes can be infrequent, of low amplitude or multifocal. Therefore, there is a need to improve and thoroughly test alternative MEG localisation approaches, particularly in challenging patient samples where spiking activity is ambiguous.

5.1.1.2 Equivalent Current Dipole Fitting

Typically in MEG, interictal epileptiform discharges are modelled into source space by manually identifying spikes in the sensors waveforms and fitting single equivalent current dipoles (ECDs) to each spike or the spike average (Guggisberg, et al., 2008). This approach is effective in cases of focal epilepsy (Wheless et al., 1999; Papanicolaou et al., 2005; Ossenblok et al., 2007) and is considered the clinical standard by the ACMEGS (Bagic et al., 2011). A number of parameters, including confidence volumes and the GOF value, can be used to evaluate the appropriateness

of each ECD model (Bagic et al., 2011). Criteria for acceptance of the model is usually met if spikes are of sufficient amplitude above background noise, with a single focal source active at the time point of interest (Sekihara et al., 1996; Shirashi et al., 2005).

There are several practical limitations associated with the ECD fitting approach: (1) time required to visually inspect 250+ sensor time series across multiple continuous recordings (Ishii et al., 2008), (2) the expertise required to identify spikes from other transients (Knowlton & Shih, 2004), (3) selection of an appropriate temporal point in the spike for modelling (Bagic et al., 2011), (4) moderate inter-rater reliability (Azuma et al., 2003; Piccinelli et al., 2005), and (5) *a priori* knowledge regarding the number of dipoles (Gaetz & Cheyne, 2003), starting position, and model to be used (e.g. stationary, rotating, or moving dipole) (Russo et al., 2016). Furthermore, some technicians choose to average interictal spikes prior to ECD fitting (Bast et al., 2004; de Jongh et al., 2005) therefore introducing further subjective judgements into the spike selection process.

5.1.1.3 Kurtosis Beamforming

Kurtosis beamforming or SAM(g2) is an alternative method developed to automatically localise spikes using an adaptive spatial filtering approach alongside a higher-level statistic to measure the excess kurtosis (g2) of each region's source time series (Robinson et al., 2004; Kirsch et al., 2006; Prendergast et al., 2013). The underlying hypothesis is that regions containing spikes increase the excess kurtosis value and thereby localise to the irritative zone. A beamformer-based approach has several advantages over ECD: (1) multiple sources can be reconstructed independently without requiring *a priori* knowledge regarding the number of active sources (Vrba & Robinson, 2001; Hillebrand et al., 2005), (2) the signal to noise ratio (SNR) is increased due to the spatial filter attenuating sources of magnetic noise (Adjamian et al., 2009), and (3) beamforming allows virtual electrodes to be computed, revealing the time series for predefined locations in the head. The visual inspection of virtual electrode time series has shown to be valuable in detecting spikes originating from deep structures that are not clearly discernible on the physical sensors (Hillebrand et al., 2016). To this extent, kurtosis beamforming is an objective virtual electrode selection tool that provides a small set of time series for which the user can determine the clinical relevance (i.e., whether they contain spikes or

artefacts). This may overcome the aforementioned limitations of manual spike marking at the sensor-level and subsequent ECD analysis.

Studies evaluating kurtosis beamforming have demonstrated a good level of concordance with other inverse models (Robinson et al., 2004; Kirsch et al., 2006; de Gooijer-van de Groep et al., 2013) and seizure onset zones identified by iEEG (Rose et al., 2013; Wu et al., 2014). Currently, there are few studies measuring the concordance between sources derived from kurtosis beamforming and subsequently resected areas (Guggisberg, et al., 2008; Zhang et al., 2011; Tenney et al., 2014). Zhang et al. (2011) evaluated lesional and nonlesional epilepsy patients and concluded that a favourable post-surgical outcome can be obtained in most patients when MEG (ECD/SAM(g2)) is concordant with either MRI or iEEG. Specifically, they reported that 15/16 MRI-MEG concordant patients achieved favourable surgery outcome after undergoing resective surgery that included the SAM(g2) zone. Tenney et al. (2014) evaluated multiple source algorithms and demonstrated an 89.5% sublobar concordance between SAM(g2) and the resected area in 20 patients, rendering 6 patients seizure free. In this context, it can be suggested that measuring the spatial concordance between the presurgical MEG results and the resected volume in seizure-free patients (i.e. the epileptogenic zone) is the gold standard when validating a particular source localisation approach.

Despite a growing body of research, the implementation of kurtosis beamforming in the clinical analysis of MEG is variable (Scott et al., 2016) and as such may still be considered a research method. This may be based on reports of poorer performances relative to ECD analysis (Guggisberg et al., 2008), or the suggestion that this technique is extensively time-consuming (Guggisberg et al., 2008; Wu et al., 2014) and does not fit into the clinical analysis routine (Guggisberg et al., 2008). Furthermore, the variable use of kurtosis beamforming may be due to clinical MEG sites not having access to kurtosis beamformer software. For example, The Elekta Spikiness beamformer is not readily available to all Elekta sites and the CTF SAM(g2) software is now outdated causing compatibility issues with more recent operating systems.

5.1.2 Aims

The aim of this chapter is to further elucidate the role of kurtosis beamforming in clinical MEG by reporting on its ability to localise the epileptogenic zone in a heterogeneous group of patients. The patients investigated had varying spike frequencies and inconclusive or conflicting MRI and EEG findings prior to MEG referral. This heterogeneous cohort reflects the type of patients often referred for MEG evaluation at the Aston Brain Centre (ABC) and the VUmc, Amsterdam. A comparison between the kurtosis beamformer localisations and the original MEG analysis (ECD fitting) is also carried out.

5.2 Methods

5.2.1 Patients

MEG recordings of 22 patients with drug resistant epilepsy were retrospectively analysed. The patients underwent preoperative evaluation and epilepsy surgery at the VUmc, Amsterdam. Surgery outcome was classified more than 12 months after surgery using the Engel classification system. As the patients only underwent routine clinical care, approval for this study and informed consent was not needed by the institutional review board and conformed with the Dutch health law of February 26, 1998 (amended March 1, 2006), i.e. Wet Medisch-Wetenschappelijk Onderzoek met mensen (WMO; Medical Research Involving Human Subjects Act), division 1, section 1.2.

5.2.2 MEG acquisition

Whole-head MEG recordings were made using an Elekta Neuromag Vectorview system (Elekta Neuromag Oy, Helsinki, Finland) with 306 channels (102 magnetometers and 204 gradiometers) in a magnetically shielded room (Vacuumschmelze GmbH, Hanau, Germany). The acquisition protocol involved eyes-closed resting-state recordings of 15 minutes in the supine position with a 1250 Hz sampling frequency and online filtering (410 Hz anti-aliasing filter and 0.1 Hz high-pass filter). A 3D head-digitizer (Fastrak, Polhemus, Colchester, VT, USA) was used to record the scalp outline and digitise the fiducial landmarks and continuous head position indicator coils. The scalp surface points were co-registered with a T1-

weighted MRI of the patient using the surface-matching algorithm described in Chapter 2.

5.2.3 MEG Preprocessing

The raw data were spatially filtered offline to remove artefacts using the temporal extension of signal space separation (tSSS) (Elekta Neuromag Oy) (Taulu and Simola, 2006). This was implemented in the MaxFilter software using a sliding windows of 10 s and a subspace correlation limit of 0.9 (Maxfilter version 2.1, Elekta Neuromag Oy). Noisy channels were visually identified and excluded before tSSS filtering. A single sphere head model was generated based on the co-registered MRI scalp surface and used in both source reconstruction approaches. The use of the same head model is important as previous studies have often used different head models when comparing analysis method (e.g. single sphere for ECD, multiple local spheres for kurtosis beamformer: Gooijer van de Groep et al., 2013; Kirsch et al., 2006; Wu et al., 2014; Guggisberg et al., 2008), thus making the comparison between methods more convoluted.

5.2.4 ECD analysis

The clinical analysis had already been performed by an experienced EEG/MEG technician. The ECD approach used was consistent with the ACMEGS guidelines (Bagic et al., 2011) and forms part of the standard analysis pipeline used at the VUmc. In summary, spikes in the sensor time series were identified and a single equivalent current dipole model was calculated at each sample from half-way up the ascending limb of the spike until the peak (using Xfit, version 5.5.18, Elekta Neuromag Oy). Typically, ECD models with GOF values above 70% were accepted for further review and were evaluated by a multidisciplinary team of clinicians, physicists and technicians.

5.2.5 Kurtosis Beamformer

The kurtosis beamformer was applied to the presurgical MEG data using the Elekta SSS-Spikiness Beamformer (Beamformer version 2.0, Elekta Neuromag Oy). The SSS-beamformer differs from a conventional beamformer in that it operates on the harmonic function amplitudes and the corresponding lead fields derived from SSS

filtering (Vrba et al., 2010). The kurtosis beamformer works by reconstructing the source time series for each voxel in the source space grid and then computes the kurtosis value for each of these time series. This results in a volumetric map whereby each voxel is represented by a single kurtosis value. A guide on how to replicate the analysis detailed in this section and an example dataset can be found here: https://osf.io/95k8f/.

To ensure that each dataset underwent the same method, a 300s time window was chosen for analysis. This time window was selected to include as many spikes as possible whilst trying to avoid artefacts. Data were band-pass filtered from 20 to 70Hz to provide an optimal contrast for spike identification (Kirsch et al., 2006; Ishii et al., 2008). For each patient, the source space grid (5mm resolution) was computed for a bounding box enclosing the entire head. Beamformer weights were then constructed and virtual electrodes representing each location in source space were computed. The excess kurtosis (g2) value was then calculated for each virtual electrode time series:

$$g_2 = \frac{\Sigma_k^N (t(k) - \mu_t)^4}{N\sigma_t^4} - 3 \qquad (5.1)$$

where *N* is the length of time series *t*, μ is the mean and σ is the standard deviation. The volumetric image was then overlaid onto the co-registered MRI and kurtosis peak locations were extracted using a local maxima algorithm in the MRIView software (MRIView version 1.0, Elekta Neuromag Oy).

Virtual electrode time series corresponding to the peak locations were recomputed using the stored beamformer weights and compared to the physical sensor time series. We considered all peaks that were localised inside the head. From these peak locations, the corresponding virtual electrodes were visually inspected to evaluate whether they contained genuine spikes or artefacts. A montage in the Graph software (Elekta Neuromag, Oy) was used to visualise the virtual electrodes alongside the physical MEG sensor time series in 10 second segments. This montage allowed the cross-validation of transients seen in the virtual electrode with those seen in the physical MEG sensors. Virtual electrodes that robustly localised epileptiform activity (e.g. multiple spikes present in the time series for that location) were selected as the candidate source. The virtual electrode number chosen as the candidate source is reported in Table 1 (e.g. VE1 represents the first volumetric peak location).

To test the value of the kurtosis beamformer in a non-hypothesis driven scenario, no other information (e.g. patient notes, surgical site, EEG, MRI) was used to guide the analysis.

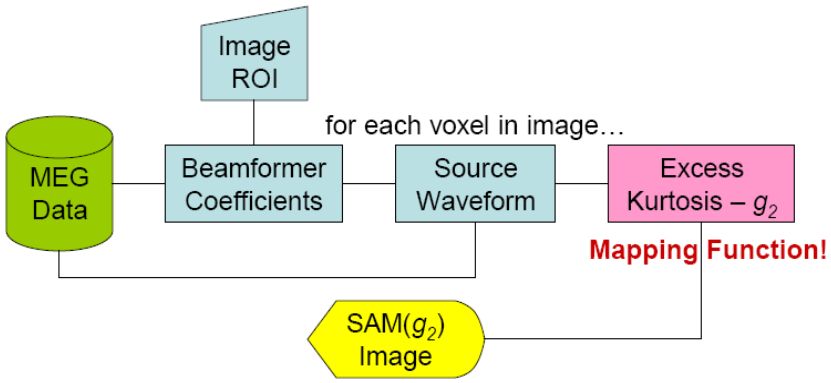

Figure 5.1. A schematic of the kurtosis beamformer pipeline. A scalar beamformer is applied to the MEG data to estimate the source time series for each voxel in source space. The excess kurtosis is then calculated for each source waveform and mapped onto a high resolution MRI.

5.2.6 Resection cavity delineation

The resection cavity was manually segmented based on the three month post-operative MRI using iPlan 3.0 software (BrainLAB AG, Feldkirchen, Germany). Firstly, the post-operative scan was linearly registered with the preoperative MRI (the one used for MEG co-registration). Secondly, the same transformation that was applied to co-register the preoperative MRI with the MEG data was also applied to the resection cavity.

5.2.7 Concordance with resection cavity

For each patient, the ECD point sources and the single kurtosis beamformer candidate (point) source were overlaid onto the presurgical MRI along with the resection cavity delineation. The ECD results were represented by the cluster or main

cluster if the ECDs were scattered. If ECDs were scattered across one lobe, then the centroid of this scatter was used to determine the overlap. In cases of more than one ECD localisation, all localisations were reported and considered. If no spikes or focal slow activity were present, or the ECDs extended across multiple lobes, then this was considered an uninterpretable localisation. The kurtosis beamformer results were represented by the location of the candidate source. An uninterpretable kurtosis beamformer localisation consisted of virtual electrodes not containing any epileptiform activity. Only interpretable results were included in the concordance calculations.

Anatomical concordance was visually assessed based on the overlap of the kurtosis beamformer candidate source, ECDs and the resection cavity. The level of concordance was determined using concordance criteria similar to that used in Kirsch et al. (2006):

I. Concordant, direct overlap of Kurtosis/ECD and resection: Kurtosis beamformer peak/ECD cluster and resection cavity directly overlap.
II. Concordant, partial overlap of Kurtosis/ECD and resection: Kurtosis beamformer peak/ECD cluster and resected cavity are concordant at the lobar level, but do not directly overlap.
III. Discordant, no overlap of Kurtosis/ECD and resection: Kurtosis beamformer/ECD results were uninterpretable or disagreed on location with resection cavity (e.g. scattered ECD results).

5.2.8 Concordance between ECD and Kurtosis Beamformer localisations

The overlay of the ECD point sources and the single kurtosis beamformer candidate source were used to establish concordance in a similar manner as described in the paragraph above:

I. Concordant, direct overlap of Kurtosis and ECDs: Kurtosis beamformer peak and ECD main cluster directly overlap.
II. Concordant, partial overlap of Kurtosis and ECDs: Kurtosis beamformer peak and ECD main cluster are contained in the same lobe, but do not directly overlap.

III. Discordant, no overlap of Kurtosis and ECDs: Kurtosis beamformer peaks and ECD main cluster are in different lobes.

5.2.9 Sensitivity, Specificity, and Accuracy

To evaluate the concordance between the two source localisation methods and the resection cavity, measures of sensitivity, specificity and accuracy were calculated in conjunction with surgery outcome. These measures were calculated only on the interpretable localisations. Sensitivity was based on the number of ECD/Kurtosis beamformer localisations that overlapped with the resection cavity in the patients that were seizure free. Specificity was based on the number of discordant ECD/Kurtosis beamformer localisation with the resection cavity in patients with persistent seizures. More specifically:

Sensitivity = Concordance with resection area in seizure-free patients / all seizure-free patients.

Specificity = Discordance with resection area in patients with persistent seizures / all patients with persistent seizures.

Accuracy = (Concordance with resection area in seizure-free patients + discordance with resection area in patients with persistent seizures) / all patients.

Furthermore, the difference in accuracy (overlap with resection area in seizure-free patients and non-overlap in patients with persistent seizures) between the two methods was tested at the lobar and sublobar level using a chi-square test.

5.3 Results

Presurgical MEG data from 22 patients who subsequently had a cortical resection were retrospectively analysed using a kurtosis beamforming approach. The presurgical findings from before the MEG referral of the patients were inconclusive or conflicting, and are displayed alongside patient characteristics in Table 5.1. The number of spikes present in the MEG recording differed from no spikes (two recordings) to 215 spikes (median: 9 spikes). The kurtosis beamformer resulted in a localisation in 18/22 patients (82%). Of the four patients with an uninterpretable kurtosis beamformer localisation; one had no spikes in the MEG recording (patient 5),

one had no spikes visible on the virtual electrodes (patient 4), and two had excessive artefacts in their recording so that the kurtosis beamformer peaks were either outside the head (patient 6) or the virtual electrodes showed only artefacts (patient 1). The ECD analysis provided interpretable localisations in 20/22 patients (91%), either in a delimited area (cluster in 14 patients) or widespread (scatter in 6 patients).

Table 5.2 shows the concordance of the kurtosis beamformer localisation with the resection cavity and ECD localisation. For the seizure-free patients, in whom the resection cavity corresponds to the epileptogenic zone, the kurtosis beamformer overlapped with the resection cavity in 9/13 patients (69%) (6 direct overlap and 3 partial overlap). Figure 5.2 shows the localisation results and virtual electrode time series for these nine patients. In the patients with persistent seizures (i.e. the epileptogenic zone was not entirely removed or disconnected), the kurtosis beamformer was discordant with the resection cavity in 3/5 patients (60%) (1 direct overlap and 1 partial overlap).

Table 5.3 shows the sensitivity (regarding overlap in seizure-free patients), specificity (regarding discordance in patients with persistent seizures), and accuracy (regarding all correct concordances and discordances). For the kurtosis beamformer, the accuracy was 56% on a sublobar level (direct overlap) and 67% on a lobar level (direct and partial overlap).

Table 5.1. Patient characteristics, MRI findings, number of spikes in the MEG recording, kurtosis beamformer and ECD localisation, location of the resection and surgery outcome (Engel class) are displayed for all patients. The kurtosis beamformer candidate source location is shown under 'Kurtosis beamformer localisation' and the VE peak number is shown under 'Kurtosis beamformer notes' (e.g. VE1 represents the first peak location).

N	Gender / Age	Interictal EEG	MRI	Spikes in recording	Kurtosis beamformer localisation	Kurtosis beamformer notes	ECD localisation	Resection	Outcome
1	F/25	R temporal	Negative	9	-	No VE candidate	L temporal (cluster)	R temporal	4A
2	F/29	L frontotemporal	MTS L	13	R parietal	VE4 best candidate	L temporal (scatter)	L temporal	1A
3	M/29	R frontal and central	Tumor RI	9	R frontal	VE1 best candidate	R frontobasal (anterior tumor boundary) (scatter)	R Frontal / Insular	3A
4	M/52	-	Tumor L frontal	2	-	No VE candidate	L frontal next to resection cavity (cluster)	L temporal	4B
5	F/46	-	Tumor L frontal	No spikes	-	-	-	L frontal	4B
6	F/26	R neocortical posterior temporal	Tumor R temporal	4	-	Artefacts / No VE candidate	R central (cluster)	R temporal	1A
7	M/28	L frontotemporal	Tumor L frontal	6	L frontal	VE4 best candidate	L frontal (scatter)	L frontal	1A
8	M/40	-	Tumor RF (extends to LF)	No spikes	L central	VE1 best candidate	L central (cluster)	R frontal	4C
9	M/23	L temporal	Tumor L temporal	16	R Frontal	VE2 best candidate	L central (cluster)	L temporal	1A
10	F/33	L neocortical fronto- and medial temporal	Mesial Temporal Sclerosis L	8	L temporal	VE2 best candidates	L temporoparietal (cluster)	L temporal	1A
11	F/52	L>R frontotemporal	Mesial Temporal Sclerosis L	4	L temporal	VE1 best candidate	-	L temporal	1A

12	F/43	R and L frontotemporal	Mesial Temporal Sclerosis R	12	R frontal	VE1 best candidate	R neocortical temporoparietal (cluster)	R temporal	1A
13	M/20	R frontal	Dysplasia R frontal	113	R frontal	VE2 best candidate	R frontal and R temporal (scatter)	R frontal	1A
14	F/29	R>L frontotemporal	Optic tumor	85	R temporal	VE1 best candidate	R medial temporal (cluster)	R temporal	1A
15	F/48	L neocortical medial and posterior temporal	Resection L temporal	9	L temporal	VE9 best candidate	L neocortical temporal (cluster)	L temporal	1A
16	F/33	-	Tumor L temporal	16	R temporal	VE3 best candidate	L temporal behind lesion (cluster) and R temporal (cluster)	L frontal	3B
17	M/38	L > R neocortical frontotemporal	Negative	4	R frontal	VE1 best candidate	L centroparietal (cluster)	L temporal	2A
18	M/47	L frontotemporal	Mesial Temporal Sclerosis L	215	L temporal	VE1 best candidate	L temporal (cluster)	L temporal	1A
19	F/28	L>R temporal	Multiple cavernomas	12	L parietal	VE3 best candidate	L temporoparietal (scatter)	L temporal	1A
20	F/30	L and R frontotemporal	Dysplasia R frontal	12	R frontal	VE1 best candidate	Frontocentral, lateralization not possible (scatter)	R frontal	1A
21	M/39	Frontotemporal, lateralization not possible	Bleeding R temporal + frontal	19	R temporal	VE1 best candidate	R temporal (cluster)	R temporal	2A
22	M/52	L>R frontotemporal	Mesial Temporal Sclerosis L	8	L temporal	VE5 best candidate	L Frontal (cluster)	L temporal	1A

Abbreviations: N: patient number, ECD: equivalent current dipoles, F: female, M: male, L: left, R: right, VE: virtual electrode, - : uninterpretable localisation.

ECD localisations were concordant with the resection cavity in 10/13 seizure-free patients (77%) (5 direct overlap and 5 partial overlap) (Table 5.3). In patients with persistent seizures, 5/7 patients (71%) (2 direct overlap) had discordant results. The accuracy was lower for the ECD localisation (50%) compared to the kurtosis beamformer localisation (56%) on a sublobar level, but was higher on a lobar level (75% for ECD analysis and 67% for kurtosis beamformer) (Table 5.3). The differences between the two methods remained non-significant at both the sublobar ($\chi 2$ (1) = 0.117, p = 0.76) and lobar level ($\chi 2$ (1) = 0.320, p = 0.72).

The concordance of the two methods were moderate to high regardless of surgery outcome (Table 5.2). For seizure-free patients with an interpretable localisation by both methods, the kurtosis beamformer coincided with ECD localisations in 7/12 patients (58%) (six direct overlap and one partial overlap). In the patients with persistent seizures, the kurtosis beamformer corresponded to the ECD localisation in 4/5 patients (80%) (three direct overlap and one partial overlap). In total, the kurtosis beamformer co-localised with the ECD analysis in 9/17 (53%) on a sublobar level and in 11/17 (65%) on a lobar level (Table 5.3).

More specifically, the kurtosis beamformer resulted in a more accurate localisation than the ECD analysis in six patients. Of these, the kurtosis beamformer candidate source directly overlapped with the resection area in two patients, whereas the ECD localisations were either uninterpretable (patient 11) or localised to another lobe (patient 22). In patients 7, 13 and 20 the ECDs were scattered and fell both inside and outside of the resection area, whereas the kurtosis beamformer produced an unambiguous source (i.e. the virtual electrode showed clear spiking activity). For example, in patient 20, the ECDs were widespread, whereas the kurtosis beamformer directly overlapped with the resection area. In a further patient (patient 10), the kurtosis beamformer candidate source was adjacent to the resection area in the anterior temporal lobe, whereas the ECDs localised to a more posterior area near the temporal-parietal junction.

Table 5.2. Concordance between kurtosis beamformer localisation, resection cavity, and ECD localisation. Surgery outcome is provided in Engel classes.

Patient	Surgery outcome	Concordance Kurtosis/resection	Concordance ECD/resection	Concordance Kurtosis/ECD
Seizure-free patients				
2	1A	Discordant	Concordant, partial overlap	Discordant
6	1A	-	Discordant	-
7	1A	Concordant, direct overlap	Concordant, direct overlap	Concordant, direct overlap
9	1A	Discordant	Discordant	Discordant
10	1A	Concordant, partial overlap	Concordant, partial overlap	Discordant
11	1A	Concordant, direct overlap	-	-
12	1A	Discordant	Concordant, partial overlap	Discordant
13	1A	Concordant, partial overlap	Concordant, direct overlap	Concordant, direct overlap
14	1A	Concordant, partial overlap	Concordant, partial overlap	Concordant, direct overlap
15	1A	Concordant, direct overlap	Concordant, direct overlap	Concordant, direct overlap
18	1A	Concordant, direct overlap	Concordant, direct overlap	Concordant, direct overlap
19	1A	Discordant	Concordant, partial overlap	Concordant, partial overlap
20	1A	Concordant, direct overlap	Concordant, direct overlap	Concordant, direct overlap
22	1A	Concordant, direct overlap	Discordant	Discordant
Patients with persistent seizures				
1	4A	-	Discordant	-
3	3A	Concordant, partial overlap	Concordant, direct overlap	Concordant, partial overlap
4	4B	-	Discordant	-
5	4B	-	-	-
8	4C	Discordant	Discordant	Concordant, direct overlap
16	3B	Discordant	Discordant	Concordant, direct overlap
17	2A	Discordant	Discordant	Discordant
21	2A	Concordant, direct overlap	Concordant, direct overlap	Concordant, direct overlap

Abbreviations: ECD: equivalent current dipoles, - : uninterpretable localisation

Table 5.3. Sensitivity, specificity and accuracy for the concordance between kurtosis beamformer localisation, resection cavity, and ECD localisation.

	Concordance Kurtosis/resection		**Concordance ECD/resection**		**Concordance Kurtosis/ECD***	
	Direct overlap (sublobar concordance)	Partial + direct overlap (lobar concordance)	Direct overlap (sublobar concordance)	Partial + direct overlap (lobar concordance)	Direct overlap (sublobar concordance)	Partial + direct overlap (lobar concordance)
Seizure-free patients	6/13	9/13	5/13	10/13	6/12	7/12
Patients with persistent seizures	1/5	2/5	2/7	2/7	3/5	4/5
Total	7/18	11/18	7/20	12/20	9/17	11/17
Sensitivity	46%	69%	38%	77%		
Specificity	80%	60%	71%	71%		
Accuracy	56%	67%	50%	75%		

Abbreviation: ECD: equivalent current dipoles

*For the concordance between kurtosis beamforming and ECD analysis, the resection area and surgery outcome was not taken into account, hence sensitivity, specificity and accuracy could is not calculated.

In patients 2, 12 and 19, the kurtosis beamformer candidate sources were discordant with the resection cavity, whereas the ECD localisations partially overlapped. These patients did produce kurtosis beamformer peaks in areas concordant with the resection area but based on our inspection of the virtual electrode time series an alternative candidate source was selected.

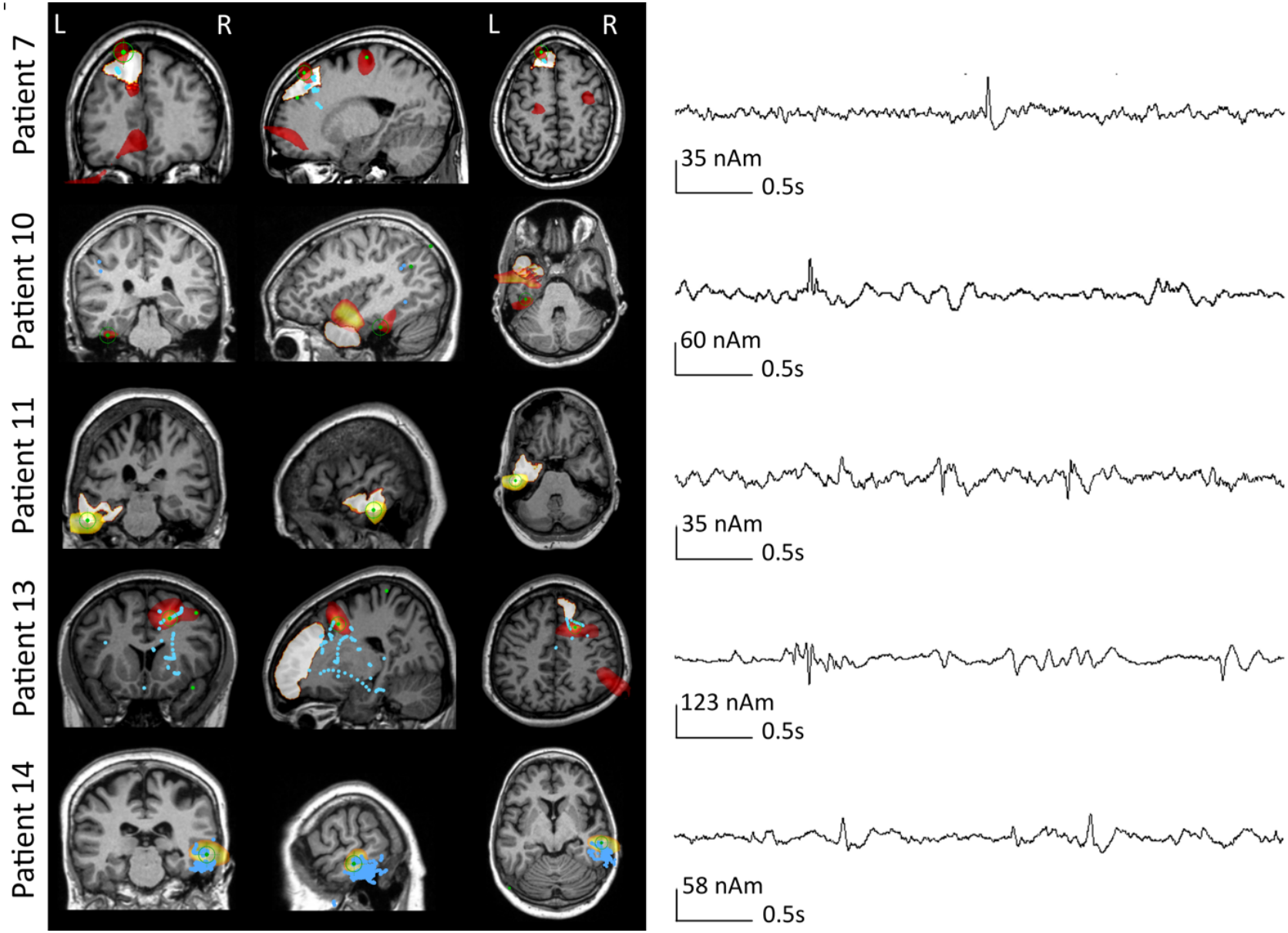
Patient 7
Patient 10
Patient 11
Patient 13
Patient 14
L
R
L
R
35 nAm
0.5s
60 nAm
0.5s
35 nAm
0.5s
123 nAm
0.5s
58 nAm
0.5s

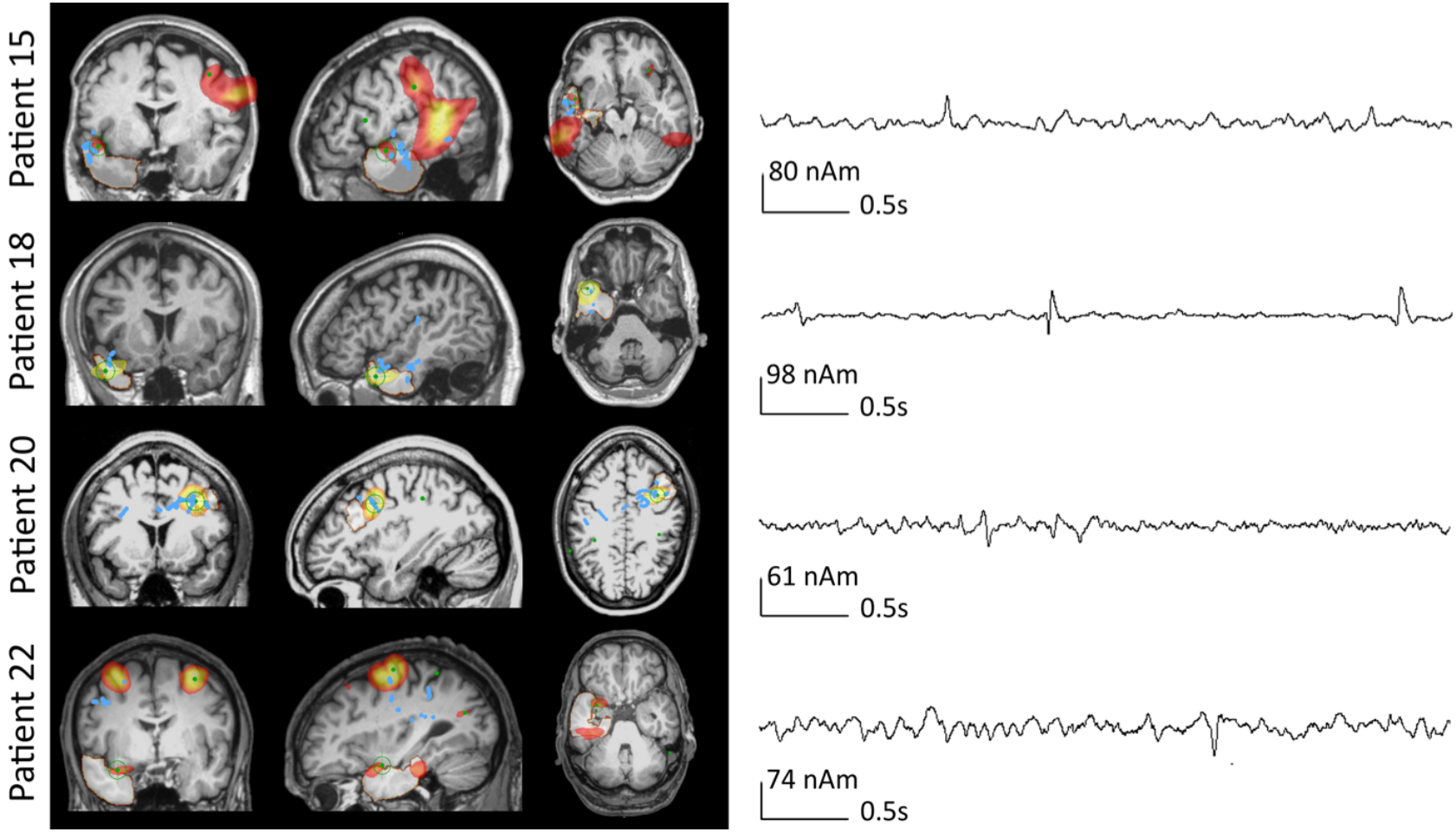

Figure 5.2. Examples of all seizure-free patients, in whom the kurtosis beamformer results were concordant (sublobar and lobar overlap) with the resection cavity. **Left:** the preoperative structural MRI is shown in three views with overlays of the resection area (milky area), kurtosis beamformer results (hot / orange), placement of the VE in the kurtosis peaks (green dots), and ECD location (blue dots). The empty green circle centres on the best VE candidate for the kurtosis beamformer results. Slice views are centred around the kurtosis beamformer candidate source, therefore not all ECD point sources are visible. **Right:** A four second segment of the virtual electrode time series corresponding to the candidate source (the virtual electrode chosen as the kurtosis beamformer localisation) for each patient.

5.4 Discussion

5.4.1 Key Findings

The kurtosis beamformer candidate sources were compared to the clinical ECD analysis and the resection area in both seizure free and seizure persistent patients. We found that the kurtosis beamformer provided an interpretable localisation in the majority of patients (18/22). Of these, the candidate source was contained within the resection lobe in 9/13 seizure-free patients and in 2/5 patients with persistent seizures, yielding an accuracy of 67% on a lobar level. The kurtosis beamformer had a higher accuracy than the ECD analysis on the sublobar level (56% and 50%, respectively) but not on the lobar level (67% and 75%, respectively).

Previous studies that have evaluated the kurtosis beamformer relative to the seizure onset zone in iEEG found lobar concordance in the majority of patients (e.g., Tenney et al. 2014: 16/20; Wu et al. 2014: 20/30 patients; Zhang et al. 2011: 13/20). It can be suggested that the gold standard for evaluating the performance of a clinical source localisation method is by measuring its spatial concordance with the resection area in seizure-free patients (i.e. the epileptogenic zone). In this study, kurtosis beamforming was evaluated by retrospectively comparing its output to the resection area in combination with surgery outcome. This study found a higher level of concordance between the kurtosis beamformer and the epileptogenic zone (9/13) relative to a similar study by Guggisberg et al. (2008) who reported a concordance of 3/11 in seizure-free patients. A key difference between the two studies is that Guggisberg and colleagues did not visually inspect the virtual electrode time series corresponding to the kurtosis beamformer peaks.

It is important to reiterate the necessity for inspecting the virtual electrode time series to rule out artefacts, ensure that kurtosis peaks contain spikes, and to determine the relationship between multiple foci (Rose et al., 2013; Scott et al., 2016). This manual verification step still involves the visual assessment of time series, but only for a small set of virtual electrodes with higher SNR relative to 250+ physical sensors. We found this step not to be as extensively time-consuming as previously suggested (Zhang et al., 2011; Wu et al., 2014). Furthermore, to reduce visual inspection time, a peak-to-

root mean square ratio algorithm can be used to automatically mark spikes in the virtual electrode time series (Kirsch et al., 2006).

In this study, visual inspection of the virtual electrodes that corresponded to the volumetric kurtosis peaks inside the head was critical (5-10 peaks per patient). The highest peaks were not necessarily the best candidates and visual inspection helped to identify sources that coincided with the EZ despite the presence of artefacts. Scott et al. (2016) suggested reviewing the first five kurtosis peaks, which may work well for artefact-free MEG recordings. In contrast, our datasets included several recordings with noisy channels and muscle artefacts, despite our efforts to minimise these. This resulted in multiple artefact-driven peaks. Patient compliance is therefore important for limiting excessive or re-occurring physiological artefacts (e.g. jaw clenching) that may bias the kurtosis metric towards spurious sources.

Another goal of this study was to compare the kurtosis beamformer to the original clinical ECD analysis. Overall, the two methods showed a moderate overlap with one another (53% sublobar, 65% lobar), which is consistent with other studies showing similar or higher lobar agreements (Kirsch et al., 2006; Wu et al., 2014; Zhang et al., 2011). The kurtosis beamformer achieved a higher accuracy at the sublobar level, whereas the ECD analysis showed a higher accuracy at the lobar level. Importantly, our findings demonstrated how the kurtosis beamformer can provide additional information to the ECD analysis. In two seizure free patients (11 and 22), the kurtosis beamformer localised sharp atypical activity to the epileptogenic zone (direct overlap) whereas the ECD analysis resulted in discordant localisations. The clinical value of localising sharp atypical activity remains to be established, however, the ability to do so may be useful in the absence of clear spikes. In three additional patients (7, 13 and 20), ECD scatters fell both inside and outside of the resection area, whereas the kurtosis beamformer gave an unambiguous localisation within the resection area. This suggests that the kurtosis beamformer may instil confidence into the ECD analysis results, particularly when ECDs are scattered.

It was also found that in three patients (2, 12, 19) ECD scatters localised the epileptogenic zone (partial overlap), whereby the kurtosis beamformer candidate

source did not. However, in these patients, the kurtosis beamformer produced multiple peaks containing spikes, some of which overlapped with the ECD scatters. The selection of the candidate source was incorrect in these patients even though the chosen source contained clear and robust localisation of spikes. This reaffirms that interictal spikes are not necessarily an index of the epileptogenic zone (Luders et al., 2006) and can occur in distant or contralateral regions (Zumsteg et al., 2005). This finding highlights the need to interpret the kurtosis beamformer (as well as ECDs) in the context of all available clinical information, which we did not do in this study in order to test its performance in an unbiased way (this included being blind to the resection zone). Evaluating the kurtosis beamformer output in the context of available presurgical findings would have potentially improved our results, and is recommend in clinical practice.

A higher accuracy for the kurtosis beamformer on the lobar and sublobar level relative to ECD has previously been reported (Tenney et al., 2014, Wu et al., 2014). Differences with our results may simply be due to differences in patient population and MEG devices, or could be due to the few spikes in our recording (median: 9 spikes) (see Table 1 for spike count). It could therefore be argued that there were too few spikes for an optimal localisation, as Guggisberg et al. (2008) has demonstrated that accuracy increases when analysing recordings with more than 50 spikes. This is reflected in this study, as the kurtosis beamformer localised the epileptogenic zone in all three patients who produced more than 50 spikes (patient 13,14, and 18). Ultimately, the overall performance of both approaches in this study were comparable.

5.4.2 Limitations

A limitation that affects the comparison of the kurtosis beamformer with ECD analysis is the spatial extent of the localisation. For instance, the kurtosis beamformer candidate source was expressed as a single point source, whereas the ECD analysis resulted in multiple point sources that could be clustered or scattered across lobes. For example, in patient 13 the kurtosis peak is adjacent to the resection area whereas the dipoles are both within and outside the resection area. Other studies comparing these two methods demonstrated a higher accuracy for the kurtosis beamformer on a sublobar level (Tenney et al., 2014) and lobar level (Tenney et al., 2014, Wu et al.,

2014). This difference may be a result of only selecting a single peak to represent the kurtosis beamformer output, whereas other studies included all localisations containing kurtosis peaks. Another limitation in comparing the kurtosis beamformer to the resection area is that the resection site may have been influenced by the ECD findings as they formed part of the original presurgical findings.

5.4.3 Future Research

Recently, a sliding SAM(g2) approach (SAMepi) has been proposed in order to maximise the kurtosis value for sources that produce very frequent spikes (Scott et al., 2016; Harpaz et al., 2015). The problem often encountered in our patient population is that patients tend to produce few interictal spike (Nissen et al., 2016) and may therefore not benefit from this approach. The dependence on spikes is a general limitation of both kurtosis beamforming and ECD analysis, hence alternative methods are needed to generate hypotheses regarding the epileptogenic zone in the absence of spikes. The placement of virtual electrodes in suspected source locations, for example based on MRI and EEG findings, may assist in this situation (Hillebrand et al., 2016). Furthermore, it has been shown that network analysis can identify the epileptogenic zone in MEG data without interictal spikes (Nissen et al., 2017). Future research should continue to focus on developing and validating methods that detect the full spectrum of epileptiform activity (e.g. high frequency oscillations, spikes, atypical slow waves), as well as investigating spike-independent approaches.

5.4.4 Conclusion

This chapter demonstrates that kurtosis beamforming performs comparably to ECD but with fewer subjective steps and less *a priori* information to guide the analysis. This objective approach allows for more time efficient analysis and is particularly useful for less experienced MEG technicians. Furthermore, kurtosis beamforming can assist the ECD analysis by instilling confidence in ECD localisations (particularly when scattered) and in some cases localise unknown or unexpected sources. Based on this, it is proposed that kurtosis beamforming should be integrated into existing clinical protocols to assist in generating hypotheses regarding the epileptogenic zone. This could be achieved with little additional effort by taking the agreement of both

approaches (similar to de Gooijer-van de Groep et al. 2013) and in cases where the methods are discordant, virtual electrodes can be placed in the kurtosis peaks and ECD centroids to determine clinical relevance. Kurtosis beamforming could also be used as a first pass analysis to estimate the number of probable sources to model and to automatically identify spikes in the time series. This may assist in the early subjective steps encountered during the ECD analysis.

The heterogeneous patient cohort used in this study is representative of the patients typically referred to MEG for presurgical evaluation in our centre. The generalisability of these findings may benefit from larger patient studies whereby kurtosis beamforming can be evaluated in subgroups, such as temporal or frontal lobe epilepsy patients. A further limitation is that proprietary software was used to analyse the data and therefore limits replication. Open source approaches to computing the kurtosis beamformer may facilitate larger multicentre studies whereby data from different sites and MEG platforms can be pooled together and analysed using a standardised set of analysis scripts. The next chapter will briefly outline an open source version of the kurtosis beamformer to help facilitate such studies.

Chapter 6: Open Source Kurtosis Beamformer Pipeline

6.1 Introduction

Standardised clinical tools, such as the kurtosis beamformer in open source software could facilitate multi-site collaborations and the pooling of data across multiple MEG platforms. This type of multicentre collaboration and the use of standardised analyses is one of the aims of the MRC-MEG UK partnership, hence the motivation for this chapter. This would allow larger clinical studies to be conducted and greater flexibility to improve and modify code (e.g. in MATLAB), as opposed to proprietary software with limited access (e.g. Elekta software). For example, Prendergast et al. (2013) suggested modifications to the source orientation selection routine to increase the accuracy of the kurtosis beamformer by optimising for kurtosis instead of power**.** This suggestion and the integration of other modifications (e.g. SAMepi, Harpaz et al., 2015) are impossible to integrate within the current Elekta and CTF software. Alternatively, an open source environment would facilitate greater access to the code, allowing improvements to be integrated and tested by the wider user community.

This brief chapter acts as an extension to the previous chapter with the aim of developing an open source kurtosis beamformer pipeline. Importantly, this pipeline can be implemented using data from any of the main MEG platforms[5]. This pipeline uses the Fieldtrip functions and is applied to two patient datasets that were acquired on the same day in both CTF and Elekta MEG systems at the ABC. For validation, the source localisations for these datasets are compared to the results gained from their respective vendor kurtosis beamformer software.

[5] Supported MEG data fromats: CTF, Elekta/Neuromag, 4D/BTi, Yokogawa.

6.2 Methods

6.2.1 Patient Data Acquisition

Two patients were recorded at the Aston Brain Centre on the same day using a 275 channel CTF MEG system (MISL, Coquitlam, Canada) and an Elekta Neuromag Triux (Elekta Neuromag Oy, Helsinki, Finland). The CTF data was sampled at 1200Hz with an anti-aliasing filter of 300 Hz, and a third order gradiometer configuration. The Elekta data was sampled at 2000 Hz with a 330 Hz anti-aliasing filter and 0.1 Hz high-pass filter. The Elekta data was tSSS filtered and motion corrected using a sliding window of 10 s and a subspace correlation limit of 0.9 (Maxfilter version 2.2, Elekta Neuromag Oy). In both MEG platforms, non-continuous epochs of data were acquired lasting between 2-5 minutes in the seated upright position. Data from both scanner platforms were coregistered using the head surface matching algorithm described in chapter 2.

6.2.2 Fieldtrip Kurtosis Beamformer

This kurtosis beamformer implementation is fundamentally the same as the pipeline described in the previous chapter, however a conventional beamformer was used as opposed to an SSS-beamformer. In the Fieldtrip toolbox for MATLAB (Oostenveld et al., 2011), data were band-pass filtered from 20 to 70Hz, a single shell head model was generated based on the segmented brain and a 5mm source space grid was used. A single covariance window spanning the entire dataset was used and a scalar LCMV beamformer was used to estimate the source time series for each location in source space. The kurtosis function in MATLAB was iteratively applied to each of the source time series to generate a volumetric kurtosis image. A peak finding algorithm written in MATLAB was then used to find local maxima within the volumetric image. For the analysis, the top peak location was plotted and the corresponding virtual electrode was reconstructed by applying the beamformer weights for that location to the data. Figure 6.1 shows a basic schematic of the fieldtrip functions used in this pipeline. Example code can be downloaded from https://osf.io/95k8f/.

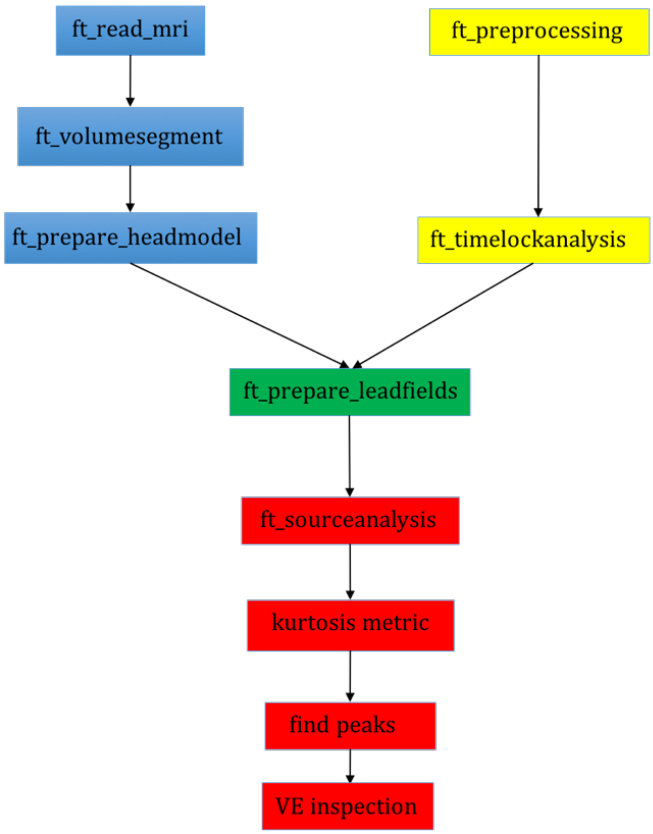

Figure 6.1. The Fieldtrip functions used in the kurtosis beamformer. Note kurtosis is applied using the MATLAB kurtosis function and the find peaks algorithm is in-house code.

6.2.3 SAM(g2) and Spikiness Beamformer

To compare the Fieldtrip localisations with some form of standard, the CTF SAM(g2) and Elekta Spikiness Beamformer was also computed in the CTF and Elekta datasets, respectively. The implementation of these methods were the same as described in the previous chapter, however the Elekta Spikiness Beamformer was computed using Beamformer version 3.0 (Elekta Neuromag Oy) and used a single shell BEM model generated in the Xfit software (version 5.5.18, Elekta Neuromag Oy). The SAM(g2) beamformer was computed in the ctf-5.1 software (MISL, Coquitlam, Canada) and used a multiple local spheres model.

6.3 Results

The open source pipeline implemented in Fieldtrip indicates concordant localisations between the CTF and Elekta datasets, and spatial concordance with the results produced in the respective vendor software.

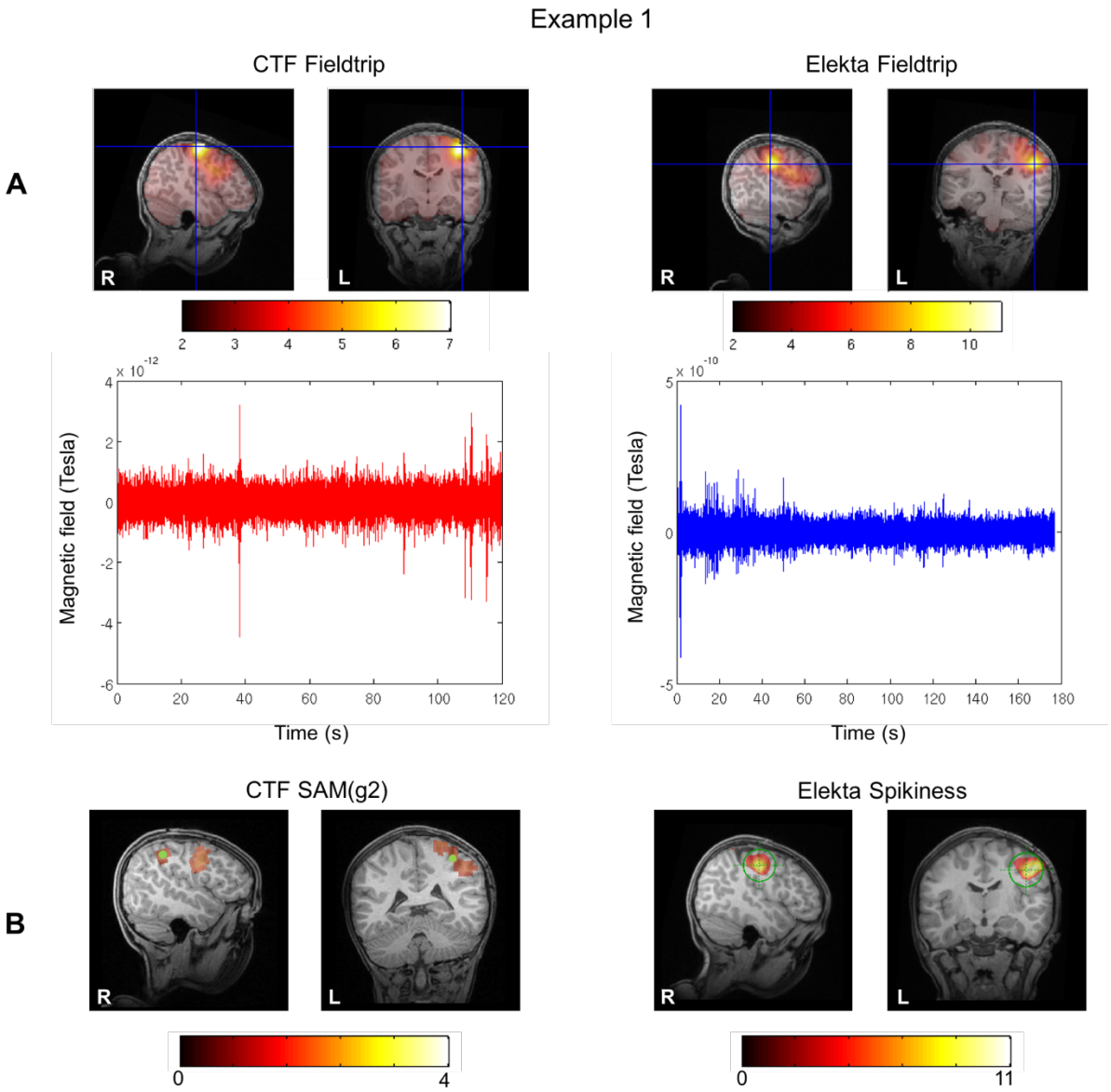

Figure 6.2. Example 1 of the Fieldtrip kurtosis beamformer. A) The Fieldtrip kurtosis beamformer volumetric images for CTF and Elekta data. The peak source localisations are indicated by the blue cross hairs and corresponding virtual electrodes are plotted underneath. B) The CTF SAM(g2) and Elekta Spikiness Beamformer localisations for the same datasets. For CTF SAM(g2) data, the peak source is indicated by a green dot. For the Elekta Spikiness data, the peak source is indicated by the green target.

In example 1 (Figure 6.2), the first volumetric peak from the Fieldtrip kurtosis beamformer show similar results for both the CTF and Elekta datasets. These peaks localise to areas adjacent to an anatomical lesion in the right parietal lobe. The virtual electrodes corresponding to the top peaks are plotted below the volumetric images and clearly show spiking activity several magnitudes larger than the background activity. For comparative purposes, the kurtosis beamformer was also implemented in the CTF SAM(g2) and in the Elekta Spikiness beamformer software for the CTF and Elekta data respectively. Both volumetric images indicate regions close to the regions identified by the Fieldtrip kurtosis beamformer, although the peak locations were not identical.

Example 2 (Figure 6.3) further demonstrates concordant localisations between the top peak locations in the CTF and Elekta datasets. The corresponding virtual electrode time series again shows clear spikes above baseline activity. The first peak in the CTF SAM(g2) volumetric image also coincides with the anatomical region identified by the Fieldtrip results. Further, the Elekta Spikiness beamformer indicates the same region, however this was the second volumetric peak. The first volumetric peak indicated a region in the right parietal lobe not visible on the slice view in Figure 6.3.

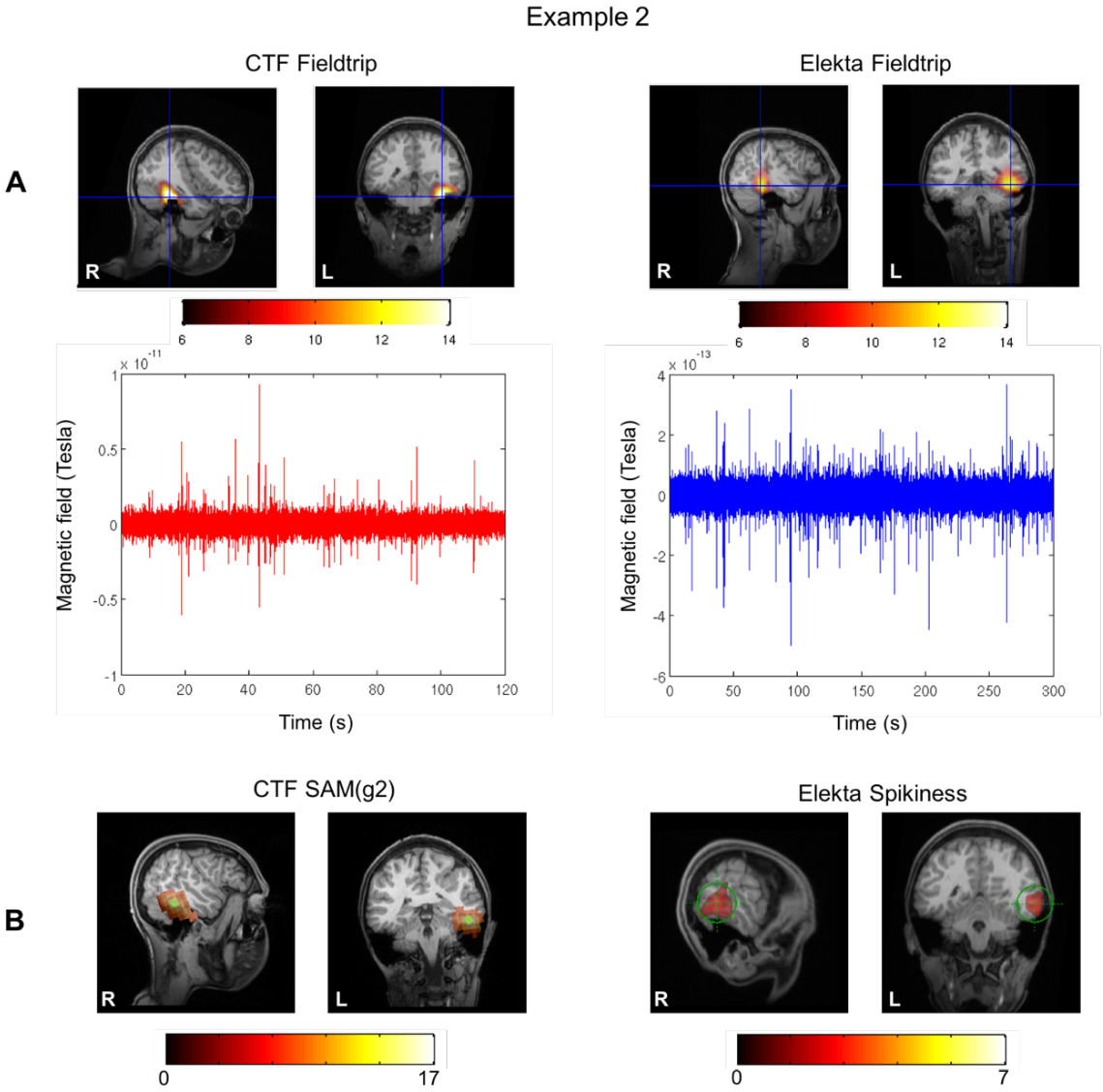

Figure 6.3. Example 2 of the Fieldtrip kurtosis beamformer. A) The Fieldtrip kurtosis beamformer volumetric images for CTF and Elekta data. The peak source localisations are indicated by the blue cross hairs and corresponding virtual electrodes are plotted underneath. B) The CTF SAM(g2) and Elekta Spikiness Beamformer localisations for the same datasets. For CTF SAM(g2) data, the peak source is indicated by a green dot. For the Elekta Spikiness data, the peak source is indicated by the green target.

6.4 Discussion

This brief chapter outlined an open source implementation of the kurtosis beamformer in order to work towards a standardised pipeline that could be used to pool data from different sites and MEG platforms to facilitate a multi-centre clinical study. The results demonstrated that the Fieldtrip kurtosis beamformer implementation is able to localise voxels that contain interictal spikes and that these localisations correlate well with the MEG vendor software. The advantage of the method used was that the same patients were measured in both CTF and Elekta MEG platforms on the same day. The results showed that for examples 1 & 2, the top peak locations were concordant but not identical. This is likely to be a result of the differences in the sensor configurations and noise profiles of the two systems, alongside physiological and spiking variability between sessions (Ou et al., 2007).

To further establish the kurtosis beamformer pipeline in Fieldtrip, a more systematic comparison will be undertaken. This will also involve an implementation in the MNE software. This comparison will compare spatial locations and corresponding virtual electrodes from a series of patients recorded in both CTF and Elekta MEG systems. This is a worthwhile venture as Elekta are no longer distributing the spikiness beamformer to new sites and the CTF software is outdated leading to compatibility issues with newer operating systems.

Chapter 7: Rank Vector Entropy

7.1 Introduction

Chapter 5 demonstrated how kurtosis beamforming can provide additional value to the clinical analysis of MEG data in patients with complex etiologies. However, as demonstrated, these techniques do not always accurately localise the epileptogenic zone and therefore additional approaches are required to improve the sensitivity of presurgical MEG. This proof of concept chapter outlines the use of a novel measure to analyse the MEG signal with the goal of providing additional value in the presurgical evaluation of drug resistant epilepsy patients.

As mentioned in the discussion of chapter 5, the dependence on spikes with a relatively good SNR is a general limitation of common clinical MEG analysis techniques. Patients referred to the ABC can often have ambiguous spiking patterns and may only exhibit atypical slow-wave activity or other transient abnormalities that do not lend themselves well to ECD fitting or kurtosis beamforming (see Figure 7.1). Furthermore, these patients may only produce low amplitude spikes that are difficult to detect and localise. Based on these observations, it is important to develop novel **s**ignal processing techniques that are able to detect the full spectrum of epileptiform activity to yield useful information in patients that do not produce high SNR interictal spikes. A way to achieve this could be by looking at the moment-to-moment variability, or entropy, within the signal.

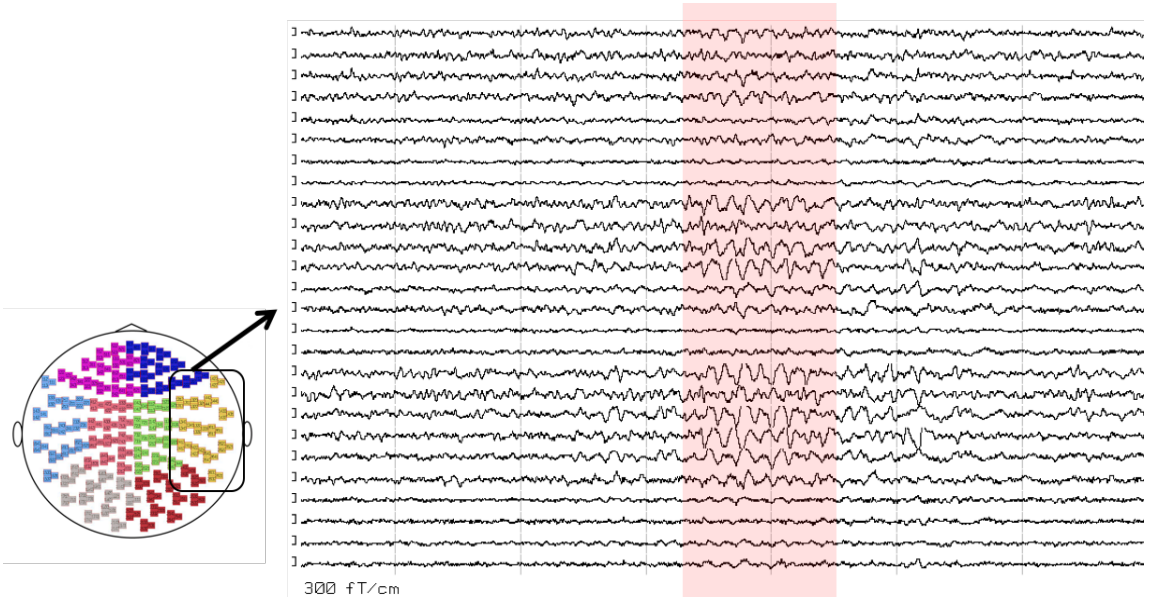

Figure 7.1. An example of a patient recorded at the Aston Brain Centre who did not produce any interictal spikes during the 45 minute recording session. This dataset contained bursts of high amplitude slow-wave activity over the right temporal sensors.

7.1.1 Entropy

Typically, neural activity is modelled by defined narrow-band oscillatory signals (theta, delta, alpha, beta, gamma) and are thought to be coupled to one another via networks (Robinson et al., 2012). A recent review by Garrett et al. (2013) proposed an alternative concept for measuring neural responses by assessing the moment-to-moment signal variability to study human brain functioning in health and disease. Entropy is a metric that can be used to quantitatively measure the variability, or disorder, in a system. Measures of source space entropy in MEG can therefore allow the spatiotemporal assessment of disorder in the brain (Brookes et al., 2014). Signals that have low predictability and high variability (e.g. Gaussian noise) result in high entropy, whereas signals with high predictability and low variability (e.g. oscillations) exhibit low entropy (Brookes et al., 2014).

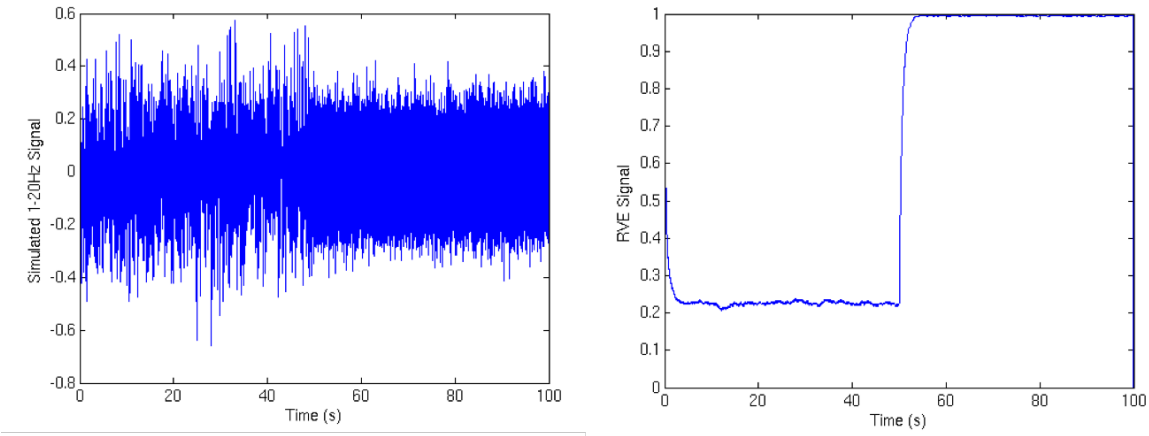

Figure 7.2. Left: Simulated signal (1-20Hz), and Right: Rank Vector Entropy (RVE) transform of the same signal. See Appendix1, for information on signal generation. The first 50 seconds of the signal are composed of 'brain-like' oscillations, and the latter 50 seconds is random noise. The RVE signal is low for the brain-like oscillatory signal and increases for the random noise, demonstrating that signals with less predictability exhibit high entropy.

7.1.2 Rank Vector Entropy

Research into entropy has often been limited by studies involving EEG/MEG sensor space analysis or by only assessing the long term properties of entropy and therefore lacking temporal resolution. This includes studies using Lempel-Ziv complexity (Fernandez et al., 2011), transfer complexity (Vakorin et al., 2010) and the comparison of multiple entropy measures (Bruna et al., 2012). Sliding block methods have previously been used to estimate temporal changes in entropy (Adler and Marcus, 1979), however are computationally inefficient when applied to thousands of voxels.

Alternatively, Robinson et al. (2013) developed a methodology, rank vector entropy (RVE), to measure the broadband, non-linear properties of the MEG signal in source space (Robinson et al., 2013). RVE is a non-parametric measure of entropy that estimates the complexity of information contained within a neurophysiological signal based on the probability distributions of "brain states" (Robinson et al., 2013). The

novel aspect of RVE is its initial encoding of the time series that rank orders n-samples in respect to their magnitude. A sliding window containing n-samples is then progressed through the time series resulting in a rank vector for each set of samples (see section 3.1.4 for method). This method is therefore invariant to the absolute signal amplitude of the time series and only regards the relative amplitude within each window.

Robinson and colleagues demonstrated the application of RVE in various MEG experiments including a resting state and auditory oddball task. It was reported that under resting state conditions there was no correlation between the temporal and spatial patterns of RVE and the Hilbert envelope of power (4-150Hz). The auditory oddball task however revealed reductions in entropy coinciding with the $N100_m$ peak for frequent and combined tones. Interestingly, for rare tones, there was a slow increase in entropy starting at approximately 250ms corresponding to the mismatch negativity signal. This asynchronous neural activity suggests that increases in entropy may therefore signify the engagement of attentional mechanisms.

The potential advantage of RVE is that it is independent of absolute amplitude and therefore sensitive to other properties of the signal that conventional approaches are not. When considering this method in the context of epilepsy patients referred for MEG at Aston (equivocal spiking patterns, low amplitude spikes, abnormal low frequency waves), RVE may be useful in detecting a range of epileptiform activity, including; typical interictal spikes (20-70Hz), slow waves (<10Hz), low SNR spikes and other transient abnormalities. RVE may therefore produce a more complete picture when attempting to detect and localise abnormal activity embedded in the patient's source time series.

Due to the limited research on RVE and its novel application in epilepsy, this chapter is exploratory to the extent that it aims to answer whether RVE is able to localise areas of interest in patients being evaluated for surgery and if so, what additional value can it provide. If we take what is known about epilepsy and the generation of ictal and interictal epileptiform activity (i.e. the hypersynchronisation of neural assemblies), it can be hypothesised that entropy will decrease during these periods of time. Interictal

spikes for example have a clear rise and drop that is likely to result in the generation of a predictable signal. Similarly, a burst of abnormal slow-waves will also have a highly predictable oscillatory signal and would be expected to cause a decrease in signal entropy.

7.1.3 Aims

To test the entropy reduction hypothesis, this chapter will first evaluate whether the RVE signal decreases in response to single virtual electrode time series containing interictal spikes. Secondly, RVE will be applied to whole-head source time series to determine whether RVE is able to provide valuable spatial localisations regarding the irritative zone and assess its suitability in detecting different types of transients. In this chapter, RVE is applied to both Elekta and CTF datasets, demonstrating the use of this methodology across different scanner platforms.

7.2 Method

The original MATLAB code for the RVE method was provided by Dr Matthew Brookes (Nottingham University) and was specific to CTF datasets. The RVE method had not yet been tested on epilepsy datasets, therefore initial testing was carried out on single virtual electrodes in CTF data (section 3.1). Based on these findings, considerable work was carried out to adapt the code to run a beamformer and RVE transformation on Elekta data (section 3.2). This was done in order to provide a pipeline for future use in the ABC. The development of the Elekta RVE code also reduced processing time to 2.5 hours (originally 22-24 hours on an 16GB, 12 core machine). This involved introducing parallel processing (parfor) in the MATLAB code where possible and the RVE computations were carried out in C++ before being saved back as a MATLAB variable. Code development was completed with the assistance from Dr Caroline Witton.

7.2.1 Patients

Eight paediatric drug resistant epilepsy patients with various spiking patterns and etiologies were included in this study. These patients were selected as they reflected the diverse range of paediatric patients that are referred to the ABC for MEG. These patients were recorded at the ABC as part of their ongoing presurgical evaluation and previous clinical analysis had been performed on them as part of their presurgical workup.

7.2.2 MEG Data Acquisition

As described above, initial testing was carried out using CTF data (patients 1-4) and further application of the RVE method was carried out on Elekta data (patients 5-8).

7.2.2.1 CTF data

MEG data was acquired from four patients (patients 1-4) using a 275 channel CTF MEG system (MISL, Coquitlam, Canada) with an anti-aliasing filter of 300 Hz, and a third order gradiometer configuration in a three layer (inner mu metal) magnetically shielded room (Vacuumschmelze GmbH, Hanau, Germany). Non-continuous epochs of data were acquired lasting between 2-5 minutes, resulting in a total recording time ranging between 45-90 minutes. Data was recorded in the seated position, and sampled at either 600, 1200, or 2400Hz. All datasets sampled above 600Hz were subsequently downsampled to 600Hz for the RVE analysis. Three fiducial coils were attached to the patient for head localisation.

7.2.2.2 Elekta data

Four patients were recorded using an Elekta Neuromag Triux system (Elekta Neuromag Oy, Helsinki, Finland) with 306 channels (102 magnetometers and 204 gradiometers) in a magnetically shielded room (Vacuumschmelze GmbH, Hanau, Germany). The acquisition protocol involves 5 minutes of eyes-open resting-state recordings obtained in the 68° seated upright position with a 2000 Hz sampling

frequency and online filtering (330 Hz anti-aliasing filter and 0.1 Hz high-pass filter). For the RVE analysis, all datasets were downsampled to 500Hz. Head localisation was performed by attaching 5 coils on the patient's head.

Data from both scanner platforms were coregistered using the head surface matching algorithm described in chapter 2.

7.2.3 Rank Vector Entropy Method

The RVE algorithm was applied to the SAM source time series to produce RVE transformed source time series. The RVE algorithm operates by selecting lagged samples, ξ, by using the sampling rate, *fs*, and the low pass-filter frequency

, *fc*:

$$\xi = \frac{fs}{2fc} \tag{7.1}$$

Therefore, a sampling rate of 600Hz and a low-pass filter of 150Hz would result in ξ=2, meaning every second sample point is selected for further analysis (ξ=2). If ξ is a non-integer then it is rounded to the nearest integer. A sliding sub-window of **W** lagged-samples (ξ intervals) starting at sample point *i* is then applied to the source times , and can be expressed as $\mathbf{W_k} = [x_i, x_{i+\xi}, x_{i+2\xi}, x_{i+3\xi} \ \ldots \ x_{i+(W-1)\xi}]$. This vector is then converted to its rank vector in relation to the magnitude order of the samples. For example, the vector $\mathbf{W_k} = [1.2 \ 3.0 \ 4.7 \ 3.2 \ 5.6]$ would yield the rank vector of $\mathbf{R_k} = [1 \ 2 \ 4 \ 3 \ 5]$.

A state symbol is then allocated to the rank vector using a generated look up table that contains every possible rank vector. Given that $\mathbf{W_k}$ contains **W** samples the look up table will contain **W**! possible symbols. For example, if **W** = 5 then the look up table will contain 120 unique rank vectors. A state symbol is allocated based on the hierarchal ordering of the rank vectors (e.g. $\mathbf{R_k} = [1, 2, 3, 4, 5]$ would be allocated a symbol of 1). The window, $\mathbf{W_k}$, then advances through the time series one lagged sample at a time ($\mathbf{W_k} = [x_{i+\xi}, x_{i+2\xi}, x_{i+3\xi}, x_{i+4\xi} \ \ldots \ x_{i+(W-1)\xi}]$) generating a new rank vector and state symbol at each iteration.

$\mathbf{W}_k$ is then advanced through the time series by incrementing *i*, generating a frequency histogram $\mathbf{F}_i$, which counts the frequency of each state symbol's occurrence. For random data (e.g. neurophysiological data) there is an equal likelihood of each state symbol occurring and a flat frequency distribution would be the likely outcome yielding only the absolute entropy. A leaky integrator is used to quantify the temporal evolution of entropy. This allows the integration of the result across a function of time whilst 'leaking out' information of previous states encountered. This leaky integrator is determined by introducing an integrator decay rate τ, whereby τ represents the time taken for histogram counts to decay by 1/e of their original value. This integrator decay rate is then used to calculate a time constant a whereby

$$\alpha = exp(-1/f\tau) \tag{7.2}$$

The time constant α is applied to each iteration of the algorithm so that $\mathbf{F}_i = \alpha\mathbf{F}_{i-1}$ where α must be <1 in order for the temporal dynamics of entropy to be estimated.

The altered frequency distribution, $\mathbf{F}_i$, is then normalised by the absolute integral of all symbol frequencies to produce a probability distribution. For each time point, Shannon's entropy is then be computed.

$$S(k) = \frac{1}{ln(w!)} \sum_{n-1}^{w!} -p_n(k) ln\left(p_n(k)\right) \tag{7.3}$$

The RVE parameters in the present study consisted of a time constant τ = 0.3s, sample lag ξ = 2, window length w = 5 and a band-pass filter frequency of 1-150Hz. These parameters are based on the original Robinson et al. (2013) study.

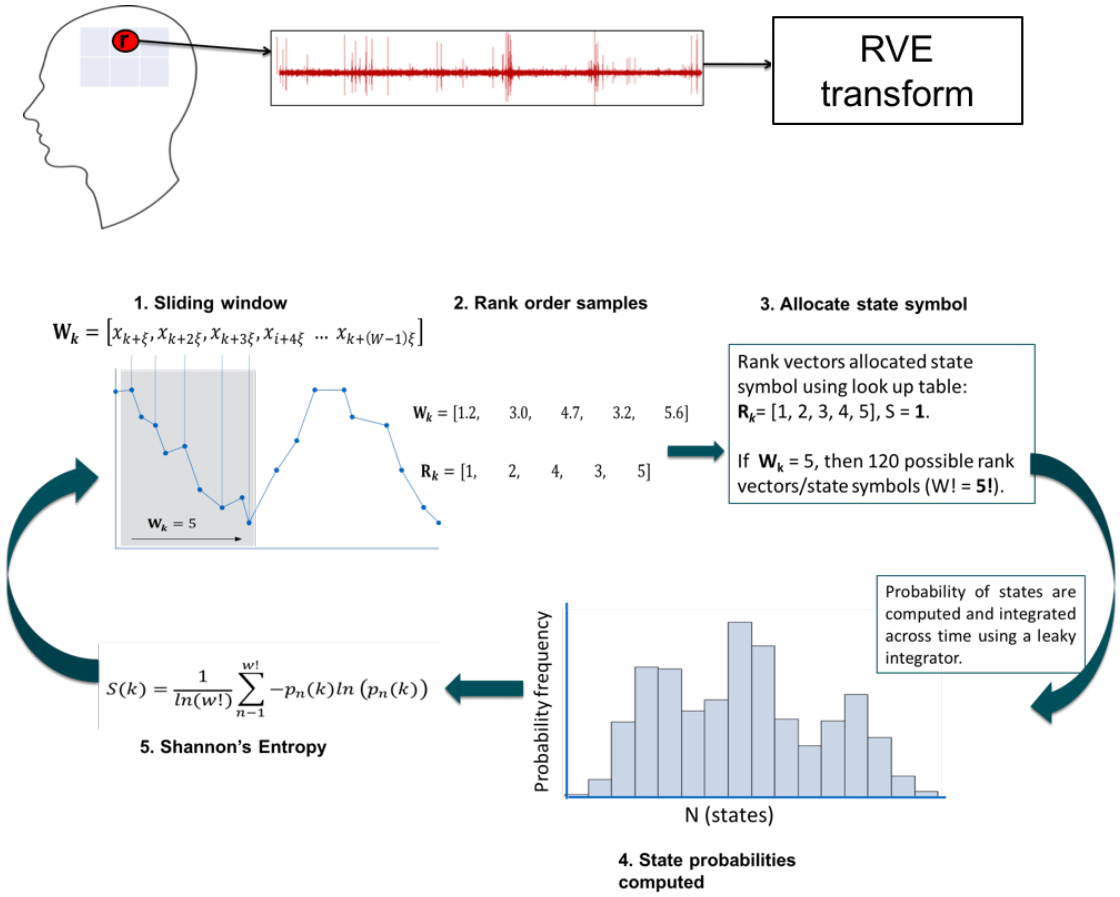

Figure 7.3. A schematic of the RVE method. Source time series are estimated using a SAM beamformer and then converted into RVE time series.

7.2.4 Virtual Electrode Selection

To investigate the temporal evolution of RVE in response to epileptiform activity, a single virtual electrode (1-150Hz) from four patients (patients 1-4) was reconstructed at a coordinate identified by the kurtosis beamformer. The kurtosis beamformer method used was the same as that described in Chapter 5, however it was computed using the CTF SAM(g2) software (20-70Hz) using a local spheres head model. Before the RVE transformation was computed, each virtual electrode was visually screened to establish it contained spikes. After RVE transformation, minima in the RVE signal were marked using an automatic detection algorithm in MATLAB. This was achieved by inverting the signal and then computing the root-mean-square (RMS) of the data and using a peak finding algorithm to mark peaks in the data that pass a threshold of 0.5. This threshold of 0.5 was arbitrary but reflected the small fluctuations observed

in the RVE signal. The original RVE signal was then plotted and time points identified by the previous step were marked on the time series. This enabled the sufficient marking of time points relating to local minima allowing decreases in entropy to be visually compared to spikes in the virtual electrodes.

7.2.5 Whole Head RVE Beamforming

Data were motion corrected and filtered offline to remove artefacts using the temporal extension of signal space separation (tSSS) with a sliding windows of 10 s and subspace correlation limit of 0.9 (Maxfilter version 2.2, Elekta Neuromag Oy). Noisy channels were visually identified and excluded prior to tSSS. A single layer BEM model was generated based on the co-registered MRI scalp surface using the Xfit software (Xfit version 5.5.18, Elekta Neuromag Oy). A scalar Elekta SSS-Basic Beamformer (Beamformer version 3.0, Elekta Neuromag Oy) was applied to the continuous data (1-150Hz) to estimate the source time series of each brain location (5mm resolution).

The beamformer source time series were then inputted into the RVE algorithm to compute RVE source time series. RVE time series were then standardised (z-score) and a functional volumetric image was computed by taking the absolute minimum value of each RVE time series. A local minima algorithm was used in the mri3dX software to generate a list of ‘peak’ (minima) locations.

7.3 Results

7.3.1 Single virtual electrode RVE analysis

To test the hypothesis that interictal discharges cause a reduction in entropy, i.e. a reduction in the RVE signal, virtual electrodes in four patients were identified using a kurtosis beamformer and then transformed into RVE time series. These virtual electrodes contained various types of epileptiform activity. To assist in the visual inspection of the time series, a peak finding algorithm was used to identify negative

peaks in the RVE signal represented by black dashed lines. The virtual electrode findings show a clear relationship between interictal activity and reductions in entropy.

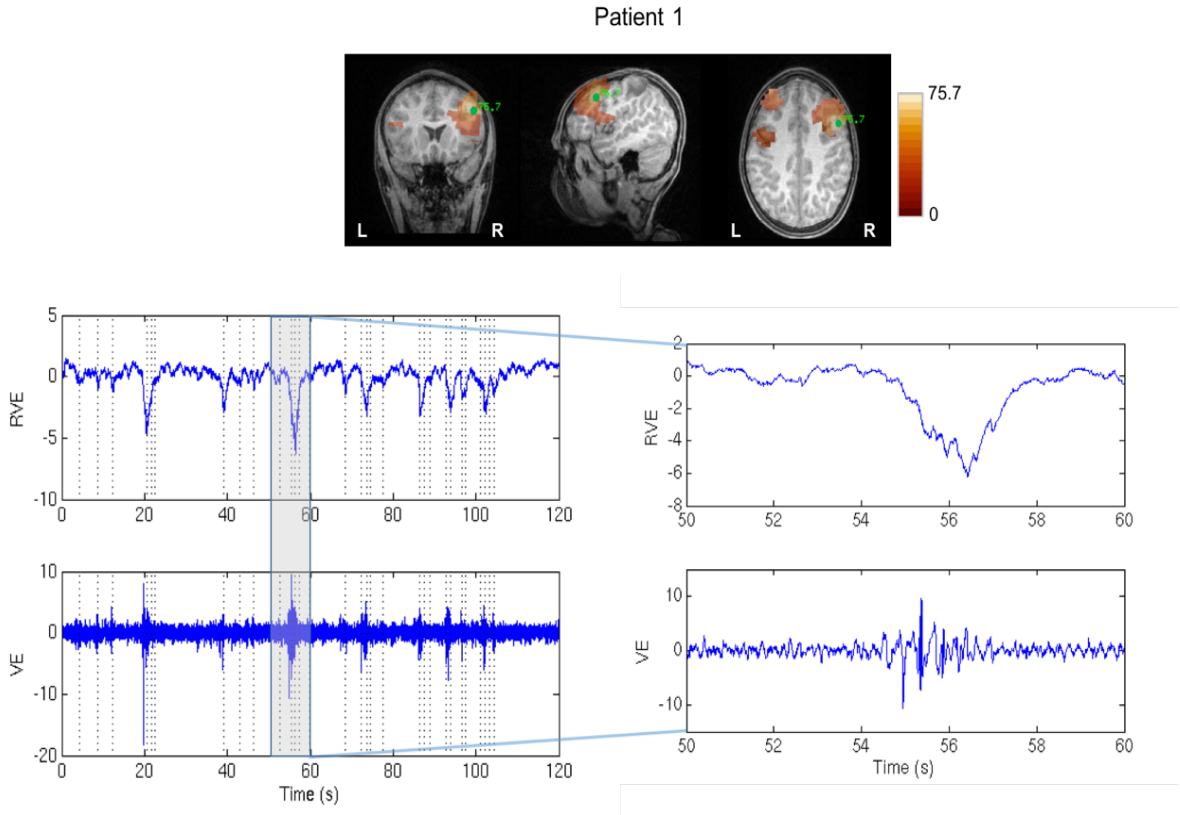

Figure 7.4. Top: Kurtosis beamformer peak localisation (green dot) overlaid onto the patients T1 anatomical MRI. The functional overlay is thresholded to half the maximum value. Bottom: The rank vector entropy (RVE) time series (top) and the virtual electrode (bottom) corresponding to the kurtosis peak location. The left set of time series shows the entire epoch (120s), the right time series show a 10s selection showing the decrease in RVE signal and the epileptiform activity in the virtual electrode.

In Figures 7.4 - 7.7, the left set of time series show the RVE and VE time series across the whole epoch (120s), with the right set of time series showing a 10 second extract indicated by the transparent grey box. In patients 1-3, the 10 second segments show polyspike complexes in the virtual electrode and clear decreases in the RVE signal during the same time period. Similarly, patient 4 shows a small, transient sharp wave at ~118 seconds, which is also shown to be sensitive by RVE. This is further demonstrated in figure 7.7, whereby a 2 second segment is extracted to clearly

visualise the sharp wave. It is also evident that there is a small lag (<1s) in the RVE decreases relative to the discharge onset.

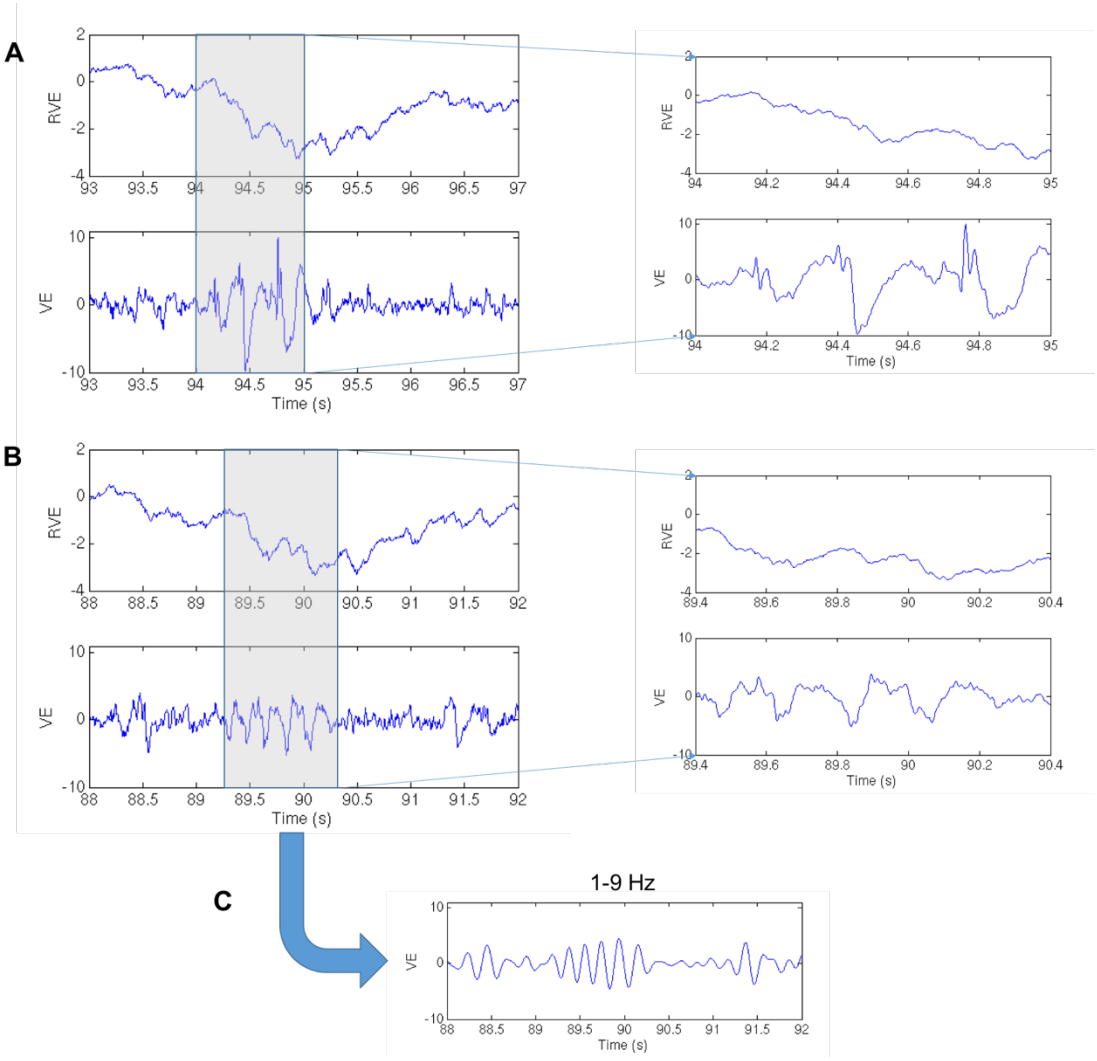

Figure 7.5. Further examples from Patient 1: Reductions in RVE in relation to (A) polyspike and wave and (B) abnormal slow-wave activity. (C): The same slow-wave activity displayed but band-pass filtered from 1-9Hz. Note the virtual electrode amplitude differences between the polyspike and wave and the slow-wave activity.

In all four patients, it is notable that interictal discharges result in a decrease in the RVE signal, with the largest RVE decreases not necessarily corresponding to the largest spikes. Figure 5, for example shows how RVE is also sensitive to atypical slow-wave rhythms, whereby there is a comparable decrease in RVE relative to the

clear polyspike complexes. Further, the polyspike and wave activity is of a much larger amplitude, yet reductions in RVE are consistent in both cases.

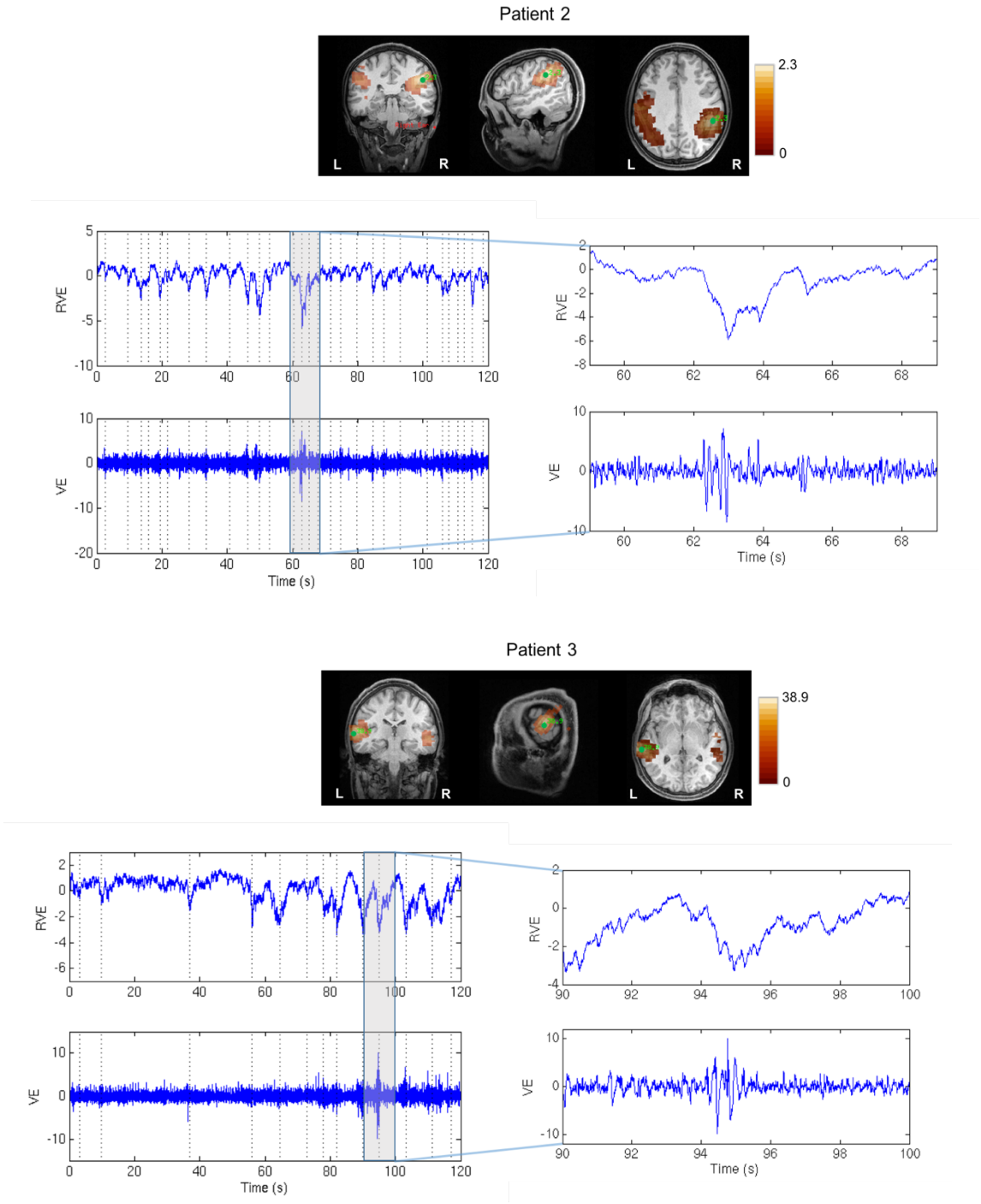

Figure 7.6. Patients 2 and 3 single virtual electrode analysis. Top row: Kurtosis beamformer peak localisation (green dot) overlaid onto the patients T1 anatomical MRI. The functional overlay is thresholded to half the maximum value. Bottom row: The rank vector entropy (RVE) time series (top) and the virtual electrode (bottom) corresponding to the kurtosis peak location. The left set of time series shows the entire epoch (120s), the right time series shows a 10s selection showing the decrease in RVE signal and the epileptiform activity in the virtual electrode.

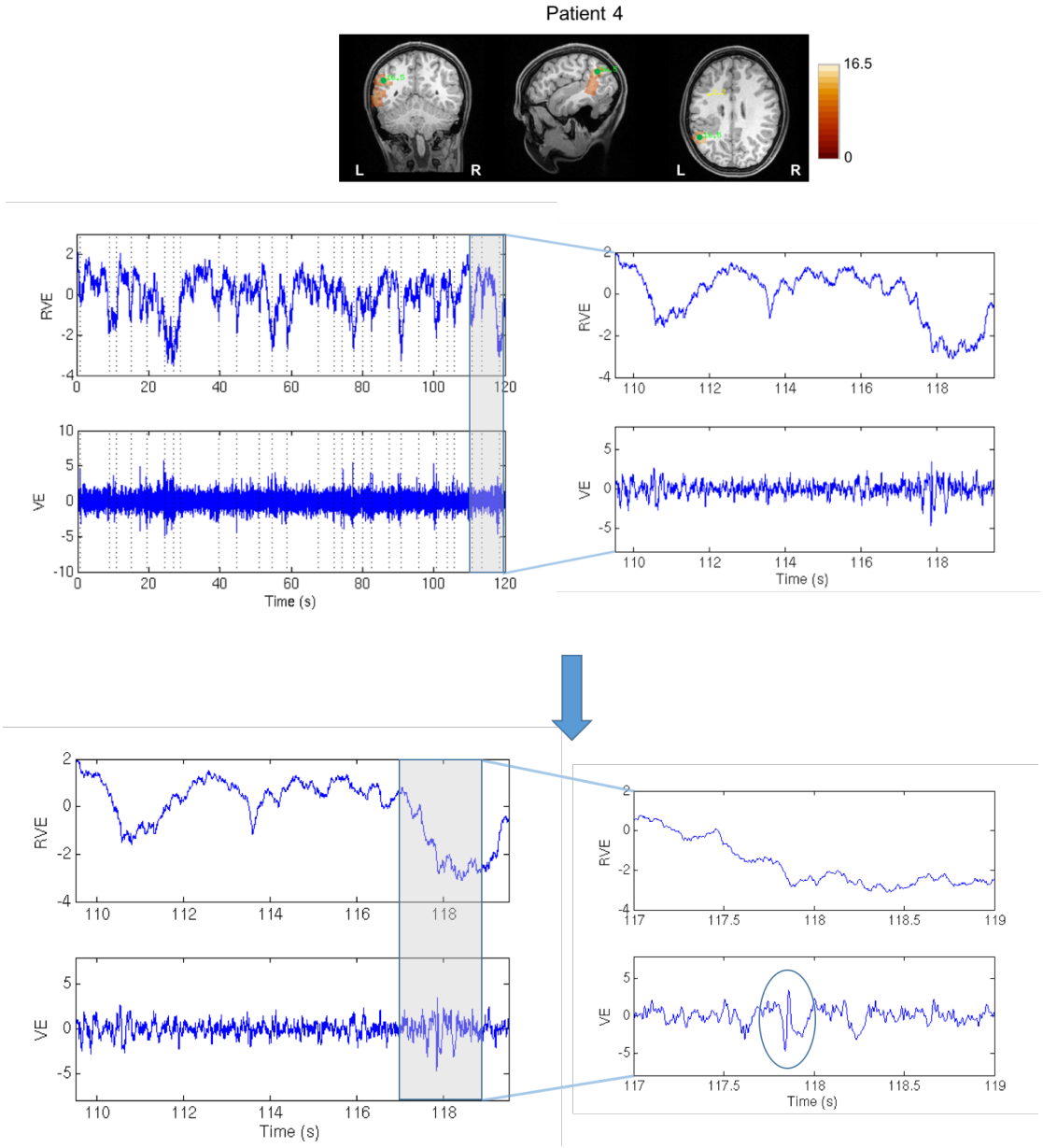

Figure 7.7. Top row: Kurtosis beamformer peak localisation (green dot) used to identify the virtual electrode (VE) containing spikes. Bottom Row: The rank vector entropy (RVE) time series (top) and the original virtual electrode. The left time series shows the entire epoch (120s), the right time series show a 10s selection showing the decrease in RVE signal and the epileptiform activity in the VE. Time series indicated by the bold blue arrow shows the same 10 second time series and a 2 second extract indicating the decrease in entropy and corresponding spike.

7.3.2 Whole Head RVE

The virtual electrode analysis demonstrated that in response to epileptiform activity there are observed decreases in the RVE signal. Based on this finding, RVE was applied to every voxel across the whole brain, and functional images were produced showing the minimum RVE value across the time series for each location in source space.

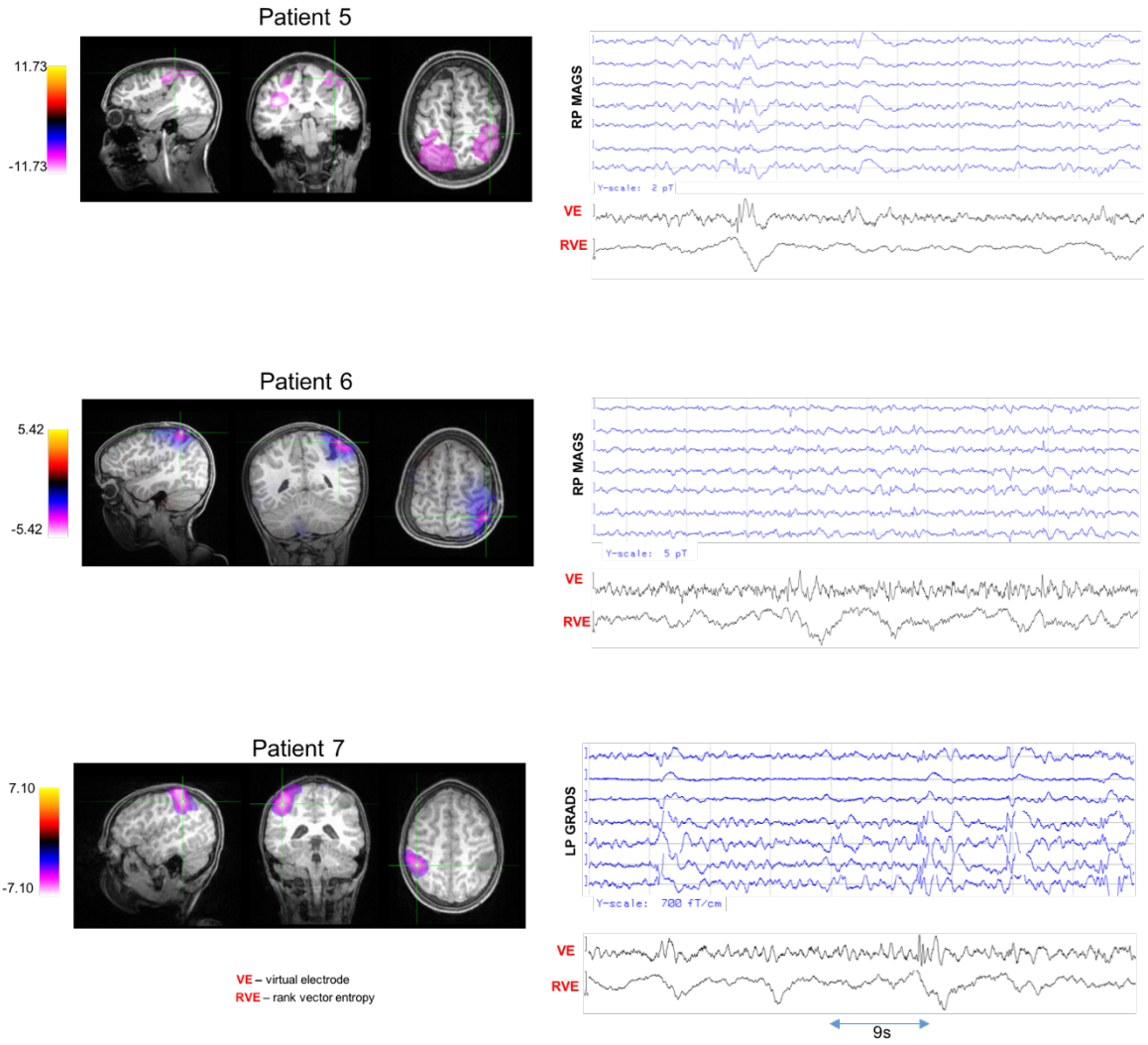

Figure 7.8. Whole head RVE source plots in three patient examples. Functional overlays are calculated by taking the minimum value of each RVE time series for every location in source space. A subset of physical MEG sensors (blue waveforms), and VE/RVE time series (black waveforms) are plotted across 9 seconds.

In Figure 7.8, the RVE localisation for patient 5 is situated in an area coinciding with a perisylvian polymicrogyria. The right parietal sensors show a polyspike and wave complex that is also reflected in the virtual electrode for the spatial location and a clear reduction in RVE. The RVE localisation for patient 6 identifies an area in the right parietal lobe that had undergone two previous resections. Due to persistent seizures post-surgery this patient was referred to MEG for further evaluation. The right parietal magnetometers and virtual electrode data contain transient sharp waves that also result in a reduction in the RVE signal. Patient 7 had spikes across multiple MEG channels, however the top RVE 'peak' localised to an area contralateral to a glioma in the right parietal lobe. Despite the lack of spatial concordance with the visible lesion, the RVE time series contains multiple decreases in RVE in response to spike and wave discharges.

7.3.3 RVE Post Surgical Example

In a further attempt to investigate whether RVE is a potentially useful tool in detecting epileptiform activity, RVE was retrospectively computed on presurgical data of a patient who subsequently had a focal resection. The postsurgical follow up at 12 months indicated that this patient was seizure-free, supporting the notion that the resected area was the epileptogenic zone. In Figure 7.9, RVE shows a spatial overlap with the resected area. This functional image is based on the time point that showed the lowest entropy value (not standardised in this example). In comparison, the kurtosis beamformer (10-80Hz) localises a source slightly posterior to the resection zone.

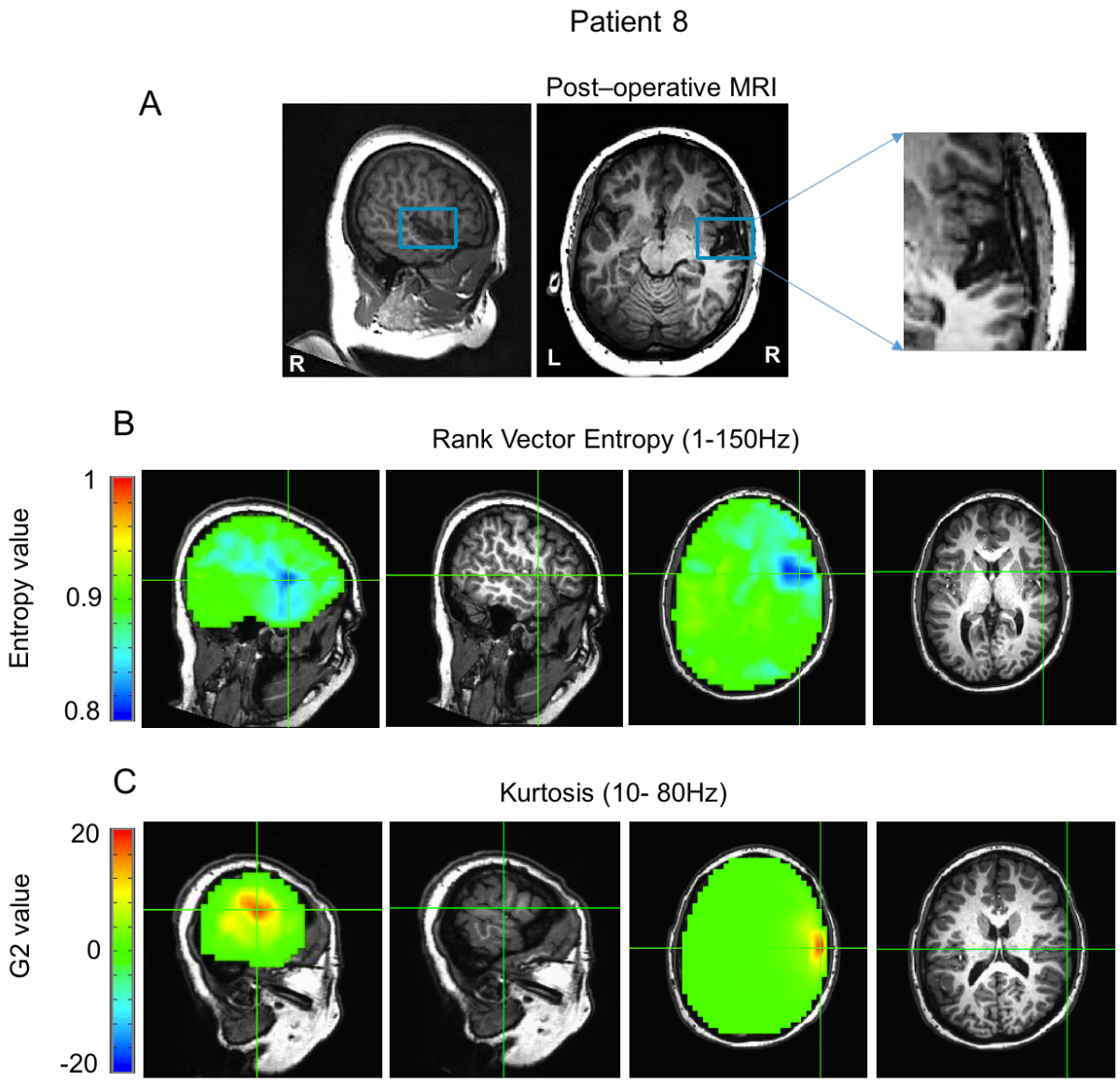

Figure 7.9. A comparison between the presurgical RVE and kurtosis beamformer localisations and subsequent resection area in a seizure free patient (at 12 months). (A) Post-operative MRI with the frontotemporal resection area indicated by the blue box. (B) RVE volumetric image at the time point showing the lowest RVE value plotted. (C) The kurtosis beamformer (10-80Hz) peak localisation.

7.4 Discussion

This chapter aimed to investigate the temporal dynamics of entropy in a series of epilepsy datasets using RVE. The hypersynchronisation of neuronal populations underlying epileptiform activity led to the hypothesis that entropy will decrease as the signal becomes more predictable. This hypothesis was evaluated by applying RVE to real virtual electrode data to investigate how the RVE signal corresponds to various types of epileptiform activity. RVE was then applied to whole-head beamformer time series to determine whether it is able to provide valuable spatial localisations in identifying probable irritative zones. Finally, in a single patient with post surgical outcome information, RVE was retrospectively applied to investigate whether the RVE localisation was spatially concordant with the resection area.

The single virtual electrode analysis revealed that RVE decreases in response to a variety of discharges including polyspike complexes, sharp waves, and abnormal slow wave rhythms. The virtual electrode analysis for patient 1 demonstrated that RVE is not necessarily dependent on amplitude, and in comparison to clear spike and wave discharges it can be equally sensitive to abnormal slow-wave activity of a lower amplitude. This finding suggests that RVE is sensitive to changes in entropy in the signal as opposed to just changes in amplitude. This could enable the identification of low amplitude spikes that are present in the source time series and assist in the visual identification of small spikes embedded in the MEG sensor time series.

The clinical value of localising abnormal low frequency signals may be particularly useful in patients with tumour-associated epilepsy (Tran et al., 1997), however it still remains unclear whether these signals are a marker of epileptogenic regions, or simply a by-product of the lesion (Baayen et al., 2003). Nevertheless, as the presence of abnormal low-frequency signals often indicates pathological changes in the brain (Baayen et al., 2003), the ability to localise these signals may still be useful in patients who do not present with any other form of abnormalities when measured in MEG. This is particularly relevant for patients that are referred to the ABC as they do not always produce clear spikes despite a presentation of drug resistant epilepsy. Furthermore, unpublished MEG data from the ABC shows that abnormal low frequency signals can

occur in patients with MRI negative findings. These localisations could assist in supporting other presurgical findings, or help the re-evaluation of MRI data (e.g. MEG guided MRI, Funke et al., 2011).

The single virtual electrode analysis demonstrated support for the hypothesis that en decreases in response to epileptiform activity. Based on these findings, probable irritative zones were identified across the whole brain by searching for volumetric peaks that contained the lowest RVE values. This was based on the notion that areas with the lowest RVE values would correspond to areas involved in the epileptic network (i.e. hypersychronised neurons). The RVE source for patient 5 localised to an area adjacent to a right lateralised perisylvian polymicrogyria and the virtual electrode for this coordinate showed multiple polyspike and waves. This patient's lesion was extensive and the question asked upon referral was if MEG could determine an area of epileptogenic focality. RVE allowed a focal region to be localised, however post surgical findings are not available to determine the accuracy of this localisation.

Patient 6 had previously undergone two fronto-parietal resections, however was referred for MEG due to persistent auras and seizures post-surgery. The volumetric image for patient 6 shows RVE peaks in an area surrounding the lesion indicating that the epileptogenic zone may not have been completely removed. This is likely due to the proximity of the epileptic focus to sensorimotor areas. Despite absent post-surgical outcomes for this patient, RVE seems to provide a sensible localisation whereby decreases in the RVE time series correspond with epileptiform activity in the virtual electrode.

The top RVE peak in patient 7 localised to an area contralateral to a right parietal glioma. Despite this localisation being discordant to the lesion, it has previously been shown that in one third of patients with a cavernoma, spikes are present in the contralateral homologous site (Jin et al., 2007). These 'mirror spikes' are thought to the be the result of rapid propagation from the perilesion epileptogenic focus (Jin et al., 2007). This rapid propagation to the contralateral homologous site is likely to be facilitated by the sensorimotor network (Biswal et al., 1995; Brookes et a., 2011).

It is important to note that patients 5,6, and 7 are all considered ‘complex’ cases whereby their MEG data suggests a distributed epileptic network containing multiple spike generators with abnormalities present on multiple sensors. This diffuse activity consists of independent and coupled spike loci meaning that an ECD analysis may not have provided valuable localisation information. In these multifocal cases, the combination of an adaptive spatial filter and a metric sensitive to paroxysmal activity such as RVE may provide unique and valuable information not currently provided by standard techniques.

Patient 8 is an example of a focal case whereby we were able to gain a post-operative MRI and surgical outcome at 12 months. The minimum RVE value localises to an area that spatially overlaps with the area that was subsequently resected, leading to a seizure free outcome. It is therefore reasonable to conclude that in this scenario RVE was able to localise the epileptogenic zone. For comparative purposes, the kurtosis beamformer localisation is also given in Figure 9, indicating a region slightly posterior and superior to the resected area. In the virtual electrode corresponding to the RVE localisation, a MATLAB based spike detection algorithm marked 112 spikes, whereas the kurtosis beamformer virtual electrode contained 105 spikes. In this scenario it is possible that the source containing fewer spikes was favoured by the kurtosis beamformer as the g2 metric is biased to rare events (Harpaz et al., 2015).

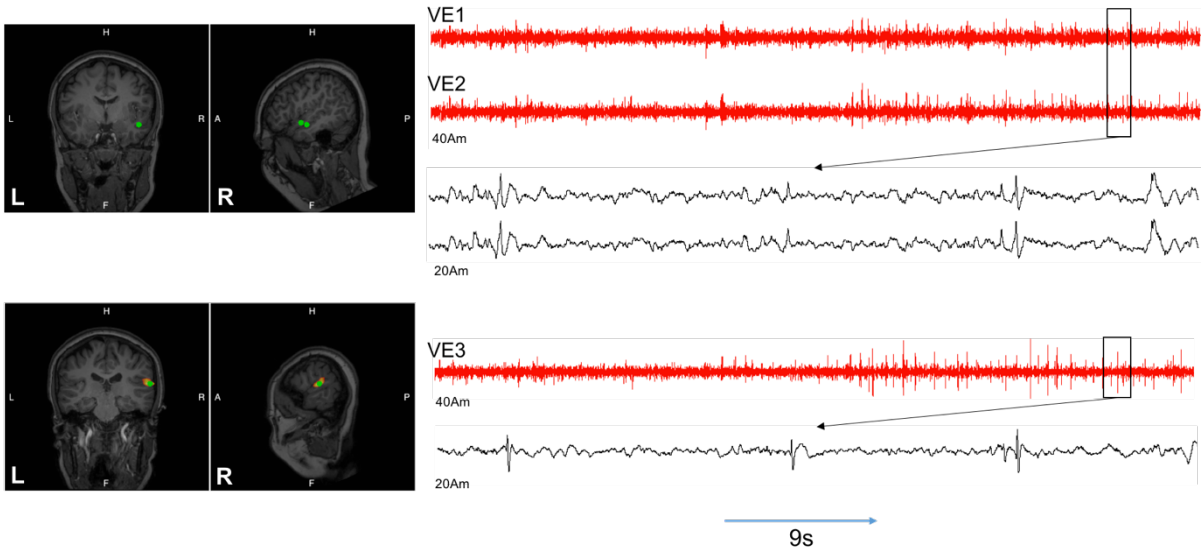

Figure 7.10. Patient 8: Two virtual electrodes (VE1 & VE2) were seeded in the area that was subsequently resected and compared to the virtual electrode corresponding to the kurtosis beamformer peak (VE3). VE1 contained 112 spikes, VE2 contained 131 spikes, and VE3 contained 105 spikes. Based on the morphology of the virtual electrode time series, VE1 and VE2 have more variable background noise and large spikes, whereas VE3 has less variable background data accompanied by more transient sharper spikes. RVE localised an area concordant with VE2.

7.4.1 RVE parameters

A key parameter of RVE is that a broadband signal is optimal (e.g. 1-150Hz) for effectively estimating entropy in order to include information across multiple frequency bands. The use of a broad-band filter is ideal for studying epilepsy as signals contain both low and high frequency components (Jirsch et al., 2006; Westmijse et al., 2009). A further advantage of RVE is that there are less tunable parameters relative to other measures of entropy (e.g. Kolmogorov Entropy, Kolomogrov, 1958), which may allow the researcher to influence the outcome by changing the bins used (Robinson et al., 2013). This allows for a simpler application and remains fairly user independent whereby the researcher is less able to bias results. However, a search for parameters optimal for epilepsy signals may be useful in order to 'tune' the RVE algorithm.

The main tuneable parameters for RVE is the sampling frequency *fs*, window size **W**, and τ (constant giving the time for the counts to decay to 1/e). In the Robinson et al. paper the sample lag ε, is determined by *fs/fc* (sampling frequency/corner frequency) rounded to the closest integer, however the sample lag can also be manually selected and therefore a tuneable parameter. Preliminary simulations shown in Appendix 1, suggest that using a higher sampling rate, with larger windows (e.g. **W**=6), may improve the sensitivity of RVE in oscillatory signals relative to random noise. The use of a larger window allows for more brain states to be computed, which could facilitate the differentiation between states due to an increase in the number of possible states (5! = 120, 6! = 720). Furthermore, using a higher sampling frequency may improve the sensitivity of RVE by allowing more samples to be included in the RVE calculations and facilitating the characterisation of transient signals. Obviously, the increase of sampling frequency and window size alsos increase the processing resources required.

7.4.2 Future Research

The functional RVE overlays represents the lowest RVE value in the time series for each voxel. A relatively unexplored aspect of this chapter is how to maximise the temporal information gained from these RVE source time series. For example, Figure 7.11 shows how 4D spatiotemporal information can be used to investigate RVE changes across time. This may be particularly useful in trying to study spike propagation through assessing the reduction in RVE across time. The study of single spikes and their propagative properties are frequently studied by MEG technicians and forms an important part of clinically oriented software (e.g. Brainstorm, Tadel et al., 2011).

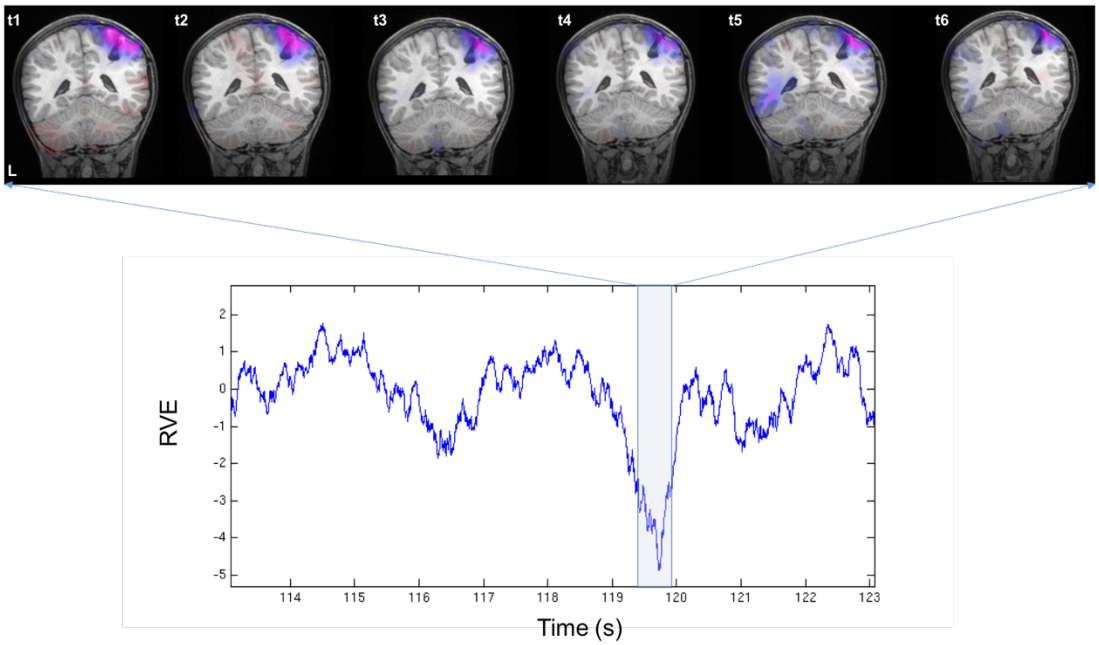

Figure 7.11. Functional RVE images plotted across 0.5 second window indicated by the transparent grey box (1 image per 0.08 seconds) demonstrating the evolution of RVE over time.

Figure 7.11 is based on time points contained within the largest decrease in RVE in patient 6, and shows how RVE changes over multiple time points, indicating an area surrounding the anatomical lesion. This could potentially provide information regarding the extent of the resection required to ensure the complete removal of the epileptogenic zone, or to study the propagation of the activity.

7.4.2.1 RVE-ICA

Other signal processing techniques may also be applied to the RVE source time series, such as independent components analysis (ICA). This could enable the identification of epileptic networks and regions that relate to spike onset and propagation. This method is similar to that used by Brookes et al., (2015) who decomposed the 4D entropy matrices into temporally independent components, thus exposing voxels with similar entropy profiles. An example of this is shown in a single

epilepsy patient below (Figure 12), whereby the top component shows changes in entropy (signal rotated), implying this entropy profile is shared by a left parietal and right frontal region. This RVE-ICA approach could allow epileptic networks to be systematically pulled apart, particularly in cases that present with different types of epileptiform activity and multiple sources.

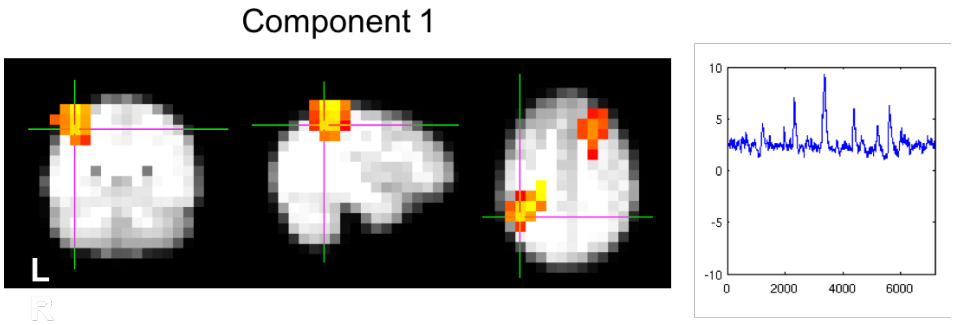

Figure 7.12. An example of RVE-ICA. The first component is plotted on the patient's downsampled MRI. This component spatially overlaps with a lesion in the the left parietal lobe and a right frontal region.

7.4.2.2 Small Scale Entropy

To further understand how pathological activity and entropy changes in the epileptic brain at the macroscopic level, it is also worth investigating the entropy of small scale entropy within local neuronal populations. This could be achieved by using multielectrode array (MEA) measurements to record both local field potentials (LFP) and single unit data simultaneously in resected human brain tissue (Jones et al., 2016). For example, Dossi et al., (2014) used planar MEA in epileptic human cortical slices to measure spontaneous interictal activity alongside drug induced ictal events (zero [Mg2+]o and high [K+]o (6 mM) artificial cerebral spinal fluid). The monitoring of single units alongside LFP/EEG signals has also been demonstrated using in vivo recordings in human epilepsy patients (Keller et al., 2010; Bower et al., 2012; Cash and Hochberg, 2015).

7.4.2.3 Seizure Detection

Extensive research since the 1970s has been carried out into the use of EEG in automatically detecting seizures (Mormann et al., 2007), including the use of discrete wavelet transform (DWT), approximate entropy (ApEn) (Ocak, 2009) and other time-frequency based methods (Tzallas et al., 2007). The application of RVE to iEEG and scalp EEG could also be useful as a seizure detection tool whereby a change in entropy (reduction) could be used to mark points in time relating to ictal activity. This may assist in the visual screening of data to identify time points of interest and to provide a measure that does not solely rely on the amplitude of the signal.

7.4.3 Limitations

This chapter is a proof of concept of the application of RVE in epilepsy MEG datasets and is not a clinical validation of this technique. In order to provide a validation of RVE, then a similar method as chapter 5 could be employed to measure the spatial concordance between RVE localisations and resection areas in a cohort of patients. A further limitation of this chapter is that the results presented are primarily qualitative and could therefore benefit from further quantitative analyses. This qualitative presentation of the data is suitable for neurophysiologists who often rely on interpreting EEG/MEG waveforms in a subjective manner. However, a quantitative analysis would assist in drawing further objective conclusions regarding the SNR of RVE and could involve comparing the SNR of decreases in RVE relative to the SNR of spikes in the virtual electrode.

7.4.4 Conclusion

This chapter demonstrates that RVE is sensitive to epileptiform activity, and may allow the localisation of a wide range of activity, including conventional spikes, abnormal slow frequency signals, and low amplitude abnormalities. The results shown in this chapter supports the hypothesis that as assemblies of neurons become hypersynchronised, the signal becomes more predictable causing a reduction in entropy. By using these reductions in entropy as a marker in time for plotting spatial

images, it has been demonstrated that regions of interest relating to the irritative zone can be localised. The overarching goal of applying novel techniques to epilepsy data is to establish multiple tools that can be used to improve the sensitivity of MEG, particularly in patients that do not present with clear spikes. RVE may allow for the localisation of low amplitude spikes, atypical slow waves, and may assist in identifying locations of interest that could then be entered into a functional connectivity analysis (e.g. granger causality). Future research should aim to provide a clinical validation of this technique and a quantitative analysis is warranted to investigate the added value of RVE in comparison to the standard clinical methods.

Chapter 8: General Discussion

8.1 Overview

This PhD project was funded by the MRC and is part of the MRC-MEG UK partnership grant (MR/K005464/1 & MR/K501086/1). The objectives of this grant were to increase the clinical research capacity of MEG in the UK and to work towards standardised data acquisition and analysis pipelines across UK MEG laboratories.

To meet the clinical goals of this grant, this thesis aimed to investigate the use of MEG to localise epileptiform activity and eloquent cortex in drug resistant epilepsy patients being considered for surgery. Therefore, this thesis consisted of two themes: The first theme aimed at refining techniques to functionally map the brain in order to identify eloquent cortex. This theme was particularly important due to the absence of a reliable beamformer implementation at the ABC. Therefore, initial methods testing had to be carried out to establish a new beamformer pipeline that could then be applied to datasets of interest (e.g. language data). The second theme shifted focus onto investigating methods to localise various forms of epileptiform activity by evaluating a pre-existing method spike detection technique and introducing a novel method. These two themes, albeit distinct in their goals are of equal importance in the presurgical evaluation of patients being considered for surgery. In this context, it has been demonstrated that MEG can be used to help form hypotheses regarding the location of the epileptogenic zone as well as identify brain regions that are important for healthy brain functioning.

This general discussion will provide a summary of the work done in this thesis and highlight the main conclusions that can be drawn from this work. The limitations of the work conducted in this thesis will also be discussed. Finally, to embed the outputs of this research into the wider picture, the future of clinical MEG will briefly be discussed in relation to recent advancements in MEG technology.

8.2 Experimental Chapter Summary

In order to facilitate the functional mapping of patients using Elekta data, additional methodological work was carried to establish a beamformer pipeline that was fit for purpose (Chapter 3). This chapter highlighted the current issues when analysing Elekta data (e.g. combining sensors, tSSS filtering) and recommended a set of parameters that can be used in future functional mapping applications. This is the first study to explore the parameters that are specific to Elekta data in the context of beamforming. The findings showed that tSSS is a necessary preprocessing step prior to source localisation in order to provide an accurate localisation. This supports previous work that indicates the requirement of tSSS when analysing Elekta data (Hillebrand et al., 2013). Furthermore, the time frequency plots indicated that using tSSS in combination with gradiometers alone produce the best sustained gamma response. As mentioned in the chapter 3 discussion, there are a number of ways to preprocess and analyse MEG data. Therefore, further work should focus on trying to establish a set of standardised guidelines on how to approach these issues, particularly when addressing issues specific to Elekta data.

The pipeline developed in Chapter 3 was then used in Chapter 4 to analyse language data. Chapter 4 had two primary goals, the first being a replication of earlier work at Aston that was conducted using the CTF 275 system, the second was piloting a passive language task. The verb generation results showed support for the key finding from the original Fisher et al. (2008) paper, demonstrating lateralised beta desynchronisations (15-25 Hz) in response to the covert generation of verbs. Secondly, the findings from the rotated speech paradigm indicated that this task could be useful in assisting to determine language dominance in a passive manner. It was found that anterior temporal regions showed a frequency specific (40-60 Hz) response in single subjects, therefore supporting previous work indicating the role of the anterior temporal pathway in speech perception (Scott et al., 2000).

The clinical significance of Chapter 4 is that probing language in a passive way could be of great practical benefit when measuring young children or patients that are unable to complete complex active tasks. Despite these initial positive findings, there were several limitations to this work including a low sample size and the need for

potentially refining the rotated speech paradigm (i.e. increasing the number of trials). Crucially, this data acts as important pilot data to form a larger study using patients whereby invasive measures of language in patients can be used to validate the MEG findings. A study of this nature is currently undergoing at the ABC.

Chapter 5 focussed on the second theme of this thesis. In this chapter, kurtosis beamformer results were compared to the resection site in patients who had undergone surgery. The rationale for this study was based on the variable clinical use of kurtosis beamforming across clinical MEG centres, despite a number of sites producing published research using this method (Scott et al., 2016). Therefore, a further evaluation of this technique to form conclusions regarding the role of kurtosis beamforming in clinical MEG analysis was conducted. The key finding from Chapter 5 was that in 9/13 of the seizure free patients the kurtosis beamformer overlapped (at the lobar level) with the subsequently resected area. It was found that there was not a significant difference in the accuracy between kurtosis beamforming and the clinical standard ECD fitting approach. However, it was demonstrated in some cases that these techniques can provide unique information that the other technique is not sensitive to. Importantly, the value of kurtosis beamforming as an objective approach was also demonstrated. Based on these findings, it was concluded that kurtosis beamforming should be integrated into existing clinical protocols, whereby this additional information may help to confirm sources implicated by ECD fitting and in some cases (e.g. sharp activity) provide unique information to help form hypotheses about the epileptogenic zone.

The evaluation conducted in Chapter 5 would benefit further from a larger study using data from multiple sites using a standardised kurtosis beamformer method. This type of multicentre collaboration and use of standardised analysis tools is one of the aims of the MRC-MEG UK partnership. Therefore, this provided motivation to develop an open source version of the kurtosis beamformer in Fieldtrip to facilitate such a collaboration. This work was described in the following short chapter (Chapter 6), which can be considered an extension of Chapter 5. In Chapter 6, it was demonstrated in 2 patients that a Fieldtrip based kurtosis beamformer could perform similarly to the CTF and Elekta proprietary software and localise interictal spikes. The advantage of

an open source pipeline is that improvements to the method can easily be implemented (e.g. Prendergast et al., 2013) and data can be pooled from multiple MEG platforms. Further research will aim to validate this pipeline, whilst also introducing variations of the kurtosis beamformer method, such as the SAMepi approach originally described by Harpaz et al. (2015).

The findings from Chapter 5 indicated that the available clinical MEG analysis tools do not always accurately localise the epileptogenic zone and therefore new approaches are required to improve the sensitivity of MEG to abnormal transients. Chapter 7 aimed to address this by introducing a novel method, RVE, to investigate whether it can provide additional information in localising a range of epileptiform activity including spikes, low amplitude transients, and abnormal slow waves. It was hypothesised that reductions in signal entropy would be observed during periods of hyperschronisation within neuronal populations, i.e. during epileptiform activity. The findings show that the RVE signal showed a decrease in entropy to a range of epileptiform activity including low amplitude signals, spikes and slow waves. The findings also demonstrated that regions showing the greatest reduction in entropy correlated with other clinical findings (e.g. lesions in the MRI) and in one patient localised to an area that was subsequently confirmed as the epileptogenic zone. There are many possible extensions of this work whereby the RVE source time series could be manipulated in a number of ways. After further clinical evaluation this method may be used for the clinical analysis of epilepsy data and potentially provide localising information of abnormalities in other conditions, such as mild traumatic brain injury (mTBI) (e.g. abnormal slow wave activity is often observed in mTBI).

8.3 Future of Clinical MEG

Finally, it is worth considering the outputs of this research in regards to recent advances in quantum sensing. New MEG and sensor developments, such as optically pumped magnetometers (OPMs) (Boto et al., 2017) and HyQuids^{TM} (Shelly et al., 2016) may provide measurements containing less low-frequency noise, which may be particularly useful for the detection of slow wave abnormalities. This feature in combination with a method such as RVE could significantly increase the sensitivity to these types of abnormalities. Another potential advantage is that these new quantum sensing devices may allow for the better detection of low amplitude high frequency oscillations (<100 Hz).

Current MEG systems are based on SQUIDS immersed in liquid helium that are housed in a dewar meaning that sensors are located at least 3-6 cm from the head surface. OPMs for example, can be positioned much closer to the head allowing increases in SNR (as the brain follows an inverse square law). Improvements in SNR has shown to provide benefits in relation to the spatial resolution in MEG (Brookes et al., 2008; Brookes et al., 2010; Hilleband & Barnes, 2002) and would benefit clinical applications, particularly in presurgical MEG when detecting low amplitude signals (e.g. small spikes, high frequency oscillations). Boto et al. (2017) recently demonstrated the potential utility of OPMs in response to a median nerve stimulation, where signals exhibited ~4 times the magnitude of equivalent measures made using SQUIDs. If these results can be replicated using whole-head arrays, then the sensitivity of presurgical MEG could increase and dramatically improve the detection and localisation of epileptiform signals in patients.

References

Abou-Khalil, B. (2007). An update on determination of language dominance in screening for epilepsy surgery: the Wada test and newer noninvasive alternatives. *Epilepsia, 48*(3), 442-455.

Adjamian, P. (2014). The application of electro-and magneto-encephalography in tinnitus research–methods and interpretations. *Frontiers in neurology, 5*.

Adjamian, P., Barnes, G. R., Hillebrand, A., Holliday, I. E., Singh, K. D., Furlong, P. L., . . . Route, P. (2004). Co-registration of magnetoencephalography with magnetic resonance imaging using bite-bar-based fiducials and surface-matching. *Clinical Neurophysiology, 115*(3), 691-698.

Adjamian, P., Holliday, I. E., Barnes, G. R., Hillebrand, A., Hadjipapas, A., & Singh, K. D. (2004). Induced visual illusions and gamma oscillations in human primary visual cortex. *European Journal of Neuroscience, 20*(2), 587-592.

Adjamian, P., Worthen, S. F., Hillebrand, A., Furlong, P. L., Chizh, B., Hobson, A. R., . . . Barnes, G. R. (2009). Effective electromagnetic noise cancellation with beamformers and synthetic gradiometry in shielded and partly shielded environments. *Journal of neuroscience methods, 178*(1), 120-127.

Adler, R. L., & Marcus, B. (1979). *Topological entropy and equivalence of dynamical systems* (Vol. 219): American Mathematical Soc.

Agirre-Arrizubieta, Z., Thai, N. J., Valentín, A., Furlong, P. L., Seri, S., Selway, R. P., . . . Alarcón, G. (2014). The value of magnetoencephalography to guide electrode implantation in epilepsy. *Brain topography, 27*(1), 197-207.

Ahonen, A. I., Hämäläinen, M., Kajola, M., Knuutila, J., Laine, P., Lounasmaa, O., . . . Tesche, C. (1993). 122-channel SQUID instrument for investigating the magnetic signals from the human brain. *Physica Scripta, 1993*(T49A), 198.

Anderson, D. P., Harvey, A. S., Saling, M. M., Anderson, V., Kean, M., Abbott, D. F., . . . Jackson, G. D. (2006). FMRI lateralization of expressive language in children with cerebral lesions. *Epilepsia, 47*(6), 998-1008.

Anhoury, S., Brown, R. J., Krishnamoorthy, E., & Trimble, M. R. (2000). Psychiatric outcome after temporal lobectomy: a predictive study. *Epilepsia, 41*(12), 1608-1615.

Azuma, H., Hori, S., Nakanishi, M., Fujimoto, S., Ichikawa, N., & Furukawa, T. A. (2003). An intervention to improve the interrater reliability of clinical EEG interpretations. *Psychiatry and clinical neurosciences, 57*(5), 485-489.

Baayen, J. C., de Jongh, A., Stam, C. J., de Munck, J. C., Jonkman, J. J., Trenité, D. G. K.-N., . . . Puligheddu, M. (2003). Localization of slow wave activity in patients with tumor-associated epilepsy. *Brain topography, 16*(2), 85-93.

Bagic, A. I., Knowlton, R. C., Rose, D. F., Ebersole, J. S., & Committee, A. C. P. G. (2011).

American Clinical Magnetoencephalography Society Clinical Practice Guideline 1: recording and analysis of spontaneous cerebral activity. *Journal of Clinical Neurophysiology, 28*(4), 348-354.

Bandettini, P. A., Jesmanowicz, A., Wong, E. C., & Hyde, J. S. (1993). Processing strategies for time-course data sets in functional MRI of the human brain. *Magnetic resonance in medicine, 30*(2), 161-173.

Barbati, G., Porcaro, C., Zappasodi, F., Rossini, P. M., & Tecchio, F. (2004). Optimization of an independent component analysis approach for artifact identification and removal in magnetoencephalographic signals. *Clinical Neurophysiology, 115*(5), 1220-1232.

Barkley, G. L., & Baumgartner, C. (2003). MEG and EEG in epilepsy. *Journal of Clinical Neurophysiology, 20*(3), 163-178.

Barnes, G. R., & Hillebrand, A. (2003). Statistical flattening of MEG beamformer images. *Human brain mapping, 18*(1), 1-12.

Barrett, A. M. (1910). A case of pure word-deafness with autopsy. *The Journal of Nervous and Mental Disease, 37*(2), 73-92.

Bast, T., Oezkan, O., Rona, S., Stippich, C., Seitz, A., Rupp, A., . . . Scherg, M. (2004). EEG and MEG source analysis of single and averaged interictal spikes reveals intrinsic epileptogenicity in focal cortical dysplasia. *Epilepsia, 45*(6), 621-631.

Belliveau, J., Kennedy, D., McKinstry, R., Buchbinder, B., Weisskoff, R., Cohen, M., . . . Rosen, B. (1991). Functional mapping of the human visual cortex by magnetic resonance imaging. *Science, 254*(5032), 716-719.

Berg, A. T., Vickrey, B. G., Langfitt, J. T., Sperling, M. R., Walczak, T. S., Shinnar, S., . . . Spencer, S. S. (2003). The multicenter study of epilepsy surgery: recruitment and selection for surgery. *Epilepsia, 44*(11), 1425-1433.

Binder, J. R., Rao, S. M., Hammeke, T., Yetkin, F., Jesmanowicz, A., Bandettini, P., . . . Haughton, V. (1994). Functional magnetic resonance imaging of human auditory cortex. *Annals of neurology, 35*(6), 662-672.

Binder, J. R., Swanson, S. J., Hammeke, T. A., & Sabsevitz, D. S. (2008). A comparison of five fMRI protocols for mapping speech comprehension systems. *Epilepsia, 49*(12), 1980-1997.

Binder, K. S., & Rayner, K. (1998). Contextual strength does not modulate the subordinate bias effect: Evidence from eye fixations and self-paced reading. *Psychonomic Bulletin & Review, 5*(2), 271-276.

Binnie, C. D., & Polkey, C. E. (2000). Commission on neurosurgery of the international league against epilepsy (ILAE) 1993–1997: recommended standards. *Epilepsia, 41*(10), 1346-1349.

Birot, G., Spinelli, L., Vulliémoz, S., Mégevand, P., Brunet, D., Seeck, M., & Michel, C. M. (2014). Head model and electrical source imaging: a study of 38 epileptic patients. *NeuroImage: Clinical, 5*, 77-83.

Biswal, B., Zerrin Yetkin, F., Haughton, V. M., & Hyde, J. S. (1995). Functional connectivity in the motor cortex of resting human brain using echo-planar mri. *Magnetic resonance in medicine, 34*(4), 537-541.

Blesser, B. (1972). Speech perception under conditions of spectral transformation: I. Phonetic characteristics. *Journal of Speech, Language, and Hearing Research, 15*(1), 5-41.

Boto, E., Meyer, S. S., Shah, V., Alem, O., Knappe, S., Kruger, P., . . . Morris, P. G. (2017). A new generation of magnetoencephalography: Room temperature measurements using optically-pumped magnetometers. *Neuroimage, 149*, 404-414.

Bower, M. R., Stead, M., Meyer, F. B., Marsh, W. R., & Worrell, G. A. (2012). Spatiotemporal neuronal correlates of seizure generation in focal epilepsy. *Epilepsia, 53*(5), 807-816.

Brainard, D. H., & Vision, S. (1997). The psychophysics toolbox. *Spatial vision, 10*, 433-436.

Broca, P. (1861). Remarks on the seat of the faculty of articulated language, following an observation of aphemia (loss of speech). *Bulletin de la Société Anatomique, 6*, 330-357.

Brodie, M. J., & French, J. A. (2000). Management of epilepsy in adolescents and adults. *The Lancet, 356*(9226), 323-329.

Bronen, R. A., Vives, K. P., Kim, J. H., Fulbright, R. K., Spencer, S. S., & Spencer, D. D. (1997). Focal cortical dysplasia of Taylor, balloon cell subtype: MR differentiation from low-grade tumors. *American journal of neuroradiology, 18*(6), 1141-1151.

Brookes, M. J., Gibson, A. M., Hall, S. D., Furlong, P. L., Barnes, G. R., Hillebrand, A., . . . Morris, P. G. (2005). GLM-beamformer method demonstrates stationary field, alpha ERD and gamma ERS co-localisation with fMRI BOLD response in visual cortex. *Neuroimage, 26*(1), 302-308.

Brookes, M. J., Hall, E. L., Robson, S. E., Price, D., Palaniyappan, L., Liddle, E. B., . . . Morris, P. G. (2015). Complexity measures in magnetoencephalography: measuring" disorder" in schizophrenia. *PLoS One, 10*(4), e0120991.

Brookes, M. J., Vrba, J., Robinson, S. E., Stevenson, C. M., Peters, A. M., Barnes, G. R., . . . Morris, P. G. (2008). Optimising experimental design for MEG beamformer imaging. *Neuroimage, 39*(4), 1788-1802.

Brookes, M. J., Woolrich, M., Luckhoo, H., Price, D., Hale, J. R., Stephenson, M. C., . . . Morris, P. G. (2011). Investigating the electrophysiological basis of resting state networks using magnetoencephalography. *Proceedings of the National Academy of Sciences, 108*(40), 16783-16788.

Brookes, M. J., Zumer, J. M., Stevenson, C. M., Hale, J. R., Barnes, G. R., Vrba, J., & Morris, P. G. (2010). Investigating spatial specificity and data averaging in MEG. *Neuroimage, 49*(1), 525-538.

Bruña, R., Poza, J., Gómez, C., García, M., Fernández, A., & Hornero, R. (2012). Analysis of spontaneous MEG activity in mild cognitive impairment and Alzheimer's disease using spectral entropies and statistical complexity measures. *Journal of neural engineering, 9*(3), 036007.

Byars, A. W., Holland, S. K., Strawsburg, R. H., Bommer, W., Dunn, R. S., Schmithorst, V. J., & Plante, E. (2002). Practical aspects of conducting large-scale functional magnetic resonance imaging studies in children. *Journal of child neurology, 17*(12), 885-889.

Cabin, R. J., & Mitchell, R. J. (2000). To Bonferroni or not to Bonferroni: when and how are the questions. *Bulletin of the Ecological Society of America, 81*(3), 246-248.

Caplan, D. (1987). Phonological representations in word production. *Motor and sensory processes of language*, 111-124.

Carne, R., O'brien, T., Kilpatrick, C., MacGregor, L., Hicks, R., Murphy, M., . . . Cook, M. (2004). MRI-negative PET-positive temporal lobe epilepsy: a distinct surgically remediable syndrome. *Brain, 127*(10), 2276-2285.

Cascino, G. D., Jack, C. R., Parisi, J. E., Sharbrough, F. W., Hirschorn, K. A., Meyer, F. B., . . . O'Brien, P. C. (1991). Magnetic resonance imaging–based volume studies in temporal lobe epilepsy: pathological correlations. *Annals of neurology, 30*(1), 31-36.

Cash, S. S., & Hochberg, L. R. (2015). The emergence of single neurons in clinical neurology. *Neuron, 86*(1), 79-91.

Cheyne, D., Bostan, A. C., Gaetz, W., & Pang, E. W. (2007). Event-related beamforming: a robust method for presurgical functional mapping using MEG. *Clinical Neurophysiology, 118*(8), 1691-1704.

Cohen-Gadol, A. A., Özduman, K., Bronen, R. A., Kim, J. H., & Spencer, D. D. (2004). Long-term outcome after epilepsy surgery for focal cortical dysplasia. *Journal of neurosurgery, 101*(1), 55-65.

Colon, A., Hofman, P., Ossenblok, P., Jansen, J., Ter Beek, L., Berting, R., . . . Boon, P. (2010). MRS-lateralisation index in patients with epilepsy and focal cortical dysplasia or a MEG-focus using bilateral single voxels. *Epilepsy research, 89*(1), 148-153.

Conner, C. R., Ellmore, T. M., Pieters, T. A., DiSano, M. A., & Tandon, N. (2011). Variability of the relationship between electrophysiology and BOLD-fMRI across cortical regions in humans. *Journal of Neuroscience, 31*(36), 12855-12865.

Cornelissen, P. L., Kringelbach, M. L., Ellis, A. W., Whitney, C., Holliday, I. E., & Hansen, P. C. (2009). Activation of the left inferior frontal gyrus in the first 200 ms of reading: evidence from magnetoencephalography (MEG). *PLoS One, 4*(4), e5359.

Cousijn, H., Haegens, S., Wallis, G., Near, J., Stokes, M. G., Harrison, P. J., & Nobre, A. C. (2014). Resting GABA and glutamate concentrations do not predict visual gamma frequency or amplitude. *Proceedings of the National Academy of Sciences, 111*(25), 9301-9306.

Crinion, J., Turner, R., Grogan, A., Hanakawa, T., Noppeney, U., Devlin, J. T., . . . Stockton, K. (2006). Language control in the bilingual brain. *Science, 312*(5779), 1537-1540.

Cross, J., Jackson, G., Neville, B., Connelly, A., Kirkham, F., Boyd, S., . . . Gadian, D. (1993). Early detection of abnormalities in partial epilepsy using magnetic resonance. *Archives of disease in childhood, 69*(1), 104-109.

D'arcy, R. C., Bardouille, T., Newman, A. J., McWhinney, S. R., DeBay, D., Sadler, R. M., . . . Esser, M. J. (2013). Spatial MEG laterality maps for language: clinical applications in epilepsy. *Human brain mapping, 34*(8), 1749-1760.

Dale, A. M., Liu, A. K., Fischl, B. R., Buckner, R. L., Belliveau, J. W., Lewine, J. D., & Halgren, E. (2000). Dynamic statistical parametric mapping: combining fMRI and MEG for high-resolution imaging of cortical activity. *Neuron, 26*(1), 55-67.

De Camargo, E. C. S., & Koroshetz, W. J. (2005). Neuroimaging of ischemia and infarction. *NeuroRx, 2*(2), 265-276.

De Ciantis, A., Barba, C., Tassi, L., Cosottini, M., Tosetti, M., Costagli, M., . . . Cossu, M. (2016). 7T MRI in focal epilepsy with unrevealing conventional field strength imaging. *Epilepsia, 57*(3), 445-454.

de Curtis, M., & Avanzini, G. (2001). Interictal spikes in focal epileptogenesis. *Progress in neurobiology, 63*(5), 541-567.

de Jongh, A., de Munck, J. C., Gonçalves, S. I., & Ossenblok, P. (2005). Differences in MEG/EEG epileptic spike yields explained by regional differences in signal-to-noise ratios. *Journal of Clinical Neurophysiology, 22*(2), 153-158.

Devinsky, O., Vickrey, B. G., Cramer, J., Perrine, K., Hermann, B., Meador, K., & Hays, R. D. (1995). Development of the quality of life in epilepsy inventory. *Epilepsia, 36*(11), 1089-1104.

Devlin, J. T., Russell, R. P., Davis, M. H., Price, C. J., Wilson, J., Moss, H. E., . . . Tyler, L. K. (2000). Susceptibility-induced loss of signal: comparing PET and fMRI on a semantic task. *Neuroimage, 11*(6), 589-600.

Dichter, M. A., & Brodie, M. J. (1996). New antiepileptic drugs. *New England Journal of Medicine, 334*(24), 1583-1590.

Diehl, B., LaPresto, E., Najm, I., Raja, S., Rona, S., Babb, T., . . . Ruggieri, P. (2003). Neocortical Temporal FDG-PET Hypometabolism Correlates with Temporal Lobe Atrophy in Hippocampal Sclerosis Associated with Microscopic Cortical Dysplasia. *Epilepsia, 44*(4), 559-564.

Dorfer, C., Widjaja, E., Ochi, A., Carter, S. I. O., & Rutka, J. (2015). Epilepsy surgery: recent advances in brain mapping, neuroimaging and surgical procedures. *Journal of neurosurgical sciences, 59*(2), 141-155.

Dossi, E., Blauwblomme, T., Nabbout, R., Huberfeld, G., & Rouach, N. (2014). Multi-electrode array recordings of human epileptic postoperative cortical tissue. *Journal of visualized experiments: JoVE*(92).

Duncan, J. S. (1997). Imaging and epilepsy. *Brain: a journal of neurology, 120*(2), 339-377.

Ebersole, J. S., & Ebersole, S. M. (2010). Combining MEG and EEG source modeling in epilepsy evaluations. *Journal of Clinical Neurophysiology, 27*(6), 360-371.

Engel, A. K., & Fries, P. (2010). Beta-band oscillations—signalling the status quo? *Current opinion in neurobiology, 20*(2), 156-165.

Engel, J. (1984). A practical guide for routine EEG studies in epilepsy. *Journal of Clinical Neurophysiology, 1*(2), 109-142.

Engel, J. (1998). Etiology as a risk factor for medically refractory epilepsy A case for early surgical intervention. *Neurology, 51*(5), 1243-1244.

Engel, J. (2003). A greater role for surgical treatment of epilepsy: why and when? *Epilepsy Currents, 3*(2), 37-40.

Engel, J., McDermott, M. P., Wiebe, S., Langfitt, J. T., Stern, J. M., Dewar, S., . . . Fried, I. (2012). Early surgical therapy for drug-resistant temporal lobe epilepsy: a randomized trial. *Jama, 307*(9), 922-930.

Engel, J., & Pedley, T. A. (1997). Introduction: what is epilepsy. *Epilepsy: A comprehensive textbook, 1*, 1-10.

Engel Jr, J. (1993). Outcome with respect to epileptic seizures. *Surgical treatment of the epilepsies*, 609-621.

Engel Jr, J. (1996). Surgery for seizures. *New England Journal of Medicine, 334*(10), 647-653.

Engel Jr, J. (2013). Why is there still doubt to cut it out? *Epilepsy Currents, 13*(5), 198-204.

Evans, L. T., Morse, R., & Roberts, D. W. (2012). Epilepsy surgery in tuberous sclerosis: a review. *Neurosurgical focus, 32*(3), E5.

Fernandez-Cortes, A., Sanchez-Moral, S., Cuezva, S., Benavente, D., & Abella, R. (2011). Characterization of trace gases' fluctuations on a ‘low energy’cave (Castañar de Íbor, Spain) using techniques of entropy of curves. *International Journal of Climatology, 31*(1), 127-143.

Ferro, M. A. (2011). A population-based study of the prevalence and sociodemographic risk factors of self-reported epilepsy among adults in the United Kingdom. *Seizure, 20*(10), 784-788.

Fiez, J. A. (1997). Phonology, semantics, and the role of the left inferior prefrontal cortex. *Human brain mapping, 5*(2), 79-83.

Fisher, A. E., Furlong, P. L., Seri, S., Adjamian, P., Witton, C., Baldeweg, T., . . . Thai, N. J. (2008). Interhemispheric differences of spectral power in expressive language: a MEG study with clinical applications. *International journal of psychophysiology, 68*(2), 111-122.

Fisher, R. S., Acevedo, C., Arzimanoglou, A., Bogacz, A., Cross, J. H., Elger, C. E., . . . Glynn, M. (2014). ILAE official report: a practical clinical definition of epilepsy.

Epilepsia, 55(4), 475-482.

Fisher, R. S., Boas, W. v. E., Blume, W., Elger, C., Genton, P., Lee, P., & Engel, J. (2005). Epileptic seizures and epilepsy: definitions proposed by the International League Against Epilepsy (ILAE) and the International Bureau for Epilepsy (IBE). *Epilepsia, 46*(4), 470-472.

Flemming, L., Wang, Y., Caprihan, A., Eiselt, M., Haueisen, J., & Okada, Y. (2005). Evaluation of the distortion of EEG signals caused by a hole in the skull mimicking the fontanel in the skull of human neonates. *Clinical Neurophysiology, 116*(5), 1141-1152.

Foley, E., Cerquiglini, A., Cavanna, A., Nakubulwa, M. A., Furlong, P. L., Witton, C., & Seri, S. (2014). Magnetoencephalography in the study of epilepsy and consciousness. *Epilepsy & Behavior, 30*, 38-42.

Fuchs, M., Kastner, J., Wagner, M., Hawes, S., & Ebersole, J. S. (2002). A standardized boundary element method volume conductor model. *Clinical Neurophysiology, 113*(5), 702-712.

Fujiwara, H., Greiner, H. M., Hemasilpin, N., Lee, K. H., Holland-Bouley, K., Arthur, T., . . . Rose, D. F. (2012). Ictal MEG onset source localization compared to intracranial EEG and outcome: improved epilepsy presurgical evaluation in pediatrics. *Epilepsy research, 99*(3), 214-224.

Fujiwara, H., Greiner, H. M., Lee, K. H., Holland-Bouley, K. D., Seo, J. H., Arthur, T., . . . Rose, D. F. (2012). Resection of ictal high-frequency oscillations leads to favorable surgical outcome in pediatric epilepsy. *Epilepsia, 53*(9), 1607-1617.

Funke, M. E., Moore, K., Orrison Jr, W. W., & Lewine, J. D. (2011). The role of magnetoencephalography in “nonlesional” epilepsy. *Epilepsia, 52*(s4), 10-14.

Furlong, P. L., Hobson, A. R., Aziz, Q., Barnes, G. R., Singh, K. D., Hillebrand, A., . . . Hamdy, S. (2004). Dissociating the spatio-temporal characteristics of cortical neuronal activity associated with human volitional swallowing in the healthy adult brain. *Neuroimage, 22*(4), 1447-1455.

Gaetz, W. C., & Cheyne, D. O. (2003). Localization of human somatosensory cortex using spatially filtered magnetoencephalography. *Neuroscience letters, 340*(3), 161-164.

Gaillard, W., Berl, M., Moore, E., Ritzl, E., Rosenberger, L., Weinstein, S., . . . Sato, S. (2007). Atypical language in lesional and nonlesional complex partial epilepsy. *Neurology, 69*(18), 1761-1771.

Gaillard, W., Berl, M., Moore, E., Ritzl, E., Rosenberger, L., Weinstein, S., . . . Sato, S. (2007). Atypical language in lesional and nonlesional complex partial epilepsy. *Neurology, 69*(18), 1761-1771.

Gaillard, W. D., Balsamo, L., Xu, B., Grandin, C., Braniecki, S., Papero, P., . . . Sachs, B. (2002). Language dominance in partial epilepsy patients identified with an fMRI reading task. *Neurology, 59*(2), 256-265.

Gaillard, W. D., Sachs, B. C., Whitnah, J. R., Ahmad, Z., Balsamo, L. M., Petrella, J. R., . . . Xu, B. (2003). Developmental aspects of language processing: fMRI of verbal fluency in children and adults. *Human brain mapping, 18*(3), 176-185.

Gallen, C., Schwartz, B., Rieke, K., Pantev, C., Sobel, D., Hirschkoff, E., & Bloom, F. (1994). Intrasubject reliability and validity of somatosensory source localization using a large array biomagnetometer. *Electroencephalography and clinical Neurophysiology, 90*(2), 145-156.

Gallen, C. C., Sobel, D. F., Waltz, T., Aung, M., Copeland, B., Schwartz, B. J., . . . Bloom, F. E. (1993). Noninvasive presurgical neuromagnetic mapping of somatosensory cortex. *Neurosurgery, 33*(2), 260-268.

Garrett, D. D., Samanez-Larkin, G. R., MacDonald, S. W., Lindenberger, U., McIntosh, A. R., & Grady, C. L. (2013). Moment-to-moment brain signal variability: A next frontier in human brain mapping? *Neuroscience & Biobehavioral Reviews, 37*(4), 610-624.

Genow, A., Hummel, C., Scheler, G., Hopfengärtner, R., Kaltenhäuser, M., Buchfelder, M., . . . Stefan, H. (2004). Epilepsy surgery, resection volume and MSI localization in lesional frontal lobe epilepsy. *Neuroimage, 21*(1), 444-449.

Gooijer-van de Groep, K. L., Leijten, F. S., Ferrier, C. H., & Huiskamp, G. J. (2013). Inverse modeling in magnetic source imaging: comparison of MUSIC, SAM (g2), and sLORETA to interictal intracranial EEG. *Human brain mapping, 34*(9), 2032-2044.

Gramfort, A., Luessi, M., Larson, E., Engemann, D. A., Strohmeier, D., Brodbeck, C., . . . Parkkonen, L. (2013). MEG and EEG data analysis with MNE-Python. *Frontiers in neuroscience, 7*.

Gramfort, A., Papadopoulo, T., Olivi, E., & Clerc, M. (2010). OpenMEEG: opensource software for quasistatic bioelectromagnetics. *Biomedical engineering online, 9*(1), 45.

Grech, R., Cassar, T., Muscat, J., Camilleri, K. P., Fabri, S. G., Zervakis, M., . . . Vanrumste, B. (2008). Review on solving the inverse problem in EEG source analysis. *Journal of neuroengineering and rehabilitation, 5*(1), 25.

Guggisberg, A. G., Kirsch, H. E., Mantle, M. M., Barbaro, N. M., & Nagarajan, S. S. (2008). Fast oscillations associated with interictal spikes localize the epileptogenic zone in patients with partial epilepsy. *Neuroimage, 39*(2), 661-668.

Haarmann, H. J., Cameron, K. A., & Ruchkin, D. S. (2002). Neural synchronization mediates on-line sentence processing: EEG coherence evidence from filler-gap constructions. *Psychophysiology, 39*(6), 820-825.

Hajek, M., Valavanis, A., Yonekawa, T., Schiess, R., Buck, A., & Wieser, H. G. (1998). Selective amobarbital test for the determination of language function in patients with epilepsy with frontal and posterior temporal brain lesions. *Epilepsia, 39*(4), 389-398.

Hall, S. D., Holliday, I. E., Hillebrand, A., Furlong, P. L., Singh, K. D., & Barnes, G. R. (2005). Distinct contrast response functions in striate and extra-striate regions of visual cortex revealed with magnetoencephalography (MEG). *Clinical*

Neurophysiology, 116(7), 1716-1722.

Hämäläinen, M., Hari, R., Ilmoniemi, R. J., Knuutila, J., & Lounasmaa, O. V. (1993). Magnetoencephalography—theory, instrumentation, and applications to noninvasive studies of the working human brain. *Reviews of modern Physics, 65*(2), 413.

Hämäläinen, M. S., & Ilmoniemi, R. J. (1994). Interpreting magnetic fields of the brain: minimum norm estimates. *Medical and biological engineering and computing, 32*(1), 35-42.

Hamalainen, M. S., & Sarvas, J. (1987). Feasibility of the homogeneous head model in the interpretation of neuromagnetic fields. *Physics in medicine and biology, 32*(1), 91.

Hamalainen, M. S., & Sarvas, J. (1989). Realistic conductivity geometry model of the human head for interpretation of neuromagnetic data. *IEEE transactions on biomedical engineering, 36*(2), 165-171.

Hamberger, M. J., & Cole, J. (2011). Language organization and reorganization in epilepsy. *Neuropsychology review, 21*(3), 240.

Hamer, H., Morris, H., Mascha, E., Karafa, M., Bingaman, W., Bej, M., . . . Hahn, J. (2002). Complications of invasive video-EEG monitoring with subdural grid electrodes. *Neurology, 58*(1), 97-103.

Hanslmayr, S., Staudigl, T., & Fellner, M.-C. (2012). Oscillatory power decreases and long-term memory: the information via desynchronization hypothesis. *Frontiers in human neuroscience, 6*.

Harding, G. F., Odom, J. V., Spileers, W., Spekreijse, H., & Vision, I. S. f. C. E. o. (1996). Standard for visual evoked potentials 1995. *Vision research, 36*(21), 3567-3572.

Hari, R., Forss, N., Avikainen, S., Kirveskari, E., Salenius, S., & Rizzolatti, G. (1998). Activation of human primary motor cortex during action observation: a neuromagnetic study. *Proceedings of the National Academy of Sciences, 95*(25), 15061-15065.

Harpaz, Y., Robinson, S. E., Medvedovsky, M., & Goldstein, A. (2015). Improving the excess kurtosis (g 2) method for localizing epileptic sources in magnetoencephalographic recordings. *Clinical Neurophysiology, 126*(5), 889-897.

Heers, M., Rampp, S., Stefan, H., Urbach, H., Elger, C. E., von Lehe, M., & Wellmer, J. (2012). MEG-based identification of the epileptogenic zone in occult peri-insular epilepsy. *Seizure, 21*(2), 128-133.

Henry, T. R., Votaw, J., Pennell, P., Epstein, C., Bakay, R., Faber, T., . . . Hoffman, J. (1999). Acute blood flow changes and efficacy of vagus nerve stimulation in partial epilepsy. *Neurology, 52*(6), 1166-1166.

Henschen, S. E. (1918). On the hearing sphere. *Acta Oto-laryngologica, 1*(1), 423-485.

Henson, R. N., Mouchlianitis, E., & Friston, K. J. (2009). MEG and EEG data fusion: simultaneous localisation of face-evoked responses. *Neuroimage, 47*(2), 581-589.

Hertz-Pannier, L., Chiron, C., Jambaqué, I., Renaux-Kieffer, V., Moortele, P. F. V. d., Delalande, O., . . . Bihan, D. L. (2002). Late plasticity for language in a child's non-dominant hemisphere: A pre-and post-surgery fMRI study. *Brain, 125*(2), 361-372.

Hillebrand, A., & Barnes, G. (2002). A quantitative assessment of the sensitivity of whole-head MEG to activity in the adult human cortex. *Neuroimage, 16*(3), 638-650.

Hillebrand, A., & Barnes, G. R. (2005). Beamformer analysis of MEG data. *International review of neurobiology, 68*, 149-171.

Hillebrand, A., Fazio, P., De Munck, J., & Van Dijk, B. (2013). Feasibility of clinical magnetoencephalography (MEG) functional mapping in the presence of dental artefacts. *Clinical Neurophysiology, 124*(1), 107-113.

Hillebrand, A., Nissen, I., Ris-Hilgersom, I., Sijsma, N., Ronner, H., van Dijk, B., & Stam, C. (2016). Detecting epileptiform activity from deeper brain regions in spatially filtered MEG data. *Clinical Neurophysiology, 127*(8), 2766-2769.

Hillebrand, A., Singh, K. D., Holliday, I. E., Furlong, P. L., & Barnes, G. R. (2005). A new approach to neuroimaging with magnetoencephalography. *Human brain mapping, 25*(2), 199-211.

Hirata, M., Goto, T., Barnes, G., Umekawa, Y., Yanagisawa, T., Kato, A., . . . Saitoh, Y. (2010). Language dominance and mapping based on neuromagnetic oscillatory changes: comparison with invasive procedures. *Journal of neurosurgery, 112*(3), 528-538.

Hirata, M., Kato, A., Taniguchi, M., Saitoh, Y., Ninomiya, H., Ihara, A., . . . Yorifuji, S. (2004). Determination of language dominance with synthetic aperture magnetometry: comparison with the Wada test. *Neuroimage, 23*(1), 46-53.

Holland, R., & Lambon Ralph, M. A. (2010). The anterior temporal lobe semantic hub is a part of the language neural network: selective disruption of irregular past tense verbs by rTMS. *Cerebral Cortex, 20*(12), 2771-2775.

Holmes, M. D., Quiring, J., & Tucker, D. M. (2010). Evidence that juvenile myoclonic epilepsy is a disorder of frontotemporal corticothalamic networks. *Neuroimage, 49*(1), 80-93.

Holmes, M. D., Quiring, J., & Tucker, D. M. (2010). Evidence that juvenile myoclonic epilepsy is a disorder of frontotemporal corticothalamic networks. *Neuroimage, 49*(1), 80-93.

Hong, K.-S., Lee, S. K., Kim, J.-Y., Lee, D.-S., & Chung, C.-K. (2002). Pre-surgical evaluation and surgical outcome of 41 patients with non-lesional neocortical epilepsy. *Seizure, 11*(3), 184-192.

Huang, M., Mosher, J. C., & Leahy, R. (1999). A sensor-weighted overlapping-sphere head model and exhaustive head model comparison for MEG. *Physics in medicine and biology, 44*(2), 423.

Humphries, C., Love, T., Swinney, D., & Hickok, G. (2005). Response of anterior temporal

cortex to syntactic and prosodic manipulations during sentence processing. *Human brain mapping, 26*(2), 128-138.

Hwang, S.-I., Kim, J. H., Park, S. W., Han, M. H., Yu, I. K., Lee, S. H., . . . Chang, K.-H. (2001). Comparative analysis of MR imaging, positron emission tomography, and ictal single-photon emission CT in patients with neocortical epilepsy. *American journal of neuroradiology, 22*(5), 937-946.

Iwasaki, M., Pestana, E., Burgess, R. C., Lüders, H. O., Shamoto, H., & Nakasato, N. (2005). Detection of epileptiform activity by human interpreters: blinded comparison between electroencephalography and magnetoencephalography. *Epilepsia, 46*(1), 59-68.

Jayakar, P., Dunoyer, C., Dean, P., Ragheb, J., Resnick, T., Morrison, G., . . . Duchowny, M. (2008). Epilepsy surgery in patients with normal or nonfocal MRI scans: integrative strategies offer long-term seizure relief. *Epilepsia, 49*(5), 758-764.

Jefferies, E. (2013). The neural basis of semantic cognition: Converging evidence from neuropsychology, neuroimaging and TMS. *Cortex*. https://doi.org/10.1016/j.cortex.2012.10.008

Jenkinson, N., & Brown, P. (2011). New insights into the relationship between dopamine, beta oscillations and motor function. *Trends in neurosciences, 34*(12), 611-618.

Jensen, M. S., & Yaari, Y. (1988). The relationship between interictal and ictal paroxysms in an in vitro model of focal hippocampal epilepsy. *Annals of neurology, 24*(5), 591-598.

Jin, K., Nakasato, N., Shamoto, H., Kanno, A., Itoyama, Y., & Tominaga, T. (2007). Neuromagnetic localization of spike sources in perilesional, contralateral mirror, and ipsilateral remote areas in patients with cavernoma. *Epilepsia, 48*(11), 2160-2166.

Jirsch, J., Urrestarazu, E., LeVan, P., Olivier, A., Dubeau, F., & Gotman, J. (2006). High-frequency oscillations during human focal seizures. *Brain, 129*(6), 1593-1608.

Jobst, B. C., Williamson, P. D., Neuschwander, T. B., Darcey, T. M., Thadani, V. M., & Roberts, D. W. (2001). Secondarily generalized seizures in mesial temporal epilepsy: clinical characteristics, lateralizing signs, and association with sleep–wake cycle. *Epilepsia, 42*(10), 1279-1287.

Johnson, K., Page, A., Williams, H., Wassemer, E., & Whitehouse, W. (2002). The use of melatonin as an alternative to sedation in uncooperative children undergoing an MRI examination. *Clinical radiology, 57*(6), 502-506.

Johnson, S., Prendergast, G., Hymers, M., & Green, G. (2011). Examining the effects of one- and three-dimensional spatial filtering analyses in Magnetoencephalography. *PLoS ONE*, *6*(8), e22251. https://doi.org/10.1371/journal.pone.0022251

Jones, R. S., da Silva, A. B., Whittaker, R. G., Woodhall, G. L., & Cunningham, M. O. (2016). Human brain slices for epilepsy research: Pitfalls, solutions and future challenges. *Journal of neuroscience methods, 260*, 221-232.

Jones-Gotman, M. (1991). Neuropsychological techniques in the identification of epileptic foci. *Epilepsy research. Supplement, 5*, 87-94.

Kaiboriboon, K., Bertrand, M. E., Osman, M. M., & Hogan, R. E. (2005). Quantitative analysis of cerebral blood flow patterns in mesial temporal lobe epilepsy using composite SISCOM. *Journal of Nuclear Medicine, 46*(1), 38-43.

Kakisaka, Y., Iwasaki, M., Alexopoulos, A. V., Enatsu, R., Jin, K., Wang, Z. I., . . . Burgess, R. C. (2012). Magnetoencephalography in fronto-parietal opercular epilepsy. *Epilepsy research, 102*(1), 71-77.

Keller, C. J., Truccolo, W., Gale, J. T., Eskandar, E., Thesen, T., Carlson, C., . . . Madsen, J. R. (2010). Heterogeneous neuronal firing patterns during interictal epileptiform discharges in the human cortex. *Brain, 133*(6), 1668-1681.

Kharkar, S., & Knowlton, R. (2015). Magnetoencephalography in the presurgical evaluation of epilepsy. *Epilepsy & Behavior, 46*, 19-26.

Kilpatrick, C., Cook, M., Kaye, A., Murphy, M., & Matkovic, Z. (1997). Non-invasive investigations successfully select patients for temporal lobe surgery. *Journal of Neurology, Neurosurgery & Psychiatry, 63*(3), 327-333.

Kirsch, H., Robinson, S., Mantle, M., & Nagarajan, S. (2006). Automated localization of magnetoencephalographic interictal spikes by adaptive spatial filtering. *Clinical Neurophysiology, 117*(10), 2264-2271.

Knake, S., Halgren, E., Shiraishi, H., Hara, K., Hamer, H., Grant, P., . . . Busa, E. (2006). The value of multichannel MEG and EEG in the presurgical evaluation of 70 epilepsy patients. *Epilepsy research, 69*(1), 80-86.

Knake, S., Triantafyllou, C., Wald, L., Wiggins, G., Kirk, G., Larsson, P., . . . Dale, A. (2005). 3T phased array MRI improves the presurgical evaluation in focal epilepsies A prospective study. *Neurology, 65*(7), 1026-1031.

Knecht, S., Deppe, M., Dräger, B., Bobe, L., Lohmann, H., Ringelstein, E.-B., & Henningsen, H. (2000). Language lateralization in healthy right-handers. *Brain, 123*(1), 74-81.

Knecht, S., Dräger, B., Deppe, M., Bobe, L., Lohmann, H., Flöel, A., . . . Henningsen, H. (2000). Handedness and hemispheric language dominance in healthy humans. *Brain, 123*(12), 2512-2518.

Knecht, S., Dräger, B., Deppe, M., Bobe, L., Lohmann, H., Flöel, A., . . . Henningsen, H. (2000). Handedness and hemispheric language dominance in healthy humans. *Brain, 123*(12), 2512-2518.

Knowlton, R., Laxer, K., Aminoff, M., Roberts, T., Wong, S., & Rowley, H. (1997). Magnetoencephalography in partial epilepsy: clinical yield and localization accuracy. *Annals of neurology, 42*(4), 622-631.

Knowlton, R. C., Elgavish, R., Howell, J., Blount, J., Burneo, J. G., Faught, E., . . . Worthington, J. (2006). Magnetic source imaging versus intracranial

electroencephalogram in epilepsy surgery: a prospective study. *Annals of neurology, 59*(5), 835-842.

Knowlton, R. C., Lawn, N. D., Mountz, J. M., & Kuzniecky, R. I. (2004). Ictal SPECT analysis in epilepsy Subtraction and statistical parametric mapping techniques. *Neurology, 63*(1), 10-15.

Knowlton, R. C., & Shih, J. (2004). Magnetoencephalography in epilepsy. *Epilepsia, 45*(s4), 61-71.

Kolmogorov, A. (1958). *On the linear dimension of topological vector spaces.* Paper presented at the Dokl. Akad. Nauk SSSR.

Kuzniecky, R. I. (2005). Neuroimaging of epilepsy: therapeutic implications. *NeuroRx, 2*(2), 384-393.

Kwan, P., Arzimanoglou, A., Berg, A. T., Brodie, M. J., Allen Hauser, W., Mathern, G., . . . French, J. (2010). Definition of drug resistant epilepsy: consensus proposal by the ad hoc Task Force of the ILAE Commission on Therapeutic Strategies. *Epilepsia, 51*(6), 1069-1077.

Kwong, K. K., Belliveau, J. W., Chesler, D. A., Goldberg, I. E., Weisskoff, R. M., Poncelet, B. P., . . . Turner, R. (1992). Dynamic magnetic resonance imaging of human brain activity during primary sensory stimulation. *Proceedings of the National Academy of Sciences, 89*(12), 5675-5679.

Lamusuo, S., Forss, N., Ruottinen, H. M., Bergman, J., Mäkelä, J., Mervaala, E., . . . Ylinen, A. (1999). [18F] FDG-PET and Whole-Scalp MEG Localization of Epileptogenic Cortex. *Epilepsia, 40*(7), 921-930.

Lantz, G., De Peralta, R. G., Spinelli, L., Seeck, M., & Michel, C. (2003). Epileptic source localization with high density EEG: how many electrodes are needed? *Clinical Neurophysiology, 114*(1), 63-69.

Larson, E., Maddox, R. K., & Lee, A. K. (2014). Improving spatial localization in MEG inverse imaging by leveraging intersubject anatomical differences. *Frontiers in neuroscience, 8*.

Lee, J. W., Tanaka, N., Shiraishi, H., Milligan, T. A., Dworetzky, B. A., Khoshbin, S., . . . Bromfield, E. B. (2010). Evaluation of postoperative sharp waveforms through EEG and magnetoencephalography. *Journal of Clinical Neurophysiology, 27*(1), 7-11.

Leidy, N. K., Elixhauser, A., Vickrey, B., Means, E., & Willian, M. (1999). Seizure frequency and the health-related quality of life of adults with epilepsy. *Neurology, 53*(1), 162-162.

Lew, S. M., Matthews, A. E., Hartman, A. L., & Haranhalli, N. (2013). Posthemispherectomy hydrocephalus: results of a comprehensive, multiinstitutional review. *Epilepsia, 54*(2), 383-389.

Litvak, V., Mattout, J., Kiebel, S., Phillips, C., Henson, R., Kilner, J., . . . Flandin, G. (2011). EEG and MEG data analysis in SPM8. *Computational intelligence and*

neuroscience, 2011.

Liu, Z., Ding, L., & He, B. (2006). Integration of EEG/MEG with MRI and fMRI. *IEEE engineering in medicine and biology magazine, 25*(4), 46-53.

Löscher, W., & Potschka, H. (2005). Drug resistance in brain diseases and the role of drug efflux transporters. *Nature reviews. Neuroscience, 6*(8), 591.

Lüders, H. O., Najm, I., Nair, D., Widdess-Walsh, P., & Bingman, W. (2006). The epileptogenic zone: general principles. *Epileptic disorders, 8*(2), 1-9.

Malviya, S., Voepel-Lewis, T., Eldevik, O. P., Rockwell, D. T., Wong, J., & Tait, A. (2000). Sedation and general anaesthesia in children undergoing MRI and CT: adverse events and outcomes. *British journal of anaesthesia, 84*(6), 743-748.

Mamelak, A. N., Lopez, N., Akhtari, M., & Sutherling, W. W. (2002). Magnetoencephalography-directed surgery in patients with neocortical epilepsy. *Journal of neurosurgery, 97*(4), 865-873.

Maris, E., & Oostenveld, R. (2007). Nonparametric statistical testing of EEG-and MEG-data. *Journal of neuroscience methods, 164*(1), 177-190.

Martinez, C., Sullivan, T., & Hauser, W. A. (2009). Prevalence of acute repetitive seizures (ARS) in the United Kingdom. *Epilepsy research, 87*(2), 137-143.

Mazoyer, B. M., Tzourio, N., Frak, V., Syrota, A., Murayama, N., Levrier, O., . . . Mehler, J. (1993). The cortical representation of speech. *Journal of Cognitive Neuroscience, 5*(4), 467-479.

McCagh, J., Fisk, J. E., & Baker, G. A. (2009). Epilepsy, psychosocial and cognitive functioning. *Epilepsy research, 86*(1), 1-14.

McIntosh, A., Wilson, S. J., & Berkovic, S. F. (2001). Seizure outcome after temporal lobectomy: current research practice and findings. *Epilepsia, 42*(10), 1288-1307.

Meunier, S., Lehéricy, S., Garnero, L., & Vidailhet, M. (2003). Dystonia: lessons from brain mapping. *The Neuroscientist, 9*(1), 76-81.

Mikuni, N., Nagamine, T., Ikeda, A., Terada, K., Taki, W., Kimura, J., . . . Shibasaki, H. (1997). Simultaneous recording of epileptiform discharges by MEG and subdural electrodes in temporal lobe epilepsy. *Neuroimage, 5*(4), 298-306.

Mohamed, I. S., Otsubo, H., Ochi, A., Elliott, I., Donner, E., Chuang, S., . . . Snead, O. C. (2007). Utility of magnetoencephalography in the evaluation of recurrent seizures after epilepsy surgery. *Epilepsia, 48*(11), 2150-2159.

Mohanraj, R., Norrie, J., Stephen, L. J., Kelly, K., Hitiris, N., & Brodie, M. J. (2006). Mortality in adults with newly diagnosed and chronic epilepsy: a retrospective comparative study. *The Lancet Neurology, 5*(6), 481-487.

Mohseni, H. R., Woolrich, M. W., Kringelbach, M. L., Probert Smith, P., & Aziz, T. (2012). Fusion of magnetometer and gradiometer sensors of MEG in a beamforming framework. *IEEE Trans Biomed*.

Morgan, C. L., & Kerr, M. P. (2002). Epilepsy and mortality: a record linkage study in a UK population. *Epilepsia, 43*(10), 1251-1255.

Mosher, J. C., & Leahy, R. M. (1998). Recursive MUSIC: a framework for EEG and MEG source localization. *IEEE transactions on biomedical engineering, 45*(11), 1342-1354.

Mosher, J. C., & Leahy, R. M. (1999). Source localization using recursively applied and projected (RAP) MUSIC. *IEEE Transactions on signal processing, 47*(2), 332-340.

Mosher, J. C., Leahy, R. M., & Lewis, P. S. (1997). Matrix kernels for the forward problem in EEG and MEG. *Los Alamos National Labs, Tech. Rep. LA-UR-97-3812*.

Mosher, J. C., Leahy, R. M., & Lewis, P. S. (1999). EEG and MEG: forward solutions for inverse methods. *IEEE transactions on biomedical engineering, 46*(3), 245-259.

Mouthaan, B. E., Rados, M., Barsi, P., Boon, P., Carmichael, D. W., Carrette, E., . . . Dimova, P. (2016). Current use of imaging and electromagnetic source localization procedures in epilepsy surgery centers across Europe. *Epilepsia, 57*(5), 770-776.

Muhlhofer, W., Tan, Y. L., Mueller, S. G., & Knowlton, R. (2017). MRI-negative temporal lobe epilepsy—What do we know? *Epilepsia, 58*(5), 727-742.

Mukamel, R., Gelbard, H., Arieli, A., Hasson, U., Fried, I., & Malach, R. (2005). Coupling between neuronal firing, field potentials, and FMRI in human auditory cortex. *Science, 309*(5736), 951-954.

Muthukumaraswamy, S. D. (2014). The use of magnetoencephalography in the study of psychopharmacology (pharmaco-MEG). *Journal of Psychopharmacology, 28*(9), 815-829.

Muthukumaraswamy, S. D., & Singh, K. D. (2008). Spatiotemporal frequency tuning of BOLD and gamma band MEG responses compared in primary visual cortex. *Neuroimage, 40*(4), 1552-1560.

Muthukumaraswamy, S. D., & Singh, K. D. (2009). Functional decoupling of BOLD and gamma-band amplitudes in human primary visual cortex. *Human brain mapping, 30*(7), 2000-2007.

Muthukumaraswamy, S. D., & Singh, K. D. (2013). Visual gamma oscillations: the effects of stimulus type, visual field coverage and stimulus motion on MEG and EEG recordings. *Neuroimage, 69*, 223-230.

Muthukumaraswamy, S. D., Singh, K. D., Swettenham, J. B., & Jones, D. K. (2010). Visual gamma oscillations and evoked responses: variability, repeatability and structural MRI correlates. *Neuroimage, 49*(4), 3349-3357.

Nagarajan, S., & Sekihara, K. (2014). Magnetoencephalographic Imaging *Magnetoencephalography* (pp. 163-182): Springer.

Nakagawa, S. (2004). A farewell to Bonferroni: the problems of low statistical power and publication bias. *Behavioral ecology, 15*(6), 1044-1045.

Narain, C., Scott, S. K., Wise, R. J., Rosen, S., Leff, A., Iversen, S., & Matthews, P. (2003). Defining a left-lateralized response specific to intelligible speech using fMRI. *Cerebral Cortex, 13*(12), 1362-1368.

Nevalainen, P., Rahkonen, P., Pihko, E., Lano, A., Vanhatalo, S., Andersson, S., . . . Lauronen, L. (2015). Evaluation of somatosensory cortical processing in extremely preterm infants at term with MEG and EEG. *Clinical Neurophysiology, 126*(2), 275-283.

Nissen, I., Stam, C., Citroen, J., Reijneveld, J., & Hillebrand, A. (2016). Preoperative evaluation using magnetoencephalography: experience in 382 epilepsy patients. *Epilepsy research, 124*, 23-33.

Nissen, I. A., Stam, C. J., Reijneveld, J. C., Straaten, I. E., Hendriks, E. J., Baayen, J. C., . . . Hillebrand, A. (2017). Identifying the epileptogenic zone in interictal resting-state MEG source-space networks. *Epilepsia, 58*(1), 137-148.

Noachtar, S., & Rémi, J. (2009). The role of EEG in epilepsy: a critical review. *Epilepsy & Behavior, 15*(1), 22-33.

Nolte, G. (2003). The magnetic lead field theorem in the quasi-static approximation and its use for magnetoencephalography forward calculation in realistic volume conductors. *Physics in medicine and biology, 48*(22), 3637.

Nowell, M., Rodionov, R., Zombori, G., Sparks, R., Winston, G., Kinghorn, J., . . . McEvoy, A. W. (2015). Utility of 3D multimodality imaging in the implantation of intracranial electrodes in epilepsy. *Epilepsia, 56*(3), 403-413.

Ocak, H. (2009). Automatic detection of epileptic seizures in EEG using discrete wavelet transform and approximate entropy. *Expert Systems with Applications, 36*(2), 2027-2036.

Oishi, M., Otsubo, H., Kameyama, S., Morota, N., Masuda, H., Kitayama, M., & Tanaka, R. (2002). Epileptic spikes: magnetoencephalography versus simultaneous electrocorticography. *Epilepsia, 43*(11), 1390-1395.

Ojemann, J. G., Akbudak, E., Snyder, A. Z., McKinstry, R. C., Raichle, M. E., & Conturo, T. E. (1997). Anatomic localization and quantitative analysis of gradient refocused echo-planar fMRI susceptibility artifacts. *Neuroimage, 6*(3), 156-167.

Okada, Y. (1983). Inferences concerning anatomy and physiology of the human brain based on its magnetic field. *Il Nuovo Cimento D, 2*(2), 379-409.

Okada, Y., Tanenbaum, R., Williamson, S., & Kaufman, L. (1984). Somatotopic organization of the human somatosensory cortex revealed by neuromagnetic measurements. *Experimental Brain Research, 56*(2), 197-205.

Okada, Y. C., Williamson, S. J., & Kaufman, L. (1982). Magnetic field of the human sensorimotor cortex. *International Journal of Neuroscience, 17*(1), 33-38.

Oostenveld, R., Fries, P., Maris, E., & Schoffelen, J.-M. (2011). FieldTrip: open source software for advanced analysis of MEG, EEG, and invasive electrophysiological

data. *Computational intelligence and neuroscience, 2011*, 1.

Ossenblok, P., De Munck, J. C., Colon, A., Drolsbach, W., & Boon, P. (2007). Magnetoencephalography is more successful for screening and localizing frontal lobe epilepsy than electroencephalography. *Epilepsia, 48*(11), 2139-2149.

Ossenblok, P., De Munck, J. C., Colon, A., Drolsbach, W., & Boon, P. (2007). Magnetoencephalography is more successful for screening and localizing frontal lobe epilepsy than electroencephalography. *Epilepsia, 48*(11), 2139-2149.

Ou, W., Golland, P., & Hämäläinen, M. (2007). *Sources of variability in MEG.* Paper presented at the International Conference on Medical Image Computing and Computer-Assisted Intervention.

Pantazis, D., Nichols, T. E., Baillet, S., & Leahy, R. M. (2005). A comparison of random field theory and permutation methods for the statistical analysis of MEG data. *Neuroimage, 25*(2), 383-394.

Papanicolaou, A. C., Pataraia, E., Billingsley-Marshall, R., Castillo, E. M., Wheless, J. W., Swank, P., . . . Simos, P. G. (2005). Toward the substitution of invasive electroencephalography in epilepsy surgery. *Journal of Clinical Neurophysiology, 22*(4), 231-237.

Papanicolaou, A. C., Simos, P. G., Castillo, E. M., Breier, J. I., Sarkari, S., Pataraia, E., . . . Maggio, V. (2004). Magnetocephalography: a noninvasive alternative to the Wada procedure. *Journal of neurosurgery, 100*(5), 867-876.

Pascual-Marqui, R. D. (2002). Standardized low-resolution brain electromagnetic tomography (sLORETA): technical details. *Methods Find Exp Clin Pharmacol, 24*(Suppl D), 5-12.

Pascual-Marqui, R. D., Michel, C. M., & Lehmann, D. (1994). Low resolution electromagnetic tomography: a new method for localizing electrical activity in the brain. *International journal of psychophysiology, 18*(1), 49-65.

Pataraia, E., Billingsley-Marshall, R., Castillo, E., Breier, J., Simos, P., Sarkari, S., . . . Papanicolaou, A. (2005). Organization of receptive language-specific cortex before and after left temporal lobectomy. *Neurology, 64*(3), 481-487.

Pataraia, E., Simos, P., Castillo, E., Billingsley, R., Sarkari, S., Wheless, J., . . . Swank, P. (2004). Does magnetoencephalography add to scalp video-EEG as a diagnostic tool in epilepsy surgery? *Neurology, 62*(6), 943-948.

Patterson, K., Nestor, P. J., & Rogers, T. T. (2007). Where do you know what you know? The representation of semantic knowledge in the human brain. *Nature reviews. Neuroscience, 8*(12), 976.

Paulini, A., Fischer, M., Rampp, S., Scheler, G., Hopfengärtner, R., Kaltenhäuser, M., . . . Stefan, H. (2007). Lobar localization information in epilepsy patients: MEG—a useful tool in routine presurgical diagnosis. *Epilepsy research, 76*(2), 124-130.

Penfield, W., & Rasmussen, T. (1950). The cerebral cortex of man; a clinical study of

localization of function.

Pfurtscheller, G., & Da Silva, F. L. (1999). Event-related EEG/MEG synchronization and desynchronization: basic principles. *Clinical Neurophysiology, 110*(11), 1842-1857.

Piccinelli, P., Viri, M., Zucca, C., Borgatti, R., Romeo, A., Giordano, L., . . . Beghi, E. (2005). Inter-rater reliability of the EEG reading in patients with childhood idiopathic epilepsy. *Epilepsy research, 66*(1), 195-198.

Prendergast, G., Green, G. G., & Hymers, M. (2013). A robust implementation of a kurtosis beamformer for the accurate identification of epileptogenic foci. *Clinical Neurophysiology, 124*(4), 658-666.

Price, C. J., Price, C., Wise, R., Warburton, E., Moore, C., Howard, D., . . . Friston, K. (1996). Hearing and saying: The functional neuro-anatomy of auditory word processing. *Brain, 119*(3), 919-931.

Pugnaghi, M., Meletti, S., Castana, L., Francione, S., Nobili, L., Mai, R., & Tassi, L. (2011). Features of somatosensory manifestations induced by intracranial electrical stimulations of the human insula. *Clinical Neurophysiology, 122*(10), 2049-2058.

Pujol, J., Deus, J., Losilla, J. M., & Capdevila, A. (1999). Cerebral lateralization of language in normal left-handed people studied by functional MRI. *Neurology, 52*(5), 1038-1038.

Rasmussen, T., & Milner, B. (1977). The role of early left-brain injury in determining lateralization of cerebral speech functions. *Annals of the New York Academy of Sciences, 299*(1), 355-369.

Rausch, R., & Babb, T. L. (1993). Hippocampal neuron loss and memory scores before and after temporal lobe surgery for epilepsy. *Archives of Neurology, 50*(8), 812-817.

Requena, I., Arias, M., Lopez-Ibor, L., Pereiro, I., Barba, A., Alonso, A., & Monton, E. (1991). Cavernomas of the central nervous system: clinical and neuroimaging manifestations in 47 patients. *Journal of Neurology, Neurosurgery & Psychiatry, 54*(7), 590-594.

Roberts, T., Rowley, H., Zusman, E., McDermott, M., & Barbaro, N. (1995). Brief Clinical Report: Correlation of Functional Magnetic Source Imaging with Intraoperative Cortical Stimulation in Neurosurgical Patients. *Journal of image guided surgery, 1*(6), 339-347.

Robinson, S., Nagarajan, S., Mantle, M., Gibbons, V., & Kirsch, H. (2004). Localization of interictal spikes using SAM (g2) and dipole fit. *Neurology & clinical neurophysiology: NCN, 2004*, 74.

Robinson, S., & Vrba, J. (1999). Recent advances in biomagnetism.

Robinson, S. E., Mandell, A. J., & Coppola, R. (2012). Spatiotemporal imaging of complexity. *Frontiers in computational neuroscience, 6*.

Rodionov, R., Vollmar, C., Nowell, M., Miserocchi, A., Wehner, T., Micallef, C., . . . McEvoy, A. W. (2013). Feasibility of multimodal 3D neuroimaging to guide implantation of

intracranial EEG electrodes. *Epilepsy research, 107*(1), 91-100.

Rogawski, M. A., & Löscher, W. (2004). The neurobiology of antiepileptic drugs. *Nature reviews. Neuroscience, 5*(7), 553.

Rose, D. F., Fujiwara, H., Holland-Bouley, K., Greiner, H. M., Arthur, T., & Mangano, F. T. (2013). Focal peak activities in spread of interictal-ictal discharges in epilepsy with beamformer MEG: evidence for an epileptic network? *Frontiers in neurology, 4*.

Rosenow, F., & Lüders, H. (2001). Presurgical evaluation of epilepsy. *Brain, 124*(9), 1683-1700.

Ryvlin, P., Cross, J. H., & Rheims, S. (2014). Epilepsy surgery in children and adults. *The Lancet Neurology, 13*(11), 1114-1126.

Ryvlin, P., & Rheims, S. (2008). Epilepsy surgery: eligibility criteria and presurgical evaluation. *Dialogues in clinical neuroscience, 10*(1), 91.

Salmelin, R. (2007). Clinical neurophysiology of language: the MEG approach. *Clinical Neurophysiology, 118*(2), 237-254.

Sander, J. (1993). Some aspects of prognosis in the epilepsies: a review. *Epilepsia, 34*(6), 1007-1016.

Sayuthi, S., Tharakan, J., Pieter, M. S., & Mar, W. (2009). Neuropsychological assessment in epilepsy surgery–preliminary experience in a rural tertiary care hospital in north east Malaysia. *The Malaysian journal of medical sciences: MJMS, 16*(1), 39.

Scherg, M., & Von Cramon, D. (1985). Two bilateral sources of the late AEP as identified by a spatio-temporal dipole model. *Electroencephalography and Clinical Neurophysiology/Evoked Potentials Section, 62*(1), 32-44.

Schevon, C. A., Carlson, C., Zaroff, C. M., Weiner, H. J., Doyle, W. K., Miles, D., . . . Vazquez, B. (2007). Pediatric language mapping: sensitivity of neurostimulation and Wada testing in epilepsy surgery. *Epilepsia, 48*(3), 539-545.

Schimmel, H. (1967). The (±) reference: accuracy of estimated mean components in average response studies. *Science, 157*(3784), 92-94.

Schmidt, D., & Gram, L. (1995). Monotherapy versus polytherapy in epilepsy. *CNS drugs, 3*(3), 194-208.

Schmidt, D., & Stavem, K. (2009). Long-term seizure outcome of surgery versus no surgery for drug-resistant partial epilepsy: A review of controlled studies. *Epilepsia, 50*(6), 1301-1309.

Schmidt, R. (1986). Multiple emitter location and signal parameter estimation. *IEEE transactions on antennas and propagation, 34*(3), 276-280.

Scott, J. M., Robinson, S. E., Holroyd, T., Coppola, R., Sato, S., & Inati, S. K. (2016). Localization of Interictal Epileptic Spikes With MEG: Optimization of an Automated Beamformer Screening Method (SAMepi) in a Diverse Epilepsy Population. *Journal of Clinical Neurophysiology, 33*(5), 414-420.

Scott, S. K., Blank, C. C., Rosen, S., & Wise, R. J. (2000). Identification of a pathway for intelligible speech in the left temporal lobe. *Brain, 123*(12), 2400-2406.

Scott, S. K., McGettigan, C., & Eisner, F. (2009). A little more conversation, a little less action-candidate roles for motor cortex in speech perception. *Nature reviews. Neuroscience, 10*(4), 295.

Seeck, M., & Spinelli, L. (2004). Intracranial monitoring. *Supplements to Clinical neurophysiology, 57*, 485-493.

Sekihara, K., Abraham-Fuchs, K., Stefan, H., & Hellstrandt, E. (1996). Suppression of background brain activity influence in localizing epileptic spike sources from biomagnetic measurements. *Brain topography, 8*(3), 323-328.

Semah, F., Picot, M.-C., Adam, C., Broglin, D., Arzimanoglou, A., Bazin, B., . . . Baulac, M. (1998). Is the underlying cause of epilepsy a major prognostic factor for recurrence? *Neurology, 51*(5), 1256-1262.

Shelly, C. D., Matrozova, E. A., & Petrashov, V. T. (2016). Resolving thermoelectric “paradox” in superconductors. *Science advances, 2*(2), e1501250.

Shin, W. C., Hong, S. B., Tae, W. S., & Kim, S. E. (2002). Ictal hyperperfusion patterns according to the progression of temporal lobe seizures. *Neurology, 58*(3), 373-380.

Shiraishi, H., Ahlfors, S. P., Stufflebeam, S. M., Takano, K., Okajima, M., Knake, S., . . . Dale, A. M. (2005). Application of Magnetoencephalography in Epilepsy Patients with Widespread Spike or Slow-wave Activity. *Epilepsia, 46*(8), 1264-1272.

Siegel, A. M., Roberts, D. W., Thadani, V. M., McInerney, J., Jobst, B. C., & Williamson, P. D. (2000). The role of intracranial electrode reevaluation in epilepsy patients after failed initial invasive monitoring. *Epilepsia, 41*(5), 571-580.

Singh, K. D., Barnes, G. R., & Hillebrand, A. (2003). Group imaging of task-related changes in cortical synchronisation using nonparametric permutation testing. *Neuroimage, 19*(4), 1589-1601.

Singh, K. D., Barnes, G. R., Hillebrand, A., Forde, E. M., & Williams, A. L. (2002). Task-related changes in cortical synchronization are spatially coincident with the hemodynamic response. *Neuroimage, 16*(1), 103-114.

Son, Y.-J., Chung, C.-K., Lee, S.-K., Chang, K. H., Lee, D. S., Yi, Y. N., & Kim, H. J. (1999). Comparison of localizing values of various diagnostic tests in non-lesional medial temporal lobe epilepsy. *Seizure, 8*(8), 465-470.

Spencer, S. S., McCarthy, G., & Spencer, D. D. (1993). Diagnosis of medial temporal lobe seizure onset Relative specificity and sensitivity of quantitative MRI. *Neurology, 43*(10), 2117-2117.

Sperling, M. R. (1997). Clinical challenges in invasive monitoring in epilepsy surgery. *Epilepsia, 38*(s4).

Sperling, M. R., Wilson, G., Engel, J., Babb, T. L., Phelps, M., & Bradley, W. (1986). Magnetic resonance imaging in intractable partial epilepsy: correlative studies.

Annals of neurology, 20(1), 57-62.

Springer, J. A., Binder, J. R., Hammeke, T. A., Swanson, S. J., Frost, J. A., Bellgowan, P. S., . . . Mueller, W. M. (1999). Language dominance in neurologically normal and epilepsy subjects: a functional MRI study. *Brain, 122*(11), 2033-2046.

Staley, K. J., & Dudek, F. E. (2006). Interictal spikes and epileptogenesis. *Epilepsy Currents, 6*(6), 199-202.

Stam, C. J., Nolte, G., & Daffertshofer, A. (2007). Phase lag index: assessment of functional connectivity from multi channel EEG and MEG with diminished bias from common sources. *Human brain mapping, 28*(11), 1178-1193.

Staudt, M., Grodd, W., Gerloff, C., Erb, M., Stitz, J., & Krägeloh-Mann, I. (2002). Two types of ipsilateral reorganization in congenital hemiparesis: a TMS and fMRI study. *Brain, 125*(10), 2222-2237.

Staudt, M., Grodd, W., Niemann, G., Wildgruber, D., Erb, M., & Krägeloh–Mann, I. (2001). Early left periventricular brain lesions induce right hemispheric organization of speech. *Neurology, 57*(1), 122-125.

Stefan, H., Hummel, C., Scheler, G., Genow, A., Druschky, K., Tilz, C., . . . Romstöck, J. (2003). Magnetic brain source imaging of focal epileptic activity: a synopsis of 455 cases. *Brain, 126*(11), 2396-2405.

Stefan, H., Rampp, S., & Knowlton, R. (2011). Magnetoencephalography adds to the surgical evaluation process. *Epilepsy & Behavior, 20*(2), 172-177.

Stefan, H., Schneider, S., Feistel, H., Pawlik, G., Schüler, P., Abraham-Fuchs, K., . . . Huk, W. (1992). Ictal and interictal activity in partial epilepsy recorded with multichannel magnetoelectroencephalography: correlation of electroencephalography/electrocorticography, magnetic resonance imaging, single photon emission computed tomography, and positron emission tomography findings. *Epilepsia, 33*(5), 874-887.

Stenroos, M., Hunold, A., & Haueisen, J. (2014). Comparison of three-shell and simplified volume conductor models in magnetoencephalography. *Neuroimage*(94), 337-348.

Stowe, L. A., Broere, C. A., Paans, A. M., Wijers, A. A., Mulder, G., Vaalburg, W., & Zwarts, F. (1998). Localizing components of a complex task: sentence processing and working memory. *Neuroreport, 9*(13), 2995-2999.

Sutherling, W., Crandall, P., Darcey, T., Becker, D., Levesque, M., & Barth, D. (1988). The magnetic and electric fields agree with intracranial localizations of somatosensory cortex. *Neurology, 38*(11), 1705-1705.

Sutherling, W., Mamelak, A., Thyerlei, D., Maleeva, T., Minazad, Y., Philpott, L., & Lopez, N. (2008). Influence of magnetic source imaging for planning intracranial EEG in epilepsy. *Neurology, 71*(13), 990-996.

Swanson, S. J., Sabsevitz, D. S., Hammeke, T. A., & Binder, J. R. (2007). Functional magnetic resonance imaging of language in epilepsy. *Neuropsychology review,*

17(4), 491-504.

Swettenham, J. B., Muthukumaraswamy, S. D., & Singh, K. D. (2009). Spectral properties of induced and evoked gamma oscillations in human early visual cortex to moving and stationary stimuli. *Journal of neurophysiology, 102*(2), 1241-1253.

Szaflarski, J. P., Holland, S. K., Schmithorst, V. J., & Byars, A. W. (2006). fMRI study of language lateralization in children and adults. *Human brain mapping, 27*(3), 202-212.

Tadel, F., Baillet, S., Mosher, J. C., Pantazis, D., & Leahy, R. M. (2011). Brainstorm: a user-friendly application for MEG/EEG analysis. *Computational intelligence and neuroscience, 2011*, 8.

Tao, J. X., Ray, A., Hawes-Ebersole, S., & Ebersole, J. S. (2005). Intracranial EEG substrates of scalp EEG interictal spikes. *Epilepsia, 46*(5), 669-676.

Taulu, S., & Simola, J. (2006). Spatiotemporal signal space separation method for rejecting nearby interference in MEG measurements. *Physics in medicine and biology, 51*(7), 1759.

Téllez-Zenteno, J. F., Dhar, R., & Wiebe, S. (2005). Long-term seizure outcomes following epilepsy surgery: a systematic review and meta-analysis. *Brain, 128*(5), 1188-1198.

Tenney, J. R., Fujiwara, H., Horn, P. S., & Rose, D. F. (2014). Comparison of magnetic source estimation to intracranial EEG, resection area, and seizure outcome. *Epilepsia, 55*(11), 1854-1863.

Thivard, L., Lehéricy, S., Krainik, A., Adam, C., Dormont, D., Chiras, J., . . . Dupont, S. (2005). Diffusion tensor imaging in medial temporal lobe epilepsy with hippocampal sclerosis. *Neuroimage, 28*(3), 682-690.

Tonini, C., Beghi, E., Berg, A. T., Bogliun, G., Giordano, L., Newton, R. W., . . . Wiebe, S. (2004). Predictors of epilepsy surgery outcome: a meta-analysis. *Epilepsy research, 62*(1), 75-87.

Tran, T. A., Spencer, S. S., Javidan, M., Pacia, S., Marks, D., & Spencer, D. D. (1997). Significance of spikes recorded on intraoperative electrocorticography in patients with brain tumor and epilepsy. *Epilepsia, 38*(10), 1132-1139.

Trenerry, M. R., Jack, C., Ivnik, R. J., Sharbrough, F., Cascino, G. D., Hirschorn, K., . . . Meyer, F. (1993). MRI hippocampal volumes and memory function before and after temporal lobectomy. *Neurology, 43*(9), 1800-1800.

Tufenkjian, K., & Lüders, H. O. (2012). Seizure semiology: its value and limitations in localizing the epileptogenic zone. *Journal of Clinical Neurology, 8*(4), 243-250.

Tzallas, A. T., Tsipouras, M. G., & Fotiadis, D. I. (2007). Automatic seizure detection based on time-frequency analysis and artificial neural networks. *Computational intelligence and neuroscience, 2007*.

Vakorin, V. A., Kovacevic, N., & McIntosh, A. R. (2010). Exploring transient transfer entropy based on a group-wise ICA decomposition of EEG data. *Neuroimage, 49*(2), 1593-

1600.

van der Kolk, A. G., Hendrikse, J., Zwanenburg, J. J., Visser, F., & Luijten, P. R. (2013). Clinical applications of 7T MRI in the brain. *European journal of radiology, 82*(5), 708-718.

van Elk, M., van Schie, H. T., Zwaan, R. A., & Bekkering, H. (2010). The functional role of motor activation in language processing: motor cortical oscillations support lexical-semantic retrieval. *Neuroimage, 50*(2), 665-677.

Van Uitert, R., Weinstein, D., & Johnson, C. (2003). Volume currents in forward and inverse magnetoencephalographic simulations using realistic head models. *Annals of Biomedical Engineering, 31*(1), 21-31.

Vandenberghe, R., Nobre, A. C., & Price, C. (2002). The response of left temporal cortex to sentences. *Journal of Cognitive Neuroscience, 14*(4), 550-560.

Vrba, J., & Robinson, S. E. (2001). Signal processing in magnetoencephalography. *Methods, 25*(2), 249-271.

Vrba, J., Taulu, S., Nenonen, J., & Ahonen, A. (2010). Signal space separation beamformer. *Brain topography, 23*(2), 128-133.

Wada, J., & Rasmussen, T. (1960). Intracarotid injection of sodium amytal for the lateralization of cerebral speech dominance: experimental and clinical observations. *Journal of neurosurgery, 17*(2), 266-282.

Walczak, T. (1997). Interictal EEG. *Epilepsy: A comprehensive textbook*.

Wang, H., Callaghan, E., Gooding-Williams, G., McAllister, C., & Kessler, K. (2016). Rhythm makes the world go round: An MEG-TMS study on the role of right TPJ theta oscillations in embodied perspective taking. *Cortex, 75*, 68-81.

Wang, Z. I., Alexopoulos, A. V., Nair, D., Krishnan, B., Mosher, J. C., Burgess, R. C., & Kakisaka, Y. (2013). Feasibility of magnetoencephalography recording in an epilepsy patient with implanted responsive cortical stimulation device. *Clinical neurophysiology: official journal of the International Federation of Clinical Neurophysiology, 124*(8), 1705.

Warburton, E., Wise, R. J., Price, C. J., Weiller, C., Hadar, U., Ramsay, S., & Frackowiak, R. S. (1996). Noun and verb retrieval by normal subjects studies with PET. *Brain, 119*(1), 159-179.

Warrington, E. K. (1975). The selective impairment of semantic memory. *The Quarterly journal of experimental psychology, 27*(4), 635-657.

Weiss, S., & Mueller, H. M. (2012). “Too many betas do not spoil the broth”: the role of beta brain oscillations in language processing. *Frontiers in Psychology, 3*.

Westmijse, I., Ossenblok, P., Gunning, B., & Van Luijtelaar, G. (2009). Onset and propagation of spike and slow wave discharges in human absence epilepsy: a MEG study. *Epilepsia, 50*(12), 2538-2548.

Wheless, J., Willmore, L., Breier, J., Kataki, M., Smith, J., King, D., . . . Clifton, G. (1999). A comparison of magnetoencephalography, MRI, and V-EEG in patients evaluated for epilepsy surgery. *Epilepsia, 40*(7), 931-941.

Widdess-Walsh, P., Jeha, L., Nair, D., Kotagal, P., Bingaman, W., & Najm, I. (2007). Subdural electrode analysis in focal cortical dysplasia Predictors of surgical outcome. *Neurology, 69*(7), 660-667.

Wiebe, S., Blume, W. T., Girvin, J. P., & Eliasziw, M. (2001). A randomized, controlled trial of surgery for temporal-lobe epilepsy. *New England Journal of Medicine, 345*(5), 311-318.

Wilenius, J., Medvedovsky, M., Gaily, E., Metsähonkala, L., Mäkelä, J. P., Paetau, A., . . . Paetau, R. (2013). Interictal MEG reveals focal cortical dysplasias: special focus on patients with no visible MRI lesions. *Epilepsy research, 105*(3), 337-348.

Williamson, P., French, J., Thadani, V., Kim, J., Novelly, R., Spencer, S., . . . Mattson, R. (1993). Characteristics of medial temporal lobe epilepsy: II. Interictal and ictal scalp electroencephalography, neuropsychological testing, neuroimaging, surgical results, and pathology. *Annals of neurology, 34*(6), 781-787.

Wilson, S. J., Baxendale, S., Barr, W., Hamed, S., Langfitt, J., Samson, S., . . . Hermann, B. P. (2015). Indications and expectations for neuropsychological assessment in routine epilepsy care: report of the ILAE Neuropsychology Task Force, Diagnostic Methods Commission, 2013–2017. *Epilepsia, 56*(5), 674-681.

Wise, R. J., Scott, S. K., Blank, S. C., Mummery, C. J., Murphy, K., & Warburton, E. A. (2001). Separate neural subsystems withinWernicke's area'. *Brain, 124*(1), 83-95.

Witton, C., Furlong, P. L., & Seri, S. (2014). Technological challenges of pediatric MEG and potential solutions: the aston experience *Magnetoencephalography* (pp. 645-655): Springer.

Woolrich, M., Hunt, L., Groves, A., & Barnes, G. (2011). MEG beamforming using Bayesian PCA for adaptive data covariance matrix regularization. *Neuroimage, 57*(4), 1466-1479.

Worthen, S. F., Hobson, A. R., Hall, S. D., Aziz, Q., & Furlong, P. L. (2011). Primary and secondary somatosensory cortex responses to anticipation and pain: a magnetoencephalography study. *European Journal of Neuroscience, 33*(5), 946-959.

Wright, J., Pickard, N., Whitfield, A., & Hakin, N. (2000). A population-based study of the prevalence, clinical characteristics and effect of ethnicity in epilepsy. *Seizure, 9*(5), 309-313.

Wu, J., Sutherling, W., Koh, S., Salamon, N., Jonas, R., Yudovin, S., . . . Mathern, G. (2006). Magnetic source imaging localizes epileptogenic zone in children with tuberous sclerosis complex. *Neurology, 66*(8), 1270-1272.

Wu, T., Ge, S., Zhang, R., Liu, H., Chen, Q., Zhao, R., . . . Jiang, T. (2014). Neuromagnetic coherence of epileptic activity: an MEG study. *Seizure, 23*(6), 417-423.

Yamazaki, M., Tucker, D. M., Fujimoto, A., Yamazoe, T., Okanishi, T., Yokota, T., . . . Yamamoto, T. (2012). Comparison of dense array EEG with simultaneous intracranial EEG for interictal spike detection and localization. *Epilepsy research, 98*(2), 166-173.

Yoshinaga, H., Kobayashi, K., Hoshida, T., Kinugasa, K., & Ohtuska, Y. (2008). Magnetoencephalogram in a postoperative case with a large skull defect. *Pediatric neurology, 39*(1), 48-51.

Zemskaya, A. (1998). *Polymorphism of the Clinical Course, Diagnosis and Surgical Treatment of Mono-and Multi-focal Epilepsy in Children.* Paper presented at the Russian-American Symposium on Clinical and Social Aspects of Epilepsy.

Zhang, R., Wu, T., Wang, Y., Liu, H., Zou, Y., Liu, W., . . . Fu, Z. (2011). Interictal magnetoencephalographic findings related with surgical outcomes in lesional and nonlesional neocortical epilepsy. *Seizure, 20*(9), 692-700.

Zotev, V. S., Matlashov, A. N., Volegov, P. L., Savukov, I. M., Espy, M. A., Mosher, J. C., . . . Kraus, R. H. (2008). Microtesla MRI of the human brain combined with MEG. *Journal of Magnetic Resonance, 194*(1), 115-120.

Zumsteg, D., Friedman, A., Wennberg, R. A., & Wieser, H. G. (2005). Source localization of mesial temporal interictal epileptiform discharges: correlation with intracranial foramen ovale electrode recordings. *Clinical Neurophysiology, 116*(12), 2810-2818.

Appendices

Appendix 1: Rank Vector Entropy Simulations

Test Signal Generation

MATLAB code:

```
freq1 = 0; % Low freq

freq2 = 10; % High Freq

%% Start freq loop

for freq = 1:30 % 1: number of bands required to reach end freq (should be 1:30 for 600Hz sampling rate with a 150Hz corner frequency).

    time = linspace(0,endtime,fs*endtime);

    sig = randn(size(time));

    sig = nut_filter2(sig','firls','bp',200,freq1,freq2,fs,0)';

    sig(fs*(endtime/2)+1:fs*endtime) = 0.1.*randn(1,fs*(endtime/2))
```

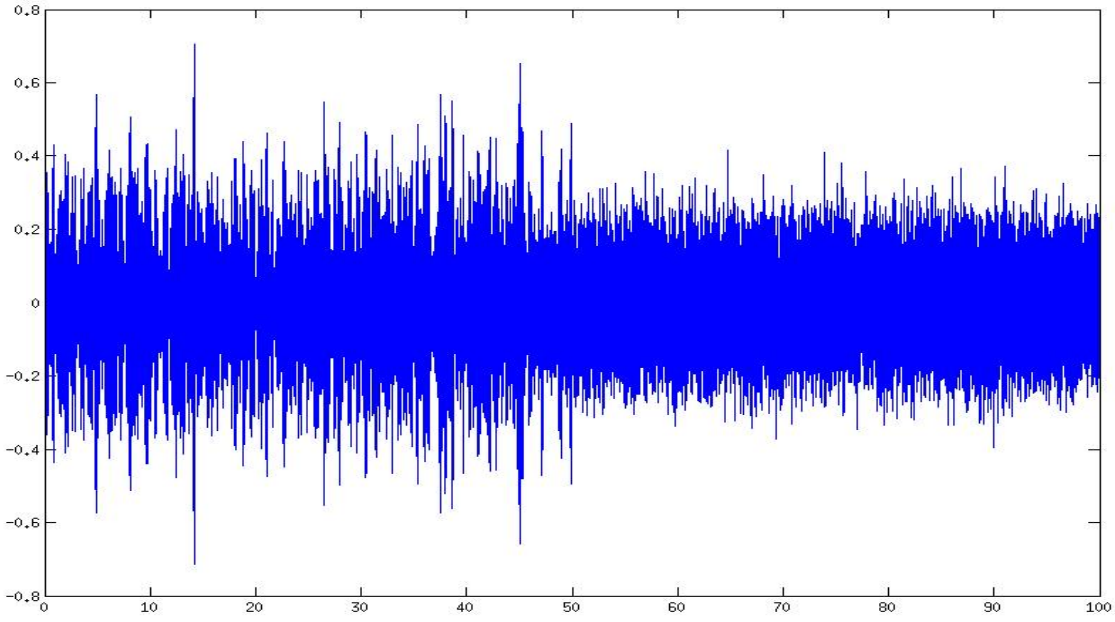

The first half of the test signal is the ‘brain-like’ oscillations within the specified frequency band, the second half is random noise.

RVE of Test Signal

For the oscillatory signal, entropy is lower relative to the noise which has an entropy value of ~1 (as expected).

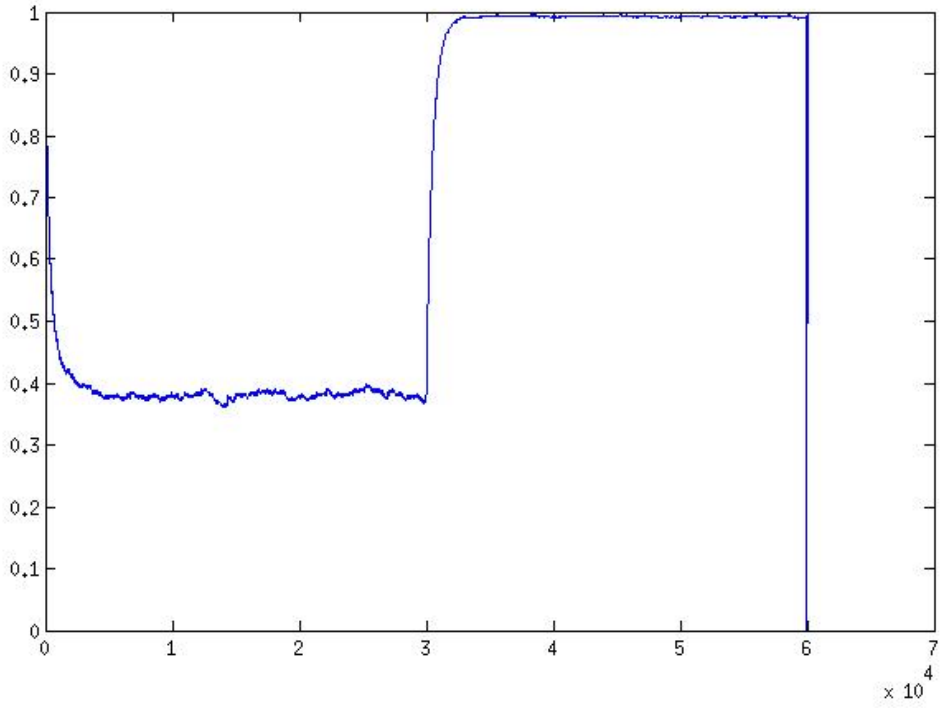

The mean of these two signals are taken (between two time points) and the difference between the means are calculated (Noise RVE mean – Osc RVE mean).

timesignal = [20 30]; % takes signal between 20 and 30 seconds.

timenoise = [70 80]; % takes signal between 70 and 80 seconds.

samplesignal = timesignal * fs;

samplenoise = timenoise * fs;

SallOsc = mean(S(samplesignal)); %takes mean between 20-30s

SallNoise = mean(S(samplenoise));% takes mean between 70-80s

SensDiff = SallNoise - SallOsc; % difference between the two

Diffs(freq, :) = SensDiff; % stores the differences

The greater the difference between the two, the more sensitive the RVE algorithm is (the vector of differences is what is plotted to see how the parameters affect the RVE sensitivity).

Sampling Frequency Comparison

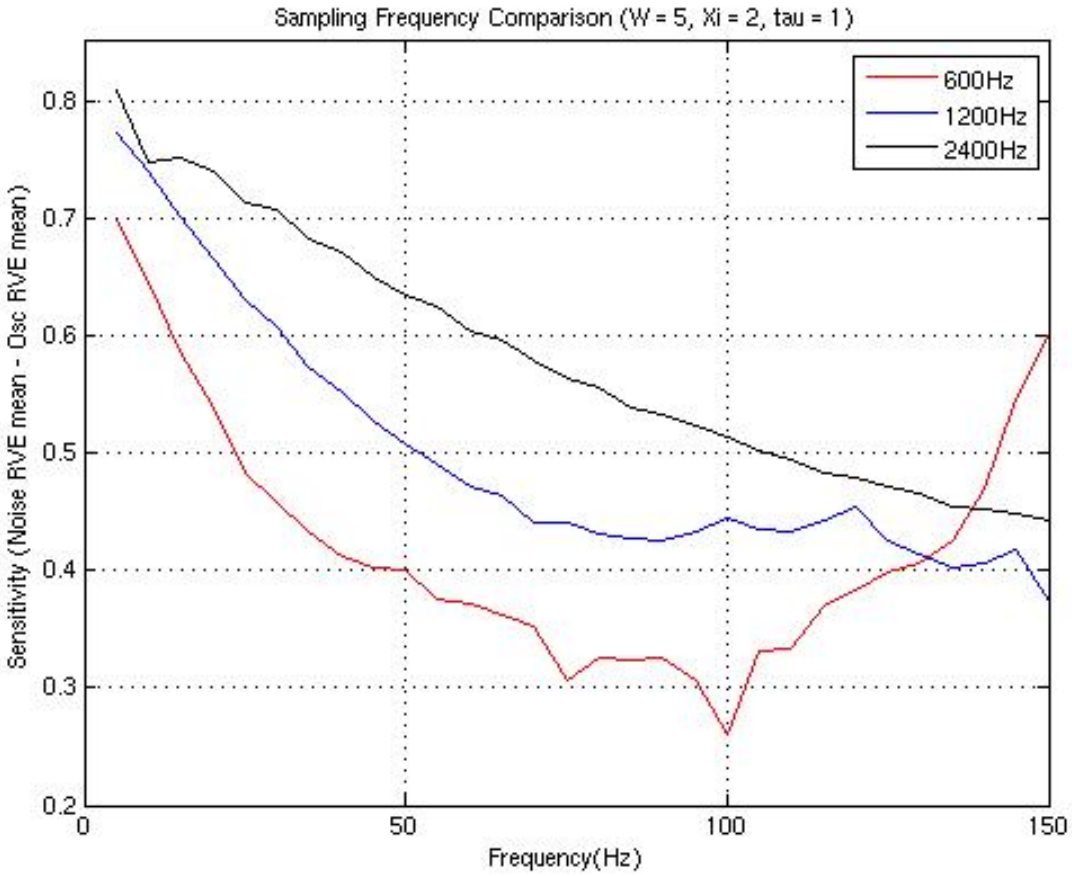

This uses the current RVE parameters but with varying sample frequencies plotted up to 150Hz. From this it is apparent that the algorithm is more sensitive to lower frequencies. Higher sampling frequencies tend to be more sensitive. Note that there is an increase in sensitivity when fc=600 Hz. This seems to be common in all sampling frequencies as the frequency band approaches the corner frequency and when Xi=2. If you change Xi to 1 then this sharp increase does not occur.

Comparing Xi (sample lag) when fs = 1200Hz

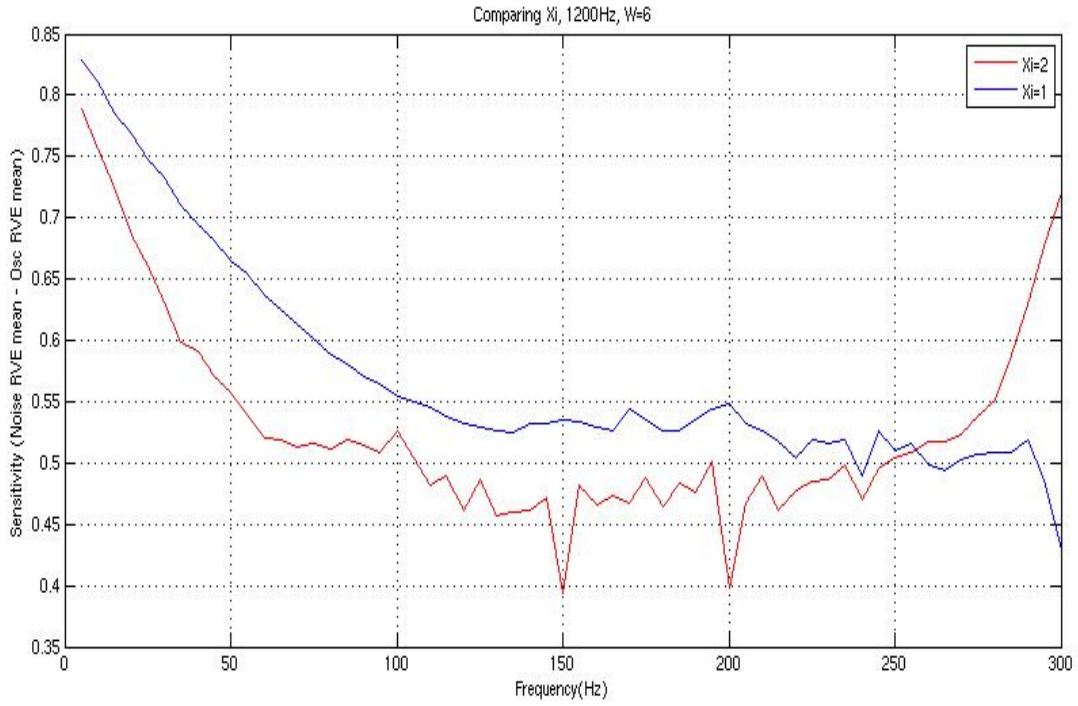

When Xi=2 there is a sharp increase as the frequency band approaches the corner frequency limit. This is apparent at all sampling frequencies tested (600, 1200, 2400 Hz). Overall, Xi=1 seems to increase the sensitivity of the RVE relative to Xi=2 as indicated by the plot above.

Comparing sampling frequency and window size (W=5, W=6)

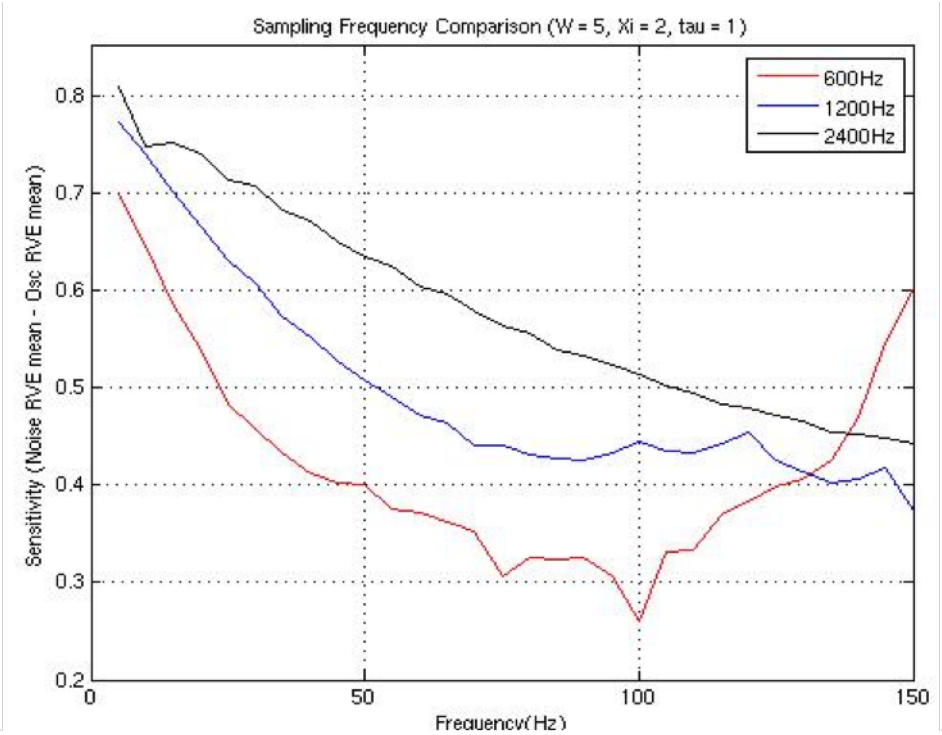

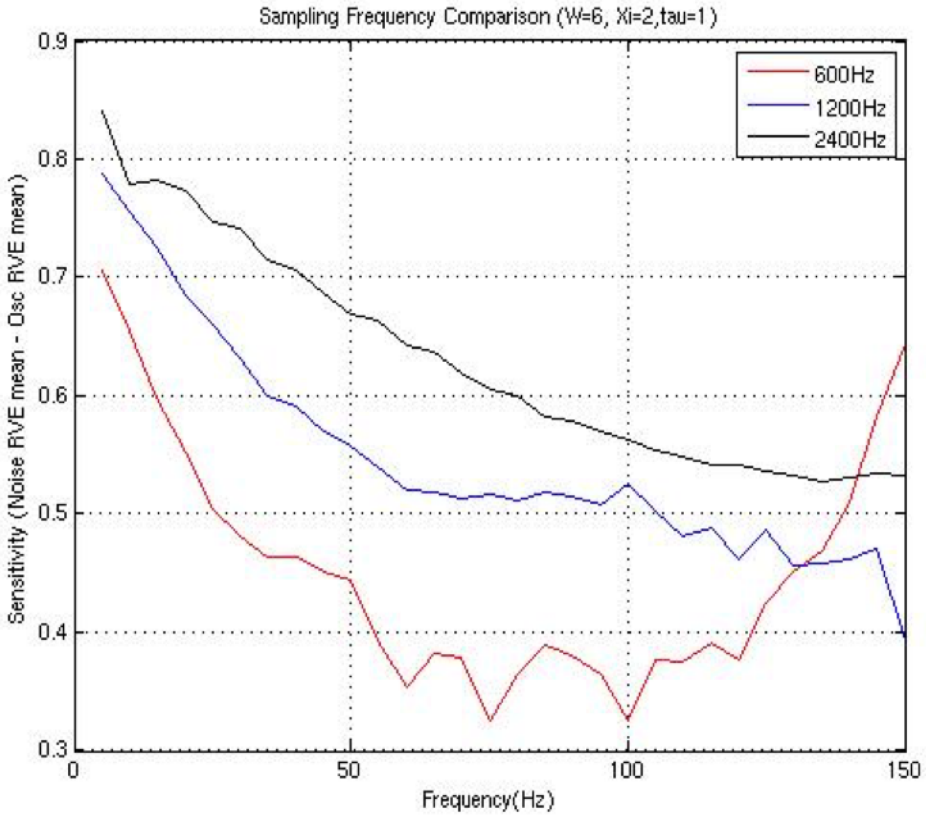

The Y axis is scaled differently for the two figures. Using W=6 (i.e. including more samples in the window), seems to increase sensitivity.

Comparing tau (600Hz *fs*)

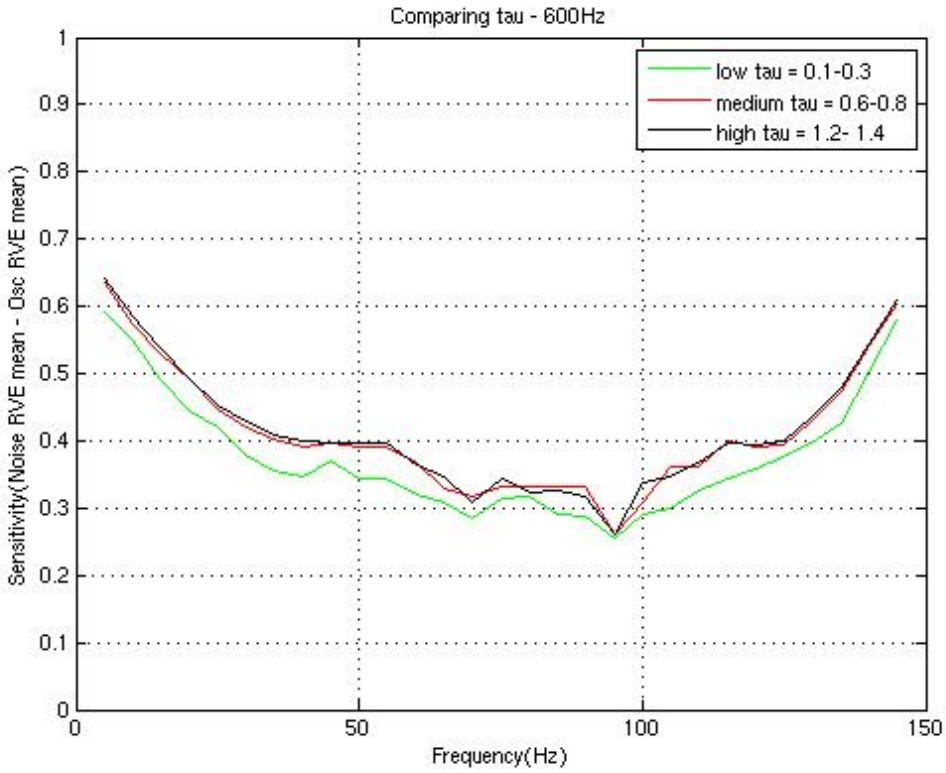

The algorithm was implemented using tau values ranging from 0.1-1.4. Three categories were used (low, mid, high tau) formed from averaging the vectors of 0.1:0.3 (low), 0.6:0.8 (mid), 1.2:1.4 (high tau). The plot indicates that there is little difference in the sensitive of RVE when using different levels of tau.